Spin Liquids, Exotic Phases and Phase Transitions

by

Ying Ran

Submitted to the Department of Physics
in partial fulfillment of the requirements for the degree of

Doctor of Philosophy

at the

MASSACHUSETTS INSTITUTE OF TECHNOLOGY

July 2007

Author .....
Department of Physics
July 27, 2007

Certified by .....
Xiao-Gang Wen
Cecil and Ida Green Professor of physics
Thesis Supervisor

Accepted by .....
Thomas J. Greytak
Professor, Associate Department Head of Education

Spin Liquids, Exotic Phases and Phase Transitions

by

Ying Ran

Submitted to the Department of Physics
on July 27, 2007, in partial fulfillment of the
requirements for the degree of
Doctor of Philosophy

Abstract

Spin liquid, or featureless Mott-Insulator, is a theoretical state of matter firstly motivated from study on High-Tc superconductor. The most striking property of spin liquids is that they do not break any physical symmetry, yet there are many types of them, meaning a phase transition is necessary from one spin liquid to another. It was a long debate about whether these exotic states can serve as the ground states in real materials or even models. In this thesis I firstly discuss a large-N model, where we show the spin liquid states can be the ground states. Because the spin liquid phases cannot be characterized by symmetry breaking, the phase transitions associated with them are naturally beyond the traditional Laudau's paradigm. I discuss a few scenarios of these exotic phase transitions to show a general picture about what can happen for such exotic transitions. Those exotic phase transitions can actually serve as a way to detect these exotic phases. Then I move to a much more realistic model: spin-1/2 Kagome lattice, where we propose a U(1)-Dirac spin liquid as the ground state. The implications on the recent material $ZnCu_3(OH)_6Cl_2$ are discussed. Finally, I come back to the high-Tc problem. A doped spin liquid can naturally be superconducting whose many properties have already been confirmed by experiments. Here I particularly study one experimental puzzle: the nodal-antinodal dichotomy in underdoped High-Tc material. This used to be one difficulty of the doped spin liquid theory. We show that a doped spin liquid can naturally has nodal-antinodal dichotomy due to further neighbor hoppings (t' and t'').

Thesis Supervisor: Xiao-Gang Wen
Title: Cecil and Ida Green Professor of physics

Acknowledgments

A few months ago there was an open house event hosted by our Physics Department for new perspective graduate students. One very talented young student asked me: "Can you tell me about your life in the condensed matter theory group? " Obviously he was trying to choose his graduate school among all the top universities. At that moment, all I said was "oh, I am having a very good time here, people here are very nice. blah blah". Immediately after I said that, I realized that my statements seemed to contain no information, and it might be beyond my English ability to convey my full feeling in a short time. Now, when I am about to finish my 6 years of study as a Ph.D student, it is the perfect moment to quantify my statements.

My advisor Xiao-Gang is the one who led me into the world of physics research. His unique way of looking at physics always shed lights on the physics problems that I work on in an unexpected way. The condensed matter theorists community happens to be very diverse; people are working on completely unrelated issues and motivated by various things: application in the real world, new experimental results, etc. However, Xiao-Gang's motivation is obviously the pleasure of discovering new directions and new ways of looking at things. He can also somehow efficiently propagate his happiness of working on physics to all his students. In a sense he acts like a charger: whenever I feel frustrated and drained, by talking to him I am refreshed and become fully energetic again.

I also want to emphasize Xiao-Gang's kindness and humility. It is always a pleasure to chat with him, because I feel no constraints in the conversation. I never have to worry about asking stupid questions, which I often do. I actually believe asking stupid questions is an inevitable way to learn how to ask the "right" questions. Finding "right" problems is always harder than solving them. The ability to raise good questions, as far as I know, probably is the single most important thing to be a good physicist. Xiao-Gang also teaches me lots of other skills to be a physicist. I remember when I was preparing for my first seminar talk, he tirelessly went through the whole presentation with me, slide by slide, bullet by bullet. He spent the whole afternoon just to make sure I can give a good talk while bypassing the frustrations he himself experienced. Not every advisor would spend such a long time for these kinds of things, and I am extremely lucky to be his student.

In addition to Xiao-Gang, I am also very fortunate to work with Patrick Lee. His warmth and approachability benefit me enormously, from private discussions to lunch conversations with him. His profound knowledge about the whole hard condensed

matter field, both theories and experiments, provides many impacts on my research and the general physics understanding, ranging from basic chemistry, crystal structure to impurity physics. Again, finding problems is always harder, and I am grateful to Patrick for feeding me important and doable problems. I also thank Patrick and Young Lee for serving on my thesis committee.

Senthil is an important part of our CMT atmosphere. He is a well-established faculty member but in person I feel he is like one of my fellow scholars. His signature laughter definitely made our corridor a more social and relaxing environment. Due to his quick and insightful response to all kinds of questions that people raised in lunch, our lunch discussions can often be productive. And certainly I should thank Mike Hermele. Collaborating with Mike not only generates lots of work with fun, it also makes me able to learn many subjects quickly. By talking to him you already know the main issues and main advances in the subject. Moreover, when we face an issue, he often quickly clears up the mist and points out what is the right thing to do. I benefit a lot by learning how he translates physical pictures and mathematical formulas back and forth.

My life in CMT is fruitful and colorful also because of my peer students and postdocs. Sung-Sik Lee, as a busy postdoc, is never too busy to answer my questions and sharing his stimulating insights. I would like to thank Michael Levin for many helpful discussions. Cody, Tiago, Saeed and Alex are my officemates over the past a few years in the group. We had uncountable number of joyful conversations. They made my office a very enjoyable place to stay, even when the air conditioner stops working in the summer. Cody actually taught me how to do projected wavefunction calculations. I also enjoy conversations with Zheng-Cheng Gu and Su-Peng Kou, who were visiting our group for short periods of time.

I also want to thank our close friends and neighbor, Ping and Wanlin. Our friendship makes my life as a Ph.D. student far more than just studying. Finally I want to thank my family members. My wife Ling is the greatest gift in my life. Her love and support draw a physicist's crazy life back to a normal and cheerful trail. My parents, although far away on the other side of the earth, keep transporting their support through the internet and phone line.

Contents

List of Figures

List of Tables

Chapter 1

Introduction

1.1 Motivation

In condensed matter physics, we are interested in phases and phase transitions. In particular, the zero-temperature phases and phase transitions, i.e., quantum phases and quantum phase transitions, due to the new physics associated with them, come into the center stage in modern theoretical condensed matter physics.

Quantum theory of condensed matter was dominated by two main themes. The first one is Fermi liquid theory [1] and the second one is Landau symmetry-breaking theory.[2, 3] Fermi liquid theory is a perturbation theory around a particular type of ground states – the states obtained by filling single-particle energy levels. Fermi liquid theory describes metals, semiconductors, magnets, superconductors, etc. Landau symmetry-breaking theory provide a deep insight into phase and phase transition. It points out that the reason that different phases are different is because they have different symmetries. A phase transition is simply a transition that changes the symmetry. Not so long ago Landau symmetry-breaking theory is believed to describe all possible phases, such as crystal phases, ferromagnetic and anti-ferromagnetic phases, superfluid phases, etc., and all of the phase transitions between them.

However, after the discovery of fractional quantum Hall (FQH) effect, people realized that different FQH states all have the same symmetry. So they contain a new kind of orders – quantum order – that is beyond Landau's symmetry breaking paradigm, therefore we call FQH phases exotic[4, 5]. Quantum order is new since it has nothing to do with symmetry breaking, long range correlation, or local order parameters. Part of this thesis is the discussion of the mathematical description of quantum order and its impact on phase transtions.

A natural question one can raise is: "are FQH liquids the only exotic phases?" or

"are there new quantum phases which do not break any physical symmetry other than fermi liquid?" Note that fermi liquid (FL) is the only conventional disordered state of matter at zero temperature. But it is conventional only because experimentally FL can describe many metals, not because theoretically it is easy to understand.

In one-dimension, people already know that there are many exotic phases, such as Luttinger liquid or spin-1/2 Heisenberg chain. However in higher dimensions, the understanding is very limited, and so far there is no conclusive experiment signature that there are any other exotic quantum phases in two or higher dimension systems than FQH liquids. Nevertheless, the theoretical studies do not have to follow experiment. Spin liquids are such theoretical exotic states of matter, which are defined to be the disordered (i.e., no spin order and no translation symmetry breaking) zero temperature state of a spin model (in particular, a spin-1/2 model by default).

Anderson firstly proposed the concept of spin liquids by his proposal of RVB states[6]. Later Baskaron[7] used slave-particle approach to give RVB liquids a mathematically description. In this thesis, we mainly follow their approach to study the physics of spin liquids. The new physics contained in spin liquids is striking. If Landau's symmetry breaking language is no longer applicable to spin liquids, what is the appropriate systematic mathematical language to describe different spin liquids? If Landau-Ginzburg-Wilson phase transition theory fails, what is the new theory replacing it? By studying spin liquids, we try to gether the information to answer these big questions.

1.2 Band insulator and Mott insulator

There is another way to apprecitate the striking features of spin liquids, which is the featureless Mott-insulator. Band insulator is a well-know concept of solid state physics, which is based on fermi liquid theory. Let us consider a lattice electron system, which has even number of electrons per unit cell. Fermi liquid theory tells us that one way to contruct the ground state of the system is to fill the electrons in the band structure one level after another. Even number of electrons per unit cell makes sure that the resulting state of the filling process is fully gapped, and thus an insulator. On the contrary, if there is odd number of electrons per unit cell, fermi liquid theory tells us that the resulting state is a metal with gapless excitations.

Can the ground state of a system with odd number of electrons per unit cell be an insulator? Mott[8] introduced the concept of Mott-insulator to describe the situation where a material should be a metal according to band theory but is insulating due

to strong replusive interactions between electrons. It is quite easy to understand it pictorically. For simplicity let us consider the square lattice with one electron per site. If the repulsive interaction is so strong that each electron is localized on one site and any charge fluctuation has a finite energy gap U, then for the energy scale much lower than U only the spin dynamics will be left and the system is insulating. Now we can ask what the ground state of the system is. The localized spin will interact with their neighbors via exchange interaction. Again for simplicity we assume only nearest neighbor interaction is present. The coupling should be anti-ferromagnetic by simple second order perturbation theory. The low energy physics is completely determined by nearest neighbor anti-ferromagnetic (AF) Heisenberg model. For the square lattice, the ground state turns out to have long range AF order which breaks the translation symmetry.

Is the above Mott insulator really different from band insulator? The answer is no. Because the translation symmetry is broken, the unit cell is actually doubled, and there are two electrons per doubled unit cell. One can actually show that the above AF Mott insulator can be connected to the band insulator of the doubled unit cell adiabatically without any phase transition. Thus the above Mott insulator is not really exotic.

What is really exotic is featureless Mott insulator, i.e., a Mott insulator which does not break translation symmetry. This is nothing but spin liquid because the low energy degrees of freedoms are spins.

1.3 Doped Mott insulator and High-Tc superconductor

The typical phase diagram of a hole-doped high-Tc superconductor is shown in Fig.1-1. At zero doping, or half-filling, the system has antiferromagnetic(AF) order and is a Mott insulator. Let us focus on zero-temperature. As we increase the doping, three things happen. First the AF order is suppressed to zero, then comes the onset of superconductivity. Finally the superconductivity(SC) disappears and the state is the usual FL. Obviously there are two ways to understand the apperance of SC, either from AF side or from FL side. However, the striking new physics, i.e., physics fundamentally differenct from BCS theory, happens from AF side. Let us focus on the low doping region. The most natural question to ask is: "how to understand the onset of superconductivity by doping the AF ordered state?"

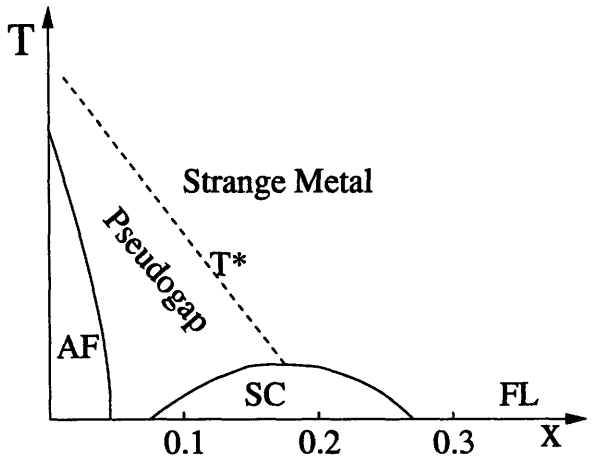

Figure 1-1: Schematic phase diagram of High-Tc superconductors. The solid curves are phase transition boundaries. There are also crossovers from pseudogap regime to strange metal and finally to fermi liquid. Note that experimentally strange metal is quite different properties from fermi liquid.

Now we have the question. The next thing to do is to mathematically write it down. The high-Tc materials can be thought as weakly coupled layers, and the minimal model that may contain the physics of the superconductivity is the one band Hubbard model on 2-dimension square lattice:

$$H_{Hubbard} = -\sum_{ij} t_{ij} c^{\dagger}_{i\sigma} c_{j\sigma} + U \sum_{i} n_{i\uparrow} n_{i\downarrow} \tag{1.1}$$

Suppose the system is slightly away from half-filling by hole-doping. In the limit of $U >> t$, the U term means that any double occupancy of electrons costs a large energy U. In the low energy sector the Hilbert space is composed of those states with no double occupancy. A second-order perturbation theory tells us that the Hubbard model can be reduced to the $t-J$ model in the low energy sector:

$$H_{t-J} = -\mathcal{P} \sum_{ij} t_{ij} c^{\dagger}_{i\sigma} c_{j\sigma} \mathcal{P} + J \sum_{\langle ij \rangle} (\vec{S}_i \cdot \vec{S}_j - \frac{1}{4} n_i n_j) \tag{1.2}$$

where $J = 4t^2/U$ and t is the nearest neighbor hopping. $\mathcal{P}$ is the projection operator removing all double occupancies. Note J is positive, i.e., antiferromagetic.

At half filling, $t-J$ model is just Heisenberg model. Weak layer-layer coupling will give a finite temperature antiferromagetic(AF) order. Now let us dope it. Numerical calculation[9, 10, 11] shows that the hole band minimum for the doped AF order state is at $(\pm\pi/2, \pm\pi/2)$, assuming only nearest neighbor hopping $t \neq 0$. The doped AF

state would have small fermi pockets at $(\pm\pi/2, \pm\pi/2)$.

If those holes in the fermi pockets experience certain attractive interaction, then one natural thing to happen is that they will pair up and condense. And the resulting state is superconductor. It seems we have a solution for High-Tc superconductor.

But wait a moment, the problem is that the onset of SC order is after the disapperance of AF order. It is not clear that starting from AF metal is a good way to access SC phase. If the SC is a result of pairing of holes in AF metal, then the coexistence of AF and SC should be observed, which is not seen in experiments.

A even bigger puzzle is the finite temperature phase diagram. A very important player of the game is the pseudogap regime, which is the "normal" state for the underdoped SC. According to BCS theory the normal state should have the gap fully closed around the fermi surface. But from all kinds of experiments including ARPES, conductivity, Kight shift, specific heat, we know that in the pseudogap regime the gap is not fully closed at all. Around the anti-nodal region ($(\pi, 0)$ and $(0, \pi)$) of the would-be fermi surface, an incoherent energy gap is observed for temperature below T^*. As one decreases the doping, T^* actually increases, as shown in Fig.1-1.

How to understand the pseudogap regime? One way to attack the problem is still to start from doped AF insulator, then consider the possible senarios which destroy the AF order by flucutations. There are recent progress along this line[senthil]. However, Anderson pointed out that the pseudogap regime can be naturally understood not by doping AF insulator, but by doping a featureless Mott-insulator, i.e., spin liquid. Strikingly, he pointed this out even before the experimental identification of the pseudogap. This is the origin of motivation for studying spin liquids from High-Tc point of view.

There have been intensive studies on understanding High-Tc superconductivity by doping a spin liquid. Instead of giving a review of previous study, here I just raise the issue that I will address in chapter 4. The important physics of doping a spin liquid is so-called spin-charge separation. After one hole is put into the spin liquid, there will be an extra charge e and spin-1/2 in the system. The charge e will be at the position of the empty site. However, because the spin degrees of freedom are not frozen but strongly fluctuating, the extra spin-1/2 will be distributed in the whole system in a certain fashion, meaning the spin-1/2 may not be bound to the charge e locally. In this picture the spin and charge degrees of freedom are not bound together and the low energy description of the system includes a charge sector and a spin sector and their interations. Let us call the charge degree of freedom holon, and the spin degree of freedom spinon.

But when we do experiments like ARPES on the system, really the electronic degrees of freedom are probed. One can imagine the electron as a bound state of the spinon and holon. An interesting and puzzling experimental fact is that, in the pseudogap regime, the APRES peak is quite coherent around the nodal region ($(\pm\pi/2, \pm\pi/2)$), but not around the antinodal region ($(\pi, 0)$ and $(0, \pi)$). In the spin-charge separation picture, it means the binding of spinon and holon are very strong at the nodal region, but not at the anti-nodal region. It is not obvious at all how the momentum space anisotropy of binding happens. In this thesis, we will show there is a simple mean-field theory and wavefunction where the origin of this anisotropy is manifest.

1.4 Low energy excitations

We stated that one fundamental difference between the exotic phases and the conventional phases is that exotic phases are not characterized by symmetry breaking. Another fundamental difference will be discussed in this section, which is the low energy excitations.

What are the low energy excitations of the conventional phases? By conventional phase we mean it is either a fermi liquid, or a symmetry breaking phase with an order parameter. For fermi liquids, the low energy excitations turn out to be free fermions. For symmetry breaking phase, the low energy excitations are the flucutations of the order parameter, which are usually free boson modes. In particular, for all *gapless* conventional phases, one can ask what the gapless modes can be. As a property of stable phases, the gapless modes should be stable against all kinds of perturbations that are consistent with the symmetry. The only such stable gapless modes are free fermion modes, which are protected by fermi liquid theory, or free Goldstone bosons, which are protected by Goldstone theorem.

Because the exotic phases have no symmetry breaking and order parameter, there are no Goldstone modes and fluctuating order parameters. What can the low energy excitations be? With the past studies of spin liquids, we know that the low energy excitations are often neither free bosons nor free fermions, and gauge interactions are usually involved in the low energy effective theory. These are fundamentally different from conventional matter. Moreover, we know that spin liquid can have gapless excitations. Those gapless modes are not protected by fermi liquid theory or Goldstone theorem. We will see in chapter 2 that they are actually protected by quantum order.

In addition, fractionalization often appears in conventional phases. Suppose we start with a microscopic model in which the fundamental degrees of freedom carry a certain set of quantum numbers. For example in the Hubbard model the fundamental degrees of freedom are electrons, which carry charge e and spin-1/2. Fractionalization does not really mean that one can literally tear apart the fundamental degrees of freedom, e.g., all the measurable quantities in Hubbard model are written in terms of electron operator. Instead fractionalization means that in the most natural way to write down the low energy effective theory, collective modes carry fraction of the fundamental quantum numbers, e.g., the spinon and holon modes in the Hubbard model. Here by "most natural way", I mean the effective theory is in a weakly interacting regime, i.e., the properties of the interacting theory are not fundamentally different from the free theory.

A stable phase can also be viewed as a stable fixed point in the renormalization group (RG) sense. The conventional stable phases corresponds to the free (gaussian) fixed points of the modes carrying the microscopic quantum numbers. On the contrary, some exotic phases, for instance the π-flux phase and U(1)-Dirac phase which will be discussed in chapter 2 and 3, corresponds to interacting fixed points, and the modes are carrying fractionalized quantum number. There are also cases, for example the Z_2-linear spin liquid discussed in chapter 2, in which the effective theory is a free fixed point of the fractionalized modes.

1.5 Conventional phase transitions and exotic phase transitions

Let us briefly review the conventional phase transitions of Landau-Ginzburg-Wilson paradigm. In Fig.1-2 we show a schematic phase diagram with one tuning parameter K. G_1 G_3 and G_2 are the symmetry group of the two phases and the transition point respectively. According to Landau's phase transition, the phase transition at K_c can be characterized by a symmetry breaking from a disordered phase to an ordered phase. If G_1 labels the disordered phase, that means G_3 must be a subgroup of G_1. Usually G_2, the symmetry group at the transition point, equals G_1. The low energy effective theory of this phase transition is the flucutation of order parameter which carries G_1 charge but not G_3 charge. The condensation of the order parameter signals the phase transition.

For an exotic phase, one cannot characterize it simply by a symmetry group. The

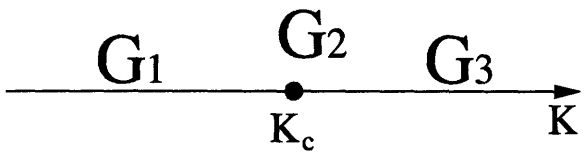

Figure 1-2: Symmetry groups and phase transition.

phase transitions between two spin liquids, if viewed in terms of symmetry group, would have $G_1 = G_2 = G_3$. Then how to understand their phase transition? We introduced the concept of quantum order to characterize different exotic phases. In chapter 2 we study in detail the mathematical language of quantum order, and the possible senarios of phase transitions between spin liquids. In addition, we also study another phase transition between spin liquids where G_3 is indeed a subgroup of G_1, i.e., a physical symmetry is broken. But due to the fact that the phase G_1 is exotic, i.e., the low energy excitations are not fluctuating order parameters, even the symmetry breaking phase transition is beyond Landau's theory.

An application of the exotic phase transitions is to detect an exotic phase experimentally. If a phase breaks a physical symmetry, then in general it will provide a finite temperature phase transition to the disordered phase. There are very sharp experimental signatures of that phase transition and one can thus detect a conventional phase. On the other hand, because exotic phases can be fully symmetric, it may not support any finite temperature phase transition. Therefore detecting them is an experimental challenge. If we understand the zero temperature phase transitions from an exotic phase to another exotic phase, or to a conventional phase, we can use the experimental signatures of those transitions to actually detect an exotic phase.

I also want to mention another type of exotic phase transitions not studied in this thesis. Senthil et.al.[12] found that if a gapless spin liquid turns out to be a unstable fixed point, it can actually connect two phases with uncompatible symmetries, i.e., G_3 is not a subgroup of G_1 and vice versa, through a single continuous phase transition.

1.6 Outline of the thesis

In this thesis, we discuss a large-N model in chapter 2 where the spin liquid states can be stable zero-temperature phases and study the phase transitions between spin liquid phases. In chapter 3 we study a more realistic model: spin-1/2 Kagome lattice and propose the U(1)-Dirac state as the ground state. Because the close relation between spin liquids and High-Tc superconductor, we study the doped spin liquids

in Chaper 4 and focus on one experimenal phenomenon: nodal-antinodal dichotomy. Finally concluding remarks are given in Chapter 5. Most of the material in this thesis has been adapted from published papers. Chapter 2 is adapted from Ref.[13], chapter 3 is adapted from Ref.[14] and chapter 4 is adapted from Ref.[15].

Chapter 2

A large-N model

2.1 Introduction

The $SU(2)$ projective construction (or, more generally, slave-boson theory [16, 17]) for 2D spin liquids in spin-1/2 systems has been studied over ten years [18, 19]. Upon doping, the $SU(2)$ projective construction provides a quite complete theory for underdoped high T_c superconductors [20, 21]. The theory explains the strange Fermi surfaces [20, 21], the strong (π, π) spin fluctuations [22, 23], and the temperature dependence of superfluid density [24, 25] for underdoped samples.

At half filling, the $SU(2)$ projective construction can also be used to describe various spin liquids. In fact, the $SU(2)$ projective construction (or more generally, the slave boson theory) have predict many different spin liquids, such as the algebraic spin liquid [26, 27, 23], chiral spin liquid [28, 29], Z_2 spin liquids [30, 31, 32, 33]. It was also shown that the $SU(2)$ projective construction is capable of describing hundreds of different spin liquids that have the same symmetry but different quantum orders [27].

The above predictions of spin liquids and the classification of spin liquids were based on mean-field calculations. At the mean-field level, it is not very hard to design a spin Hamiltonian that realizes a spin liquid that has one of a few hundreds quantum orders. It is also not hard to find the mean-field ground state for a given spin Hamiltonian. The real issue is whether we should trust the mean-field results. It was argued [31, 27] that, if the obtained mean-field ground state is unstable (i.e. if the mean-field fluctuations cause diverging interactions at low energies), then the mean-field result cannot be trusted and the mean-field state does not correspond to any real physical spin state. It was also argued that, if the mean-field ground state is stable (if the mean-field fluctuations cause vanishing interactions at low energies),

then the mean-field result can be trusted and the mean-field state does correspond to a real physical spin liquid state.

However, the above statement about stable mean-field states is too optimistic. A 'stable mean-field state' does not have diverging fluctuations at low energies. So it does not have to be unstable. On the other hand, it does not have to be stable either. This is because short-distance fluctuations, if strong enough, can also cause phase transitions and instabilities. Therefore, in order for a mean-field result to be reliable, the mean-field state must be stable (*i.e.* no infrared divergence) *and* the short-distance fluctuations must be weak. As we do not have any small parameters in the $SU(2)$ slave-boson theory for spin-1/2 systems, the short-distance fluctuations are not weak, even for stable mean-field states. Because of this, it is not clear if the mean-field results, even for the stable states, can be applied to the spin-1/2 model or not.

In this chapter, we will generalize the spin-1/2 model to a large-N model. The large-N model can be solved approximately using the $SU(2)$ projective construction. We will show that the $SU(2)$ projective construction for the large-N model have weak short-distance fluctuations. Thus, the stable $SU(2)$ mean-field states for the large-N model do correspond to real physical spin liquid states. The $SU(2)$ mean-field results for the stable states, such as fractionalization, emergent gauge structures and emergent Fermi statistics, can be applied to the large-N model.

We concentrate on a model with nearest-neighbor J_1 coupling and next-nearest-neighbor J_2 coupling. We find several mean-field phases that include $SU(2)$ π-flux state, $SU(2)$ chiral spin state and Z_2 spin liquid state.

The $SU(2)$ π-flux state is described by a low energy effective theory that includes gapless Dirac fermions coupled to $SU(2)$ gauge fields. Due to the non-vanishing interaction between the fermions and the gauge bosons down to zero energy, there is no free fermioninc or bosonic low energy quasiparticles in the $SU(2)$ π-flux state. Despite this, we show that the $SU(2)$ π-flux state is a stable spin liquid state. It is a realization of algebraic spin liquids. [27, 23]

The $SU(2)$ chiral spin state and Z_2 spin liquid state are both gapped and, thus, naturally stable. Both state carry non-trivial topological orders.

Within our J_1-J_2 model, the quantum transition (i.e. the zero-temperature transition) between the $SU(2)$ π-flux state and the $SU(2)$ chiral spin state turns out to be a continuous transition. The transition breaks the time-reversal symmetry and has a well defined Z_2 order parameter. However, we show that the critical properties of the transition are not described by the 3D Ising universality class of the Ginzburg-

Landau theory. This is because the transition not only break the Z_2 symmetry, it also changes the quantum/topological order. The continuous quantum transition between the $SU(2)$ π-flux state and the $SU(2)$ chiral spin state is a new class of quantum transition.

It has been shown that continuous quantum transitions are possible between two states with the same symmetry (but different topological orders). [34, 35, 36, 37, 38] The continuous quantum transitions are also possible between two states with the *incompatible*[1] symmetries. In this chapter, we show that even symmetry-breaking transitions with well defined order parameters, sometimes are not described by Landau's symmetry breaking theory. So it appear that most quantum continuous transitions are not described by Ginzburg-Landau theory, regardless if they have symmetry breaking and order parameter or not.

We also study the transitions from the $SU(2)$ π-flux state to a Z_2-linear spin liquid state, and from the $SU(2)$ π-flux state to a $U(1)$-linear spin liquid state. The transtion between the $SU(2)$ π-flux state to the Z_2-linear state is found to be a continuous quantum transition that does not break any symmetry. The transtion between the $SU(2)$ π-flux state to the $U(1)$-linear state, on the other hand, is a continuous quantum transition that breaks lattice rotaion and translation symmetry. What is surprising is that the two seemingly very different transitions are described by the same critical point with the same set of critical exponents.

2.2 Formulation of $SU(2)$ projective construction

First we would like to briefly review the $SU(2)$ projective construction. We will mainly follow the notation of Ref. [27, 39]. Let us start with spin-1/2 Heisenberg Model, and introduce the fermion representation of spins:

$$H = \sum_{\langle ij \rangle} J_{ij}\, \mathbf{S}_i \cdot \mathbf{S}_j \tag{2.1}$$

$$\mathbf{S}_i = \frac{1}{2} f^\dagger_{i\alpha} \boldsymbol{\sigma}_{\alpha\beta} f_{i\beta} \tag{2.2}$$

If we regard H as an operator acting on the fermion Hilbert space, then we have enlarged the Hilbert space. Therefore we have to add extra constraints to reduce the

[1] If the symmetry group of one phase is not a subgroup of the other phase and vice versa, then the two phases are said to have incompatible symmetries[12]. According to Landau's symmetry breaking theory, two phases with incompatible symmetries cannot have continuous phase transition between them.

enlarged Hilbert space to the original one for the spin system. The constraints are the one-particle per site constraints:

$$f_{i\alpha}^{\dagger} f_{i\alpha} = 1 \tag{2.3}$$

$$\Rightarrow f_{i\alpha} f_{i\beta} \epsilon_{\alpha\beta} = 0, \quad f_{i\alpha}^{\dagger} f_{i\beta}^{\dagger} \epsilon_{\alpha\beta} = 0 \tag{2.4}$$

The two extra constraints in Eq. (2.4) are results of the first one in Eq. (2.3). However in path integral formalism, if we enforce all constraints simultaneously by introducing some Lagrangian multipliers, a lattice gauge theory with $SU(2)$ gauge group can be derived. Let us introduce some notations:

$$\hat{\eta}_{ij}^{\dagger} = f_{i\alpha}^{\dagger} \epsilon_{\alpha\beta} f_{j\beta}^{\dagger} \tag{2.5}$$

$$\hat{\chi}_{ij} = f_{i\alpha}^{\dagger} \delta_{\alpha\beta} f_{j\beta}. \tag{2.6}$$

These are the only singlet bilinear forms of the pairing between site i and j. After some rearrangements, one has:

$$\mathbf{S_i} \cdot \mathbf{S_j} = -\frac{1}{4} \hat{\eta}_{ij}^{\dagger} \hat{\eta}_{ij} - \frac{1}{4} \hat{\chi}_{ij}^{\dagger} \hat{\chi}_{ij} + \frac{1}{4}.$$

Ignoring the irrelevant constant, the path integral Lagrangian of the Heisenberg model Eq. (2.1) turn out to be:

$$\begin{aligned} L' = & \sum_{i} f_{i\alpha}^{\dagger} i \partial_t f_{i\alpha} \\ & - \sum_{i} \left(\frac{1}{2} a_{0,i}^{-} \hat{\eta}_{ii}^{\dagger} + \frac{1}{2} a_{0,i}^{+} \hat{\eta}_{ii} + \frac{1}{2} a_{0,i}^{3} (\hat{\chi}_{ii}^{\dagger} - 1) \right) \\ & + \frac{1}{4} \sum_{\langle ij \rangle} J_{ij} \left(\hat{\eta}_{ij}^{\dagger} \hat{\eta}_{ij} + \hat{\chi}_{ij}^{\dagger} \hat{\chi}_{ij} \right) \end{aligned}$$

The constraint of one particle per site has been encoded by the Lagrangian multipliers in the second line:

$$\begin{pmatrix} a_{0,i}^{-} \\ a_{0,i}^{+} \\ a_{0,i}^{3} \end{pmatrix} = \begin{pmatrix} \frac{1}{2}(a_{0,i}^{1} - i a_{0,i}^{2}) \\ \frac{1}{2}(a_{0,i}^{1} + i a_{0,i}^{2}) \\ a_{0,i}^{3} \end{pmatrix}$$

If we do a particle-hole transformation of the spin-down fermions $f_{i\downarrow}$ together with a Hubbard-Stratonovich transformation, the Lagrangian can be written in a form with

the explicit $SU(2)$ gauge invariance:

$$L = \sum_i \left[\psi_i^\dagger (i\partial_t - a_{0,i}^l \tau^l)\psi_i\right] - \sum_{\langle ij\rangle} \frac{1}{4} J_{ij} \left[\frac{1}{2}\mathrm{Tr} U_{ij} U_{ij}^\dagger + \left(\psi_i^\dagger U_{ij} \psi_j + h.c.\right)\right] \tag{2.7}$$

where

$$\psi_i = \begin{pmatrix} f_{i\uparrow} \\ f_{i\downarrow}^\dagger \end{pmatrix} \tag{2.8}$$

$$U_{ij} = \begin{pmatrix} \chi_{ij} & \eta_{ij} \\ \eta_{ij}^* & -\chi_{ij}^*. \end{pmatrix} \tag{2.9}$$

The path integral that describes the spin-1/2 system is given by

$$Z = \int D(\psi) D(a_{0,i}^l) D(U_{ij}) e^{i\int dt\, L}$$

The $SU(2)$ gauge transformation is given by

$$\begin{aligned} \psi_i &\to \psi_i' = W_i \psi_i, \\ a_{0,i}^l \tau^l &\to a_{0,i}'^l = W_i a_{0,i}^l \tau^l W_i^\dagger + (i\partial_t W_i) W_i^\dagger \\ U_{ij} &\to W_{ij}' = W_i U_{ij} W_j^\dagger \end{aligned}$$

where all $W_i \in SU(2)$.

There are some other useful relations. For each site, the conjugate of fundamental representation of $SU(2)$ is equivalent to the fundamental representation itself. One therefore can introduce another $SU(2)$ doublet (neglecting the site label):

$$\widehat{\psi} = i\sigma_2 \psi^* = \begin{pmatrix} f_\downarrow \\ -f_\uparrow^\dagger \end{pmatrix} \tag{2.10}$$

Thus there are only three $SU(2)$ gauge invariant bilinear forms for ψ fields on the same site

$$S^+ = \frac{1}{2}\psi_\alpha^\dagger \widehat{\psi}_\alpha = f_\uparrow^\dagger f_\downarrow \tag{2.11}$$

$$S^- = \frac{1}{2}\widehat{\psi}_\alpha^\dagger \psi_\alpha = f_\downarrow^\dagger f_\uparrow \tag{2.12}$$

$$S^3 = \frac{1}{2}\left(\psi_\alpha^\dagger \psi_\alpha - 1\right) = \frac{1}{2}\left(1 - \widehat{\psi}_\alpha^\dagger \widehat{\psi}_\alpha\right) = \frac{1}{2}\left(f_\uparrow^\dagger f_\uparrow - f_\downarrow^\dagger f_\downarrow\right) \tag{2.13}$$

They turned out to be the generators of the spin rotation symmetry.

In the zeroth order approximation, or at the mean-field level, one assumes that the boson fields $a^l_{0,i}$ and U_{ij} get condensed, or more specifically, can be replaced by some time-independent c-numbers. In this approximation, the system is described by the following mean-field Hamiltonian

$$H_{mean} = \sum_i \psi^\dagger_i a^l_{0,i} \tau^l \psi_i + \sum_{\langle ij \rangle} \frac{1}{4} J_{ij} \left[\frac{1}{2} \mathrm{Tr} U_{ij} U^\dagger_{ij} + \left(\psi^\dagger_i U_{ij} \psi_j + h.c. \right) \right] \tag{2.14}$$

2.3 A large-N limit of $SU(2)$ projective construction

The above mean-field approximation is a good one only when there are some reasons to suppress the fluctuations of the boson fields $a^l_{0,i}$ and U_{ij}. One way to suppress these fluctuations is to go to a large-N limit. Actually the mean-field result is exact when $N = \infty$. In this section, we try to answer the following questions:

- What is the lattice spin model that the large-N limit corresponds to?
- What is ground state of this lattice spin model?

Here we present our answers of these problems first. Later we will see the detailed derivation of these answers:

- The lattice spin model is a $Sp(2N)$ spin model described by Eq. 2.18. The $Sp(2N)$ spin model is a generalization of the usual $SU(2)$ spin model (which corresponds to $N = 1$ case).
- The ground states of the model are $Sp(2N)$ singlets. For small J_2 (the next-nearest-neighbor coupling), The system is in an algebraic spin liquid state.[27, 23] The excitations are the fractionalized particles (spinons) coupled to $SU(2)$ gauge fields. The gauge field is deconfined. For larger $J2/J1$, there is a continuous quantum phase transition and the system goes into the chiral spin state which breaks the time reversal symmetry.[29]

It was debated for long time the existence of featureless Mott insulator if the unit cell does not have even number of electrons. In that case, it seems that in order to have a Mott insulator state, the ground state must break translation symmetry to enlarge the unit cell such that the number of electrons per unit cell becomes even.

Here we present a counter-example. The ground state of $Sp(2N)$ when N is large can be featureless Mott insulator with odd numbers of electrons per unit cell.

We want to introduce a large-N limit and maintain the $SU(2)$ gauge structure. The simplest way to do this is to introduce N flavors of fermions (later in this chapter we also denote N as N_f to emphasize it represents the number of flavors of fermions):

$$\psi_i^a = \begin{pmatrix} f_{i\uparrow}^a \\ f_{i\downarrow}^{a\dagger} \end{pmatrix}, \quad a = 1, 2, \cdots N.$$

Then the Lagrangian of the N-flavor model is:

$$L = \sum_i \psi_i^{\dagger a}(i\partial_t - a_{0,i}^l \tau^l)\psi_i^a + \sum_{\langle ij \rangle} \frac{1}{4} J_{ij} \left[\frac{N}{2} \mathrm{Tr} U_{ij} U_{ij}^\dagger + (\psi_i^{\dagger a} U_{ij} \psi_j^a + h.c.) \right]$$

where the repeated index a is summed. The large-N model is clearly invariant under the $SU(2)$ gauge transformation. Comparing with the original model Eq. (2.7), after integrating out the fermions, the effect of the N-flavor is to put a factor of N in front of the boson fields Lagrangian, which controls the fluctuation of them when N is large.

Now we want to find out the corresponding spin model for this large-N theory. It should be some generalization of the spin-1/2 Heisenberg model. To do so, we need to integrate out the boson fields. If we go back to the f picture, we have:

$$\begin{aligned} L = & \sum_i f_{i\alpha}^{\dagger a} i\partial_t f_{i\alpha}^a - \sum_i \left[\frac{1}{2} a_{0,i}^- \hat{\eta}_{ii}^{aa\dagger} + \frac{1}{2} a_{0,i}^+ \hat{\eta}_{ii}^{aa} + \frac{1}{2} a_{0,i}^3 (\hat{\chi}_{ii}^{aa\dagger} - N) \right] \\ & + \sum_{\langle ij \rangle} \frac{J_{ij}}{4N} \left(\hat{\eta}_{ij}^{aa\dagger} \hat{\eta}_{ij}^{bb} + \hat{\chi}_{ij}^{aa\dagger} \hat{\chi}_{ij}^{bb} \right), \end{aligned}$$

where

$$\begin{aligned} \hat{\eta}_{ij}^{ab\dagger} &= f_{i\alpha}^{\dagger a} \epsilon_{\alpha\beta} f_{j\beta}^{b\dagger} = \psi_{i1}^{\dagger a} \psi_{j2}^b - \psi_{i2}^a \psi_{j1}^{b\dagger} \\ \hat{\chi}_{ij}^{ab\dagger} &= f_{i\alpha}^{\dagger a} \delta_{\alpha\beta} f_{j\beta}^{b\dagger} = \psi_{i1}^{\dagger a} \psi_{j1}^b + \psi_{i2}^a \psi_{j2}^{b\dagger} \end{aligned}$$

Here one immediately see the constraints become $\chi_{ii}^{aa} = N$ and $\eta_{ii}^{aa} = 0$, or

$$f_{i\alpha}^{a\dagger} f_{i\alpha}^a = N \qquad\qquad f_{i\alpha}^{a\dagger} \epsilon_{\alpha\beta} f_{i\beta}^{a\dagger} = h.c. = 0 \tag{2.15}$$

for each site. The Hamiltonian under these constraints are:

$$H = -\sum_{\langle ij \rangle} \frac{J_{ij}}{4N} \left(\hat{\eta}_{ij}^{aa\dagger} \hat{\eta}_{ij}^{bb} + \hat{\chi}_{ij}^{aa\dagger} \hat{\chi}_{ij}^{bb} \right) \tag{2.16}$$

$$= \sum_{\langle ij \rangle} -\frac{J_{ij}}{4N} \left(-f_{i\alpha}^{a\dagger} f_{i\beta}^{b} f_{j\beta}^{a\dagger} f_{j\alpha}^{b} - f_{i\alpha}^{a\dagger} f_{i\beta}^{b} f_{j\beta}^{b\dagger} f_{j\alpha}^{a} + f_{i\alpha}^{a\dagger} f_{i\alpha}^{b} f_{j\beta}^{a\dagger} f_{j\beta}^{b} + N \right) \tag{2.17}$$

We want to understand the symmetry of this model and try to rewrite it in a form of spin coupling. Here, the symmetry that we are studying is not the local gauge invariance, but some global physical symmetry in analogy with the spin rotation symmetry for the $N = 1$ model. Motivated by Eq. (2.11-2.13), we construct all the gauge invariant bilinear forms of ψ for each site (neglecting the site label). Let

$$\widehat{\psi}^{a} \equiv i\sigma_2 \psi^{\dagger a} = \begin{pmatrix} f_{\downarrow}^{a} \\ -f_{\uparrow}^{a\dagger} \end{pmatrix}$$

The $SU(2)$ gauge invariant bilinears are

$$S^{ab+} \equiv \frac{1}{2} \psi_{\alpha}^{a\dagger} \widehat{\psi}_{\alpha}^{b} = \frac{1}{2} \left(f_{\uparrow}^{a\dagger} f_{\downarrow}^{b} + f_{\uparrow}^{b\dagger} f_{\downarrow}^{a} \right)$$

$$S^{ab-} \equiv \frac{1}{2} \widehat{\psi}_{\alpha}^{a\dagger} \psi_{\alpha}^{b} = \frac{1}{2} \left(f_{\downarrow}^{a\dagger} f_{\uparrow}^{b} + f_{\downarrow}^{b\dagger} f_{\uparrow}^{a} \right)$$

$$S^{ab3} \equiv \frac{1}{2} \left(\psi_{\alpha}^{a\dagger} \psi_{\alpha}^{b} - \delta^{ab} \right) = \frac{1}{2} \left(\delta^{ab} - \widehat{\psi}_{\alpha}^{b\dagger} \widehat{\psi}_{\alpha}^{a} \right) = \frac{1}{2} \left(f_{\uparrow}^{a\dagger} f_{\uparrow}^{b} - f_{\downarrow}^{b\dagger} f_{\downarrow}^{a} \right)$$

What is the group generated by these S operators? First let us count how many of them there are. For S^{ab+} or S^{ab-}, the label is symmetric for a and b, so there are $\frac{N(N+1)}{2}$ operators of each type. For S^{ab3}, the labels are not symmetric, so there are simply N^2 of them. Totally we have $N(N+1) + N^2 = 2N^2 + N$ of them. One can further examine their commutation relations:

$$\left[S^{ab-},\ S^{cd-} \right] = 0, \quad \left[S^{ab+},\ S^{cd+} \right] = 0$$

$$\left[S^{ab3},\ S^{cd3} \right] = \frac{1}{2} \left(\delta^{bc} S^{ad3} - \delta^{ad} S^{cb3} \right)$$

$$\left[S^{ab3},\ S^{cd+} \right] = \frac{1}{2} \left(\delta^{bc} S^{ad+} + \delta^{bd} S^{ac+} \right)$$

$$\left[S^{ab3},\ S^{cd-} \right] = -\frac{1}{2} \left(\delta^{ad} S^{bc-} + \delta^{ac} S^{bd-} \right)$$

$$\left[S^{ab+},\ S^{cd-} \right] = \frac{1}{2} \left(\delta^{ac} S^{bd3} + \delta^{ad} S^{bc3} + \delta^{bc} S^{ad3} + \delta^{bd} S^{ac3} \right)$$

These are the relations for $SP(2N)$ algebra, so all the S operators are the $2N^2+N$ generators which generate an $SP(2N)$ group. When $N=1$, $SP(2)$ is isomorphic to $SO(3)$. After some rearrangements, the Hamiltonian Eq. (2.17) can be rewritten as:

$$H=\sum_{\langle ij\rangle}\frac{J_{ij}}{N}\left[\frac{1}{2}S_i^{ab+}S_j^{ab-}+\frac{1}{2}S_i^{ab-}S_j^{ab+}+S_i^{ab3}S_j^{ba3}\right] \tag{2.18}$$

If we define:

$$\begin{aligned}S_i^{ab1}&=S_i^{ba1}=\frac{1}{2}\left(S_i^{ab+}+S_i^{ab-}\right)\\ S_i^{ab2}&=S_i^{ba2}=\frac{1}{2i}\left(S_i^{ab+}-S_i^{ab-}\right),\end{aligned}$$

then the vector

$$\boldsymbol{S}_i^{ab}=\left(S_i^{ab1},S_i^{ab2},S_i^{ab3}\right)$$

can simplify the Hamiltonian to:

$$H_{Sp(2N)}=\sum_{\langle ij\rangle}\frac{J_{ij}}{N}\,\mathbf{S}_i^{ab}\cdot\mathbf{S}_j^{ba} \tag{2.19}$$

Here we have to mention that the three components of $\boldsymbol{S}_i^{ab}$ are actually not on the same footing, since the first two are symmetric with respect to the flavor labels but the third one is not. It is a simple task to check that all the generators commute with the Hamiltonian. And one can even check that the $SP(2N)$ is indeed the full symmetry group of it.

Now we want to know what the physical Hilbert space is. It should be the subspace of the enlarged Hilbert space in which the constraints Eq. (2.15) are satisfied. When $N=1$, the physical Hilbert space is the spin-1/2 Heisenberg's, where we have only two states on each site:

$$|\uparrow\rangle,\quad |\downarrow\rangle$$

When $N=2$, we have 5 states on each site:

$$|1_\uparrow 2_\uparrow\rangle,\quad |1_\uparrow 2_\downarrow\rangle,\quad |1_\downarrow 2_\uparrow\rangle,\quad |1_\downarrow 2_\downarrow\rangle,\quad \frac{1}{\sqrt{2}}\left(|1_{\uparrow\downarrow}2_0\rangle-|1_0 2_{\uparrow\downarrow}\rangle\right)$$

Here, for example, $|1_\uparrow 2_\downarrow\rangle$ represents a fermion of flavor 1 and spin up and another fermion of flavor 2 and spin down; and $|1_{\uparrow\downarrow} 2_0\rangle$ represents a fermion of flavor 1 and spin up, another fermion of flavor 1 and spin down, and no fermion of flavor 2. One can check the dimension of the Hilbert space on each site for larger N's:

$$\begin{aligned} &\text{N=3} \quad \text{dimension} = 14, \\ &\text{N=4} \quad \text{dimension} = 43, \\ &\text{N=5} \quad \text{dimension} = 142, \\ &\text{N=6} \quad \text{dimension} = 429, \cdots \end{aligned}$$

This Hilbert space turns out to be an irreducible representation of the $SP(2N)$ symmetry group. If we label an irreducible representation by its highest weight state for a particular Cartan basis. The Cartan basis for $SP(2N)$ can be chosen to be the z-component spins of each flavor:

$$S^{aa3}, \text{ where } a = 1, 2, \cdots, N,$$

with N generators. Then the highest weight state in our Hilbert space is simply:

$$|1_\uparrow 2_\uparrow 3_\uparrow \ldots N_\uparrow\rangle$$

2.4 Phase diagram of the $Sp(2N)$ model on 2D square lattice

In this section we would like to calculate the zero temperature phase diagram for the $Sp(2N)$ model Eq. (2.19) on 2D square lattice. We assume that only the nearest-neighbor couplings and the next-nearest-neighbor couplings are non-zero

$$\begin{aligned} J_{i,i+\boldsymbol{x}} = J_{i,i+\boldsymbol{y}} = J_1, \\ J_{i,i+\boldsymbol{x}+\boldsymbol{y}} = J_{i,i+\boldsymbol{x}-\boldsymbol{y}} = J_2. \end{aligned}$$

We also assume $J_1 + J_2 = 1$.

There are two mean-field approaches to the $Sp(2N)$ model. In the first mean-field

approach, we use the ground state $|\Phi^{(m_i^{ab})}\rangle$ of a trial Hamiltonian

$$H_{trial} = \sum_{ij} \frac{J_{ij}}{N} \mathbf{m}_i^{ab} \cdot \mathbf{S}_j^{ba} \tag{2.20}$$

as the trivial wave function and obtain the mean-field ground state of the $Sp(2N)$ model Eq. (2.19) by minimizing

$$\langle \Phi^{(m_i^{ab})} | H_{Sp(2N)} | \Phi^{(m_i^{ab})} \rangle$$

as we vary the variational parameters m_i^{ab}. The obtained ground state corresponds to a $Sp(2N)$ spin polarized state. One can show that the ground state energy obtained in this mean-field approach is always of order 1 per site in the large N limit.

In the second mean-field approach (the projective construction),[16, 39] we start with a fermion trial Hamiltonian

$$H_{trial} = \sum_{\langle ij \rangle} \psi_i^{a\dagger} u_{ij} \psi_j^a \tag{2.21}$$

where $u_{ij} = u_{ij}^{\mu} \tau^{\mu}$ are two by two complex matrices that satisfy

$$u_{ij}^{\dagger} = u_{ji}, \qquad u_{ij}^0 = \text{imaginary}, \qquad u_{ij}^l|_{l=1,2,3} = \text{real}$$

Let $|\Phi_{mean}^{(u_{ij})}\rangle$ be the ground state of the above trial Hamiltonian. $u_{ii}^l \equiv a_{0,i}^l$ are chosen such that the constraints $\psi_i^{a\dagger} \tau^l \psi_i^b = 0$ are satisfied on average:

$$\langle \Phi_{mean}^{(u_{ij})} | \psi_i^{a\dagger} \tau^l \psi_i^b | \Phi_{mean}^{(u_{ij})} \rangle = 0$$

We then project $|\Phi_{mean}^{(u_{ij})}\rangle$ to the physical Hilbert space and obtain $P|\Phi_{mean}^{(u_{ij})}\rangle$. The physical Hilbert space is formed by states $|phys\rangle$ that satisfy the constraints Eq. (2.15) or

$$\psi_i^{a\dagger} \tau^l \psi_i^b |phys\rangle = 0$$

The projected wave function $P|\Phi_{mean}^{(u_{ij})}\rangle$ is our trial wave function with u_{ij} as variational parameters. Minimzing

$$\langle \Phi_{mean}^{(u_{ij})} | P H_{Sp(2N)} P | \Phi_{mean}^{(u_{ij})} \rangle$$

by varying u_{ij}, we obtain the approximated ground state.

Since in the large-N limit, the fluctuations of the Lagrangian multiplier $a_{0,i}^l(t)$ are weak, we expect that removing the projection P only causes an error of order $1/N$.

Also, other mean-field fluctuations are weak in the large-N limit, so we expect that the minimized mean-field energy

$$\begin{aligned} E &= \langle \Phi_{mean}^{(u_{ij})} | H_{Sp(2N)} | \Phi_{mean}^{(u_{ij})} \rangle \\ &= -\sum_{\langle ij \rangle} \frac{J_{ij}}{4N} \left(\eta_{ij}^{aa\dagger} \eta_{ij}^{bb} + \chi_{ij}^{aa\dagger} \chi_{ij}^{bb} \right) + O(1) \end{aligned}$$

to be the true ground state energy at the leading order in the large-N expansion. Here

$$\chi_{ij}^{ab} = \langle \Phi_{mean}^{(u_{ij})} | \hat{\chi}_{ij}^{ab} | \Phi_{mean}^{(u_{ij})} \rangle, \qquad \eta_{ij}^{ab} = \langle \Phi_{mean}^{(u_{ij})} | \hat{\eta}_{ij}^{ab} | \Phi_{mean}^{(u_{ij})} \rangle$$

note that the above minimized energy is of order $-N$ per site. Thus the states obtained in the first mean-field approximation Eq. 2.20 cannot be the ground state.

Within the $SU(2)$ projective construction and using the translation invariant ansatz u_{ij} with only nearest- and next-nearest-neighbor couplings, we find many local minima of $-\sum_{\langle ij \rangle} (\eta_{ij}^{aa\dagger} \eta_{ij}^{bb} + \chi_{ij}^{aa\dagger} \chi_{ij}^{bb})$ as we vary u_{ij}. We plot those minima in Fig. 2-1 as functions of J_2 (note $J_1 + J_2 = 1$).

As we change J_2, the energy of the state changes smoothly along each curve. So there is no quantum phase transition as we move from one point of a curve to another point on the same curve. The ansatzs on the same curve belong to the same phase. However, if two curves cross each other, the crossing point represents a quantum phase transition. This is because the ground state energy is not analytic at the crossing point. If the slopes of the curves at the crossing point are different, the quantum phase transition is first order. If the slopes at the crossing point are the same, the quantum phase transition is second order.

From Fig. 2-1, we see second-order (or continuous) phase transitions (at mean-field level) between the following pairs of phases: (A,D), (A,G), (B,G), (C,E), and (B,H). We used to believe that all the second-order phase transitions are caused by symmetry breaking. So a natural question is what symmetries are broken for the above five second-order phase transitions?

It turns out that, except phase (D) and phase (E), all other phases have the same symmetry. In other words, the projected ground state wave functions $P|\Phi_{mean}^{(u_{ij})}\rangle$ for the ansatz u_{ij} associated with those phases have identical symmetry. Thus the three continuous transitions (B,G), (B,H) and (A,G) do not change any symmetries. It was pointed out that those phases, despite having the same symmetry, contain different *quantum orders* [27]. The projective symmetry group (PSG), defined as the invariant group of the ansatz u_{ij}, is introduced to describe this new class of orders [27].

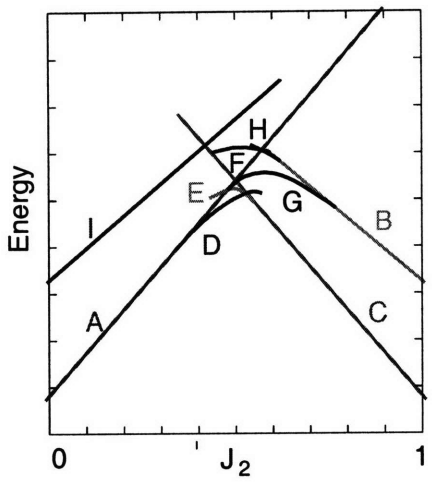

Figure 2-1: The mean-field energies for various phases in a J_1-J_2 spin system. (A) the π-flux state (the $SU(2)$-linear state SU2Bn0). (B) the $SU(2) \times SU(2)$-gapless state. (C) the $SU(2) \times SU(2)$-linear state. (D) the chiral spin state (an $SU(2)$-gapped state). (E) the $U(1)$-linear state Eq. (2.26) which breaks 90° rotation symmetry. (F) the $U(1)$-gapped state U1Cn00x. (G) the Z_2-linear state Z2Azz13. (H) the Z_2-linear state Z2A0013. (I) the uniform RVB state (the $SU(2)$-gapless state SU2An0).

The ansatzs on the same curve have the same PSG and correspond to the same quantum phase. On the other hand, the ansatzs on the different curves have different PSG's. We see that a quantum phase transition is characterized by a change in PSG. Those quantum phase transitions represent a new class of phase transitions beyond the Landau's symmetry breaking theory. Other examples of phase transitions beyond the Landau's theory can be found in Ref. [40, 34, 35, 36, 37, 38].

In the following we will discuss quantum orders (or PSG's) for mean-field phases in Fig. 2-1. The PSG's for those quantum orders are labeled by labels which look like Z2A0013 [27].

The phase (A) [41] is the π-flux state, or the SU2Bn0 state

$$u_{i,i+x} = i\chi, \qquad u_{i,i+y} = i(-)^{i_x}\chi \qquad a_0^l = 0. \tag{2.22}$$

The low energy excitations are described by massless Dirac fermions with a linear dispersion and gapless $SU(2)$ gauge fluctuations. Therefore we also call such a state $SU(2)$-linear state.

The phase (B) [27] is a state with two independent uniform RVB states [16] on the diagonal links. The gapless fermions have finite Fermi surfaces. The fermions interact with $SU(2) \times SU(2)$ gauge fluctuations. Such a state is called $SU(2) \times SU(2)$-gapless

state ($SU(2) \times SU(2)$ indicates the low energy gauge group and "gapless" indicates finite Fermi surface). Its ansatz is given by

$$u_{i,i+x+y} = \chi\tau^3, \qquad u_{i,i+x-y} = \chi\tau^3, \qquad a_0^l = 0. \tag{2.23}$$

The phase (C) [27] is a state with two independent π-flux states on the diagonal links. It has $SU(2) \times SU(2)$ gauge fluctuations at low energies and will be called an $SU(2) \times SU(2)$-linear state. Its ansatz is given by

$$u_{i,i+x+y} = \chi(\tau^3 + \tau^1) \qquad u_{i,i+x-y} = \chi(\tau^3 - \tau^1) \qquad a_0^l = 0 \tag{2.24}$$

The low energy excitations are $SU(2) \times SU(2)$ gauge fluctuations and massless Dirac fermions.

The phase (D) is the chiral spin state[29]

$$\begin{aligned} \chi_{i,i+x} &= i\chi_1, & \chi_{i,i+y} &= i\chi_1(-)^{i_x}, & a_0^l &= 0, \\ \chi_{i,i+x+y} &= -i\chi_2(-)^{i_x}, & \chi_{i,i+x-y} &= i\chi_2(-)^{i_x}. \end{aligned} \tag{2.25}$$

Both fermionic excitations and $SU(2)$ gauge excitations are gapped. The gap of the $SU(2)$ gauge excitations is due to an $SU(2)$ Chern-Simons term.

The phase (E) [27] is described by an ansatz

$$\begin{aligned} u_{i,i+x+y} &= \chi_1\tau^1 + \chi_2\tau^2 & u_{i,i+x-y} &= \chi_1\tau^1 - \chi_2\tau^2 \\ u_{i,i+y} &= \eta\tau^3 & a_0^l &= 0 \end{aligned} \tag{2.26}$$

which breaks the 90° rotation symmetry. It is a $U(1)$-linear state, i.e., the low lying excitations are massless $U(1)$ gauge fluctuations interacting with massless Dirac fermions.

The phase (F) [27] is described by the following U1Cn00x ansatz

$$\begin{aligned} u_{i,i+x} &= \eta\tau^1 & u_{i,i+y} &= \eta\tau^1 \\ u_{i,i+x+y} &= \chi\tau^3 & u_{i,i+x-y} &= \chi\tau^3 \\ a_0^3 &= \lambda, \qquad a^{1,2} = 0 \end{aligned} \tag{2.27}$$

The U1Cn00x state can be a $U(1)$-linear state where fermions are gapless with a linear dispersion relation (if a_0^3 is small) or a $U(1)$-gapped state where the fermions are gapped (if a_0^3 is large). The state for phase (F) turns out to be a $U(1)$-gapped

state. The only low energy excitations are massless $U(1)$ gauge bosons.

The phase (G) [27] is described by the Z2Azz13 ansatz

$$\begin{aligned} u_{i,i+x} &= \chi\tau^1 - \eta\tau^2, & u_{i,i+y} &= \chi\tau^1 + \eta\tau^2, \\ u_{i,i+x+y} &= -\gamma\tau^1, & u_{i,i-x+y} &= +\gamma\tau^1, \\ u_{i,i+2x} &= u_{i,i+2y} = 0, & a_0^{1,2,3} &= 0. \end{aligned} \tag{2.28}$$

The $SU(2)$ gauge structure is broken down to a Z_2 gauge structure. Hence there is no gapless gauge fluctuations. The only low energy excitations are massless Dirac fermions. Such a state is called Z_2-linear state.

The phase (H) [33] is described by the Z2A0013 ansatz

$$\begin{aligned} a_0^3 &\neq 0, \qquad a_0^{1,2} = 0, \\ u_{i,i+x} &= \chi\tau^3 + \eta\tau^1, & u_{i,i+y} &= \chi\tau^3 - \eta\tau^1, \\ u_{i,i+x+y} &= +\gamma\tau^3, & u_{i,i-x+y} &= +\gamma\tau^3. \end{aligned} \tag{2.29}$$

It is also a Z_2-linear state.

The phase (I) is the uniform RVB state [16], i.e., the $SU(2)$-gapless state SU2An0

$$u_{i,i+x} = i\chi, \qquad u_{i,i+y} = i\chi, \qquad a_0^l = 0. \tag{2.30}$$

It has gapless $SU(2)$ gauge fluctuations and gapless fermionic excitations that form a finite Fermi surface.

From Fig. 2-1, we see continuous phase transitions (at mean-field level) between the following pairs of phases: (A,D), (A,G), (B,G), (C,E), and (B,H). For the three continuous transitions (B,G), (B,H) and (A,G) that do not change any symmetries, we observe that the $SU(2)$ gauge structure in the phase (A) breaks down to Z_2 in the continuous transition from the phase (A) to the phase (G). The $SU(2) \times SU(2)$ gauge structure in the phase (B) breaks down to Z_2 in the two transitions (B,G) and (B,H).

2.5 A stable algebraic spin liquid – $SU(2)$-linear spin liquid

In this section, we will study the $SU(2)$-linear state given by Eq.(2.22) which describes the phase A in phase diagram Fig. 2-1. In the mean-field theory, the interactions

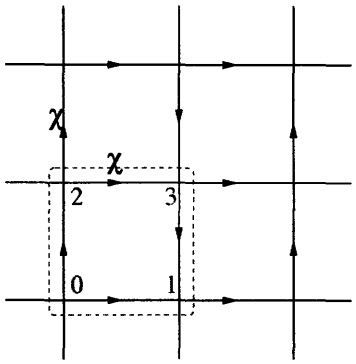

Figure 2-2: We choose the unit cell of $SU(2)$-linear state to contain *four* lattice sites when we go to the k-space.

between the excitations are ignored. In this section, we include those interactions and study how those interactions affect the low energy properties of the mean-field $SU(2)$-linear state. We will show that, after including those interactions, the gapless excitations in the mean-field $SU(2)$-linear state remain gapless, which leads to a stable algebraic spin liquid.

2.5.1 The low energy effective theory of the $SU(2)$-linear state

To obtain the low energy effective theory of the $SU(2)$-linear state in the continuum limit, we choose the unit cell as in Fig. 2-2. It contains 4 sites; each site has spin up and down, so totally 8 fermions. Let us write down the mean field Hamiltonian:

$$\begin{aligned}
H_{mean} =& \sum_i i\chi \left[\psi^\dagger_{i0}\psi_{i1} + \psi^\dagger_{i1}\psi_{i+x,0} + \psi^\dagger_{i2}\psi_{i3} + \psi^\dagger_{i3}\psi_{i+x,2}\right. \\
&\left. +\psi^\dagger_{i0}\psi_{i2} - \psi^\dagger_{i1}\psi_{i3} + \psi^\dagger_{i2}\psi_{i+y,0} - \psi^\dagger_{i3}\psi_{i+y,1}\right] + h.c. \\
=& \sum_k i\chi \left[\psi^\dagger_{k0}\psi_{k1} + \psi^\dagger_{k2}\psi_{k3} + \psi^\dagger_{k1}\psi_{k0}e^{ik_x} + \psi^\dagger_{k3}\psi_{k2}e^{ik_x}\right] \\
&+ \sum_k i\chi \left[\psi^\dagger_{k0}\psi_{k2} - \psi^\dagger_{k1}\psi_{k3} + \psi^\dagger_{k2}\psi_{k0}e^{ik_y} - \psi^\dagger_{k3}\psi_{k1}e^{ik_y}\right] + h.c. \\
=& \sum_k \left(\psi^\dagger_{k0}, \psi^\dagger_{k1}, \psi^\dagger_{k2}, \psi^\dagger_{k3}\right) \mathbf{M} \begin{pmatrix} \psi_{k0} \\ \psi_{k1} \\ \psi_{k2} \\ \psi_{k3} \end{pmatrix}
\end{aligned} \tag{2.31}$$

where

$$\mathbf{M} = \chi \begin{pmatrix} 0 & i - ie^{-ik_x} & i - ie^{-ik_y} & 0 \\ -i + ie^{ik_x} & 0 & 0 & -i + ie^{-ik_y} \\ -i + ie^{ik_y} & 0 & 0 & i - ie^{-ik_x} \\ 0 & i - ie^{ik_y} & -i + ie^{ik_x} & 0 \end{pmatrix} \tag{2.32}$$

Here we have assumed the lattice constant to be $1/2$, so we have $-\pi < k_x, k_y < \pi$. Note that here $\psi_{k,i}$ is actually $SU(2)$-doublet, corresponding to the spin up and down components in the f-formalism; so still totally 8 fermions. After some rearrangements:

$$\mathbf{M} = 2\chi \cdot \begin{pmatrix} 0 & -e^{-ik_x}\sin k_x & -e^{-ik_y}\sin k_y & 0 \\ -e^{ik_x}\sin k_x & 0 & 0 & e^{-ik_y}\sin k_y \\ -e^{ik_y}\sin k_y & 0 & 0 & -e^{-ik_x}\sin k_x \\ 0 & e^{ik_y}\sin k_y & -e^{ik_x}\sin k_x & 0 \end{pmatrix} \tag{2.33}$$

In the continuous limit, the energy spectrum for fermion is characterized by a single fermi point at $(0,0)$. When $k \approx 0$:

$$\mathbf{M} = 2\chi \begin{pmatrix} 0 & -k_x & -k_y & 0 \\ -k_x & 0 & 0 & k_y \\ -k_y & 0 & 0 & -k_x \\ 0 & k_y & -k_x & 0 \end{pmatrix} \tag{2.34}$$

We can do an extra rotation to make it the usual form of Dirac fermion:

$$\psi \to \tilde{\psi} = \mathbf{R}^\dagger \psi \tag{2.35}$$

$$\mathbf{R} = \begin{pmatrix} 0 & \frac{i}{\sqrt{2}} & \frac{1}{\sqrt{2}} & 0 \\ \frac{-1}{\sqrt{2}} & 0 & 0 & \frac{-i}{\sqrt{2}} \\ \frac{-i}{\sqrt{2}} & 0 & 0 & \frac{-1}{\sqrt{2}} \\ 0 & \frac{-1}{\sqrt{2}} & \frac{-i}{\sqrt{2}} & 0 \end{pmatrix} \psi \tag{2.36}$$

Then

$$H_{mean} = \tilde{\psi}^\dagger \gamma_0 \left[ik_x\gamma_1 + ik_y\gamma_2 \right] \tilde{\psi} \tag{2.37}$$

where the γ matrices in Euclidean space are:

$$\gamma_0 = \begin{pmatrix} \sigma_3 & \\ & -\sigma_3 \end{pmatrix} \gamma_1 = \begin{pmatrix} \sigma_1 & \\ & -\sigma_1 \end{pmatrix} \gamma_2 = \begin{pmatrix} \sigma_2 & \\ & -\sigma_2 \end{pmatrix} \tag{2.38}$$

Here we can also introduce the other two γ matrices:

$$\gamma_3 = \begin{pmatrix} & I \\ I & \end{pmatrix} \qquad \gamma_5 = \gamma_0\gamma_1\gamma_2\gamma_3 = i \begin{pmatrix} & I \\ -I & \end{pmatrix} \tag{2.39}$$

where I is the 2 by 2 identity matrix. Notice that both γ_3 and γ_5 anticommute with all space-time components of γ matrices: γ_0, γ_1 and γ_2. We should also include gauge field fluctuations above the mean-field theory. The full lagrangian is:

$$L = \bar{\tilde{\psi}} \left(\partial_\mu - i a_\mu^l \tau^l\right) \gamma_\mu \tilde{\psi} + \frac{1}{2g^2} \mathrm{Tr}\left[f_{\mu\nu}^l f_{\mu\nu}^l\right] + \cdots \tag{2.40}$$

where $\bar{\tilde{\psi}} = \tilde{\psi}^\dagger \gamma_0$. So the low energy effective theory of the $SU(2)$-linear state is a QCD_3 with a $SU(2)$ gauge field and two massless 4-component Dirac fermions (or $2N_f$ 4-component Dirac fermions which form N_f $SU(2)$ gauge doublets in the large N_f limit, notice $N_f = 1$ is the physical Heisenberg model's case).

The $\cdots$ in Eq. (2.40) represents other terms which may be generated by the interactions as we integrate out high energy fluctuations. Understanding those terms is the key to understand the low energy behavior of the model. Those terms must be consistent with the underlying lattice symmetry. So in the following, we will study the symmetry properties of the effective theory Eq. (2.40). We will show that none of terms allowed by the symmetry are relevant at low energies. None of those terms can cause infrared instability. As a result the mean-field $SU(2)$-linear state leads to a stable algebraic spin liquid.

2.5.2 Space translation and rotation symmetry

Now let us think about the corresponding lattice symmetry in continuous limit. Firstly let us discuss translation by one lattice site along x-direction T_x, in terms of the lattice fields:

$$T_x : \{ \begin{array}{ll} \psi_{\boldsymbol{i}} & \to \psi'_{\boldsymbol{i}} = \psi_{\boldsymbol{i}-\boldsymbol{x}} \\ u_{\boldsymbol{ij}} & \to u'_{\boldsymbol{ij}} = u_{\boldsymbol{i}-\boldsymbol{x},\boldsymbol{j}-\boldsymbol{x}} \end{array} \tag{2.41}$$

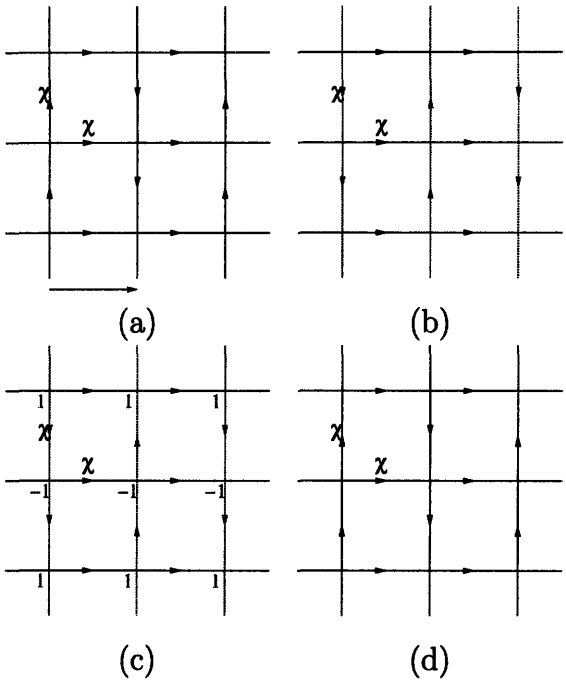

Figure 2-3: Figures (a)–(d) illustrate how the $SU(2)$-linear state respects translation symmetry T_x: (a) original ansatz (b) after T_x (c)do W_{T_x} (d) go back to original ansatz.

It seems that the translation symmetry is broken since u_{ij} is not invariant:

$$\{ \begin{array}{ll} u_{i,i+x} = & i\chi, \\ u_{i,i+y} = & i(-)^{i_x}\chi \end{array} \rightarrow \{ \begin{array}{ll} u'_{i,i+x} = & i\chi, \\ u'_{i,i+y} = & -i(-)^{i_x}\chi \end{array} \tag{2.42}$$

But as shown in Fig.2-3 one can do an extra local $SU(2)$ gauge transformation W_{T_x} to transform u_{ij} back. Let

$$W_i = (-)^{i_y} \tag{2.43}$$

Then

$$W_{T_x} : \{ \begin{array}{ll} \psi'_i & \rightarrow \psi''_i = W_i\psi'_i = (-)^{i_y}\psi_{i-x} \\ u'_{ij} & \rightarrow u''_{ij} = W_i u'_{ij} W_j^\dagger \end{array} \tag{2.44}$$

where

$$\{ \begin{array}{ll} u''_{i,i+x} & = u'_{i,i+x} = i\chi = u_{i,i+x} \\ u''_{i,i+y} & = -u'_{i,i+y} = i(-)^{i_x}\chi = u_{i,i+y} \end{array} \tag{2.45}$$

Here we point out that the combination of W_{T_x} and T_x is a transformation leaving

U_{ij} invariant. We call such a transformation an element of PSG. PSG, by definition, is the collection of all transformations leaving the ansatz $U_{ij}, a^l_{0,i}$ invariant. Here in $SU(2)$-linear state, $a^l_{0,i}$ is zero, so it is also invariant.

After choosing the unit cell as in Fig.2-2, in terms of the four component ψ fermion, the combination of W_{T_x} and T_x transforms:

$$\begin{pmatrix} \psi_{i0} \\ \psi_{i1} \\ \psi_{i2} \\ \psi_{i3} \end{pmatrix} \rightarrow \begin{pmatrix} \psi'_{i0} \\ \psi'_{i1} \\ \psi'_{i2} \\ \psi'_{i3} \end{pmatrix} = \begin{pmatrix} 0 & 1 & 0 & 0 \\ 1 & 0 & 0 & 0 \\ 0 & 0 & 0 & -1 \\ 0 & 0 & -1 & 0 \end{pmatrix} \begin{pmatrix} \psi_{i0} \\ \psi_{i1} \\ \psi_{i2} \\ \psi_{i3} \end{pmatrix} \tag{2.46}$$

Here we assumed in the continuous limit, ψ_i and ψ_{i+x} are on the same position. We can do the extra rotation to transform into $\tilde{\psi}$, the usual Dirac fermion:

$$\tilde{\psi} \rightarrow \tilde{\psi}' = \mathbf{R}^\dagger \psi' = \mathbf{R}^\dagger \begin{pmatrix} 0 & 1 & 0 & 0 \\ 1 & 0 & 0 & 0 \\ 0 & 0 & 0 & -1 \\ 0 & 0 & -1 & 0 \end{pmatrix} \mathbf{R}\tilde{\psi} = \begin{pmatrix} 0 & 0 & -1 & 0 \\ 0 & 0 & 0 & -1 \\ -1 & 0 & 0 & 0 \\ 0 & -1 & 0 & 0 \end{pmatrix} \tilde{\psi} = -\gamma_3 \tilde{\psi} \tag{2.47}$$

Eventually we know that the PSG element $W_{T_x} \circ T_x$, which is the lattice symmetry, if translated into continuous limit, is the internal symmetry $-\gamma_3$. Note that the minus sign actually corresponds to a global $SU(2)$ transformation: $W_i = -1$. So we have the correspondence:

$$W_{T_x} \circ T_x \longleftrightarrow \gamma_3 \tag{2.48}$$

Similarly one can study the translation by one lattice site along y-direction; we find:

$$W_{T_y} \circ T_y \longleftrightarrow \gamma_5 \tag{2.49}$$

For the reflection $P_x : x \rightarrow -x$:

$$W_{P_x} \circ P_x \longleftrightarrow \gamma_1 \tag{2.50}$$

For the reflection $P_y : y \rightarrow -y$:

$$W_{P_y} \circ P_y \longleftrightarrow \gamma_2 \tag{2.51}$$

For the reflection $P_{xy} : x \to y, y \to x$:

$$W_{P_{xy}} \circ P_{xy} \longleftrightarrow \frac{1}{2}(\gamma_1 - \gamma_2)(\gamma_3 + \gamma_5) \tag{2.52}$$

Note that $T_x, T_y, P_x, P_y, P_{xy}$ already give the full space-time symmetry. For example, rotation by 90 degree $R_{90} : x \to y, y \to -x$ is a combination of P_x and P_{xy}:

$$R_{90} = P_{xy} \circ P_x \tag{2.53}$$

2.5.3 Time-reversal symmetry

Now let us study the time-reversal symmetry T. In terms of spin operator:

$$T : \mathbf{S} \to -\mathbf{S} \tag{2.54}$$

One should be cautious that T is not a usual linear operator, instead it is an anti-linear operator:

$$Ti = -iT \tag{2.55}$$

What does this operator correspond to in terms of lattice fermion and bond variable U_{ij}? We know that

$$\mathbf{S} = \frac{1}{2} f^\dagger \boldsymbol{\sigma} f \tag{2.56}$$

So the corresponding transformation on f fermion is:

$$T : f \to i\sigma_2 f, \qquad T : f^\dagger \to f^\dagger (i\sigma_2)^\dagger \tag{2.57}$$

$$\begin{aligned} T\mathbf{S}T^{-1} &= T f^\dagger T^{-1} T \boldsymbol{\sigma} T^{-1} T f T^{-1} \\ &= f^\dagger (i\sigma_2)^\dagger (\sigma_1, -\sigma_2, \sigma_3) (i\sigma_2) f \\ &= f^\dagger (-\sigma_1, -\sigma_2, -\sigma_3) f \\ &= -\mathbf{S} \end{aligned} \tag{2.58}$$

Here we used the anti-linear property of T operator. Therefore the T transformation on ψ fermion is:

$$T : \psi = \begin{pmatrix} f_\uparrow \\ f_\downarrow^\dagger \end{pmatrix} \to \begin{pmatrix} f_\downarrow \\ -f_\uparrow^\dagger \end{pmatrix} = i\tau_2\psi^* \tag{2.59}$$

Our convention of notation is that in terms of f fermion, we use σ to denote Pauli matrices; while in terms of ψ fermion, we use τ to denote them.

What is the time-reversal transformation on U_{ij}? Here we notice that U_{ij} has two meanings: in Eq.(2.7) it means the operator defined as in Eq.(2.6); while in Eq.(2.14) it means the average value of the operator on mean-field ground state. Let us take a look at how the operator transform under time-reversal:

$$\begin{aligned} T\hat{\chi_{ij}}T^{-1} &= Tf_{i\alpha}^\dagger f_{j\alpha}T^{-1} = Tf_{i\alpha}^\dagger T^{-1}Tf_{j\alpha}T^{-1} \\ &= f_i^\dagger(i\sigma_2)^\dagger(i\sigma_2)f_j = f_i^\dagger f_j = \hat{\chi_{ij}} \end{aligned} \tag{2.60}$$

$$\begin{aligned} T\hat{\eta}_{ij}^\dagger T^{-1} &= Tf_{i\alpha}^\dagger\epsilon_{\alpha\beta}f_{j\beta}^\dagger T^{-1} = Tf_{i\alpha}^\dagger T^{-1}\epsilon_{\alpha\beta}Tf_{j\beta}^\dagger T^{-1} \\ &= f_{i\gamma}^\dagger(i\sigma_2)_{\gamma\alpha}^\dagger\epsilon_{\alpha\beta}(i\sigma_2)_{\delta\beta}^\dagger f_{j\delta} = f_{i\gamma}^\dagger\epsilon_{\gamma\delta}f_{j\delta} = \hat{\eta}_{ij}^\dagger \end{aligned} \tag{2.61}$$

Therefore we know that the $\hat{U_{ij}}$, as an operator, is invariant under T. Here it is helpful to write down $\hat{U_{ij}}$ in terms of ψ operators:

$$\hat{U_{ij}} = \begin{pmatrix} \hat{\chi}_{ij} & \hat{\eta}_{ij} \\ \hat{\eta}_{ij}^\dagger & -\hat{\chi}_{ij}^\dagger \end{pmatrix} = -\psi_j\psi_i^\dagger - (i\tau_2\psi_j^*)(i\tau_2\psi_i^*)^\dagger \tag{2.62}$$

Notice Eq.(2.59), under T transformation, the first term transforms into the second term, and the second transforms into the first. So the whole $\hat{U_{ij}}$ is invariant. One can also check that together with transformation Eq.(2.59), the Lagrangian Eq.(2.7) is invariant under T. This is expected since the original Heisenberg Hamiltonian Eq.(2.1) is T invariant.

But things are different if $\hat{U_{ij}}$ condense, more specifically, if it has some non-zero average value: $U_{ij} = \langle\Psi|\hat{U_{ij}}|\Psi\rangle$. Because T is an anti-linear operator, it transforms U_{ij} into U_{ij}^*. We know that for two arbitrary states $|\alpha\rangle$, $|\beta\rangle$, the anti-linear property of T gives

$$\langle\alpha|\beta\rangle = \langle T\beta|T\alpha\rangle \tag{2.63}$$

Therefore for an arbitrary linear operator $\hat{O}$,

$$\langle\alpha|\hat{O}|\beta\rangle = \langle\hat{O}^\dagger\alpha|\beta\rangle = \langle T\beta|T\hat{O}^\dagger\alpha\rangle = \langle T\beta|T\hat{O}^\dagger T^{-1}|T\alpha\rangle \tag{2.64}$$

let $\hat{O} = \hat{\chi}^\dagger_{ij}$, and $|\alpha\rangle = |\beta\rangle = |\Psi\rangle$, one immediately see that under T transformation, the average value of $\hat{\chi}_{ij}$ operator transforms as:

$$\begin{aligned}\chi_{ij} = \langle\Psi|\hat{\chi}_{ij}|\Psi\rangle \rightarrow \chi'_{ij} &= \langle T\Psi|\hat{\chi}_{ij}|T\Psi\rangle \\ &= \langle\Psi|\hat{\chi}^\dagger_{ij}|\Psi\rangle = \chi^*_{ij}\end{aligned} \tag{2.65}$$

Here we know that the mean-field variable U_{ij}, as the average value of $\hat{U}_{ij}$ operator, transforms into U^*_{ij} under T. This is consistent with our understanding of anti-linear T operator, since it transforms any c-number into its complex conjugate.

$$T : U_{ij} \rightarrow TU_{ij}T^{-1} = U^*_{ij} \tag{2.66}$$

In general, U_{ij} can be written as:

$$U_{ij} = u^0_{ij}\tau_0 + u^1_{ij}\tau_1 + u^2_{ij}\tau_2 + u^3_{ij}\tau_3 \tag{2.67}$$

where τ_0 is identity matrix. For spin rotation invariant system, one can show that u^0_{ij} is pure imaginary, while u^i_{ij} $i = 1, 2, 3$ are pure real.

How does mean-field Hamiltonian transform under T? Here we need combine transformations on ψ and U_{ij}:

$$\begin{aligned}\psi^\dagger_i U_{ij}\psi_j \rightarrow &\psi^T_i(i\tau_2)^\dagger U^*_{ij}(i\tau_2)\psi^*_j \\ \text{(using Eq.(2.67))} \quad =&\psi^T_i(-U_{ij})\psi^*_j \\ =&\psi^\dagger_j(U_{ij})^T\psi_i \\ (U_{ij} = U^\dagger_{ji}) \quad =&\psi^\dagger_j U^*_{ji}\psi_i\end{aligned} \tag{2.68}$$

Comparing with the term in original mean-field Hamiltonian $\psi^\dagger_j U_{ji}\psi_i$, one concludes that the transformation of mean-field hamiltonian under T can be simply expressed as $U_{ij} \rightarrow U^*_{ij}$, with no fermion transformation. If U^*_{ij} and original U_{ij} can be related by a $SU(2)$ gauge transformation, the system has time-reversal symmetry; otherwise the T was broken.

For our $SU(2)$-linear state, U^*_{ij} and U_{ij} are indeed related by a gauge transforma-

tion W_T.

$$W_T : W_i = -(-)^{i_x+i_y} \tag{2.69}$$

After choosing unit cell, in terms of four-component fermion ψ,

$$W_T : \begin{pmatrix} \psi_{i0} \\ \psi_{i1} \\ \psi_{i2} \\ \psi_{i3} \end{pmatrix} \to \begin{pmatrix} -1 & & & \\ & 1 & & \\ & & 1 & \\ & & & -1 \end{pmatrix} \begin{pmatrix} \psi_{i0} \\ \psi_{i1} \\ \psi_{i2} \\ \psi_{i3} \end{pmatrix} \tag{2.70}$$

In terms of usual Dirac fermion $\tilde{\psi}$:

$$W_T : \tilde{\psi} \to \begin{pmatrix} 1 & & & \\ & -1 & & \\ & & -1 & \\ & & & 1 \end{pmatrix} \tilde{\psi} = \gamma_0 \tilde{\psi} \tag{2.71}$$

The combined transformation $W_T \circ T$ leaves U_{ij} invariant. So $W_T \circ T$ is another element if PSG. And we know in terms of Dirac fermion $\tilde{\psi}$,

$$W_T \circ T : \quad \tilde{\psi} \to \tilde{\psi}' = (i\tau_2)\gamma_0 \tilde{\psi} \tag{2.72}$$

This is very similar to the time-reversal transformation in usual Dirac field theory.

2.5.4 Spin rotation: "charge conjugation"

There is another important symmetry, the global spin rotation. Let us think about rotation around y-axis by 180 degree:

$$R_{spin} : (S_x, S_y, S_z) \to (-S_x, S_y, -S_z) \tag{2.73}$$

In terms of f spinon,

$$R_{spin} : f \to f' = (i\sigma_2) f = \begin{pmatrix} f_\downarrow \\ -f_\uparrow \end{pmatrix} \tag{2.74}$$

In terms of ψ fermion,

$$R_{spin} : \psi = \begin{pmatrix} f_\uparrow \\ f_\downarrow^\dagger \end{pmatrix} \rightarrow \psi' = \begin{pmatrix} f_\downarrow \\ -f_\uparrow^\dagger \end{pmatrix} = (i\tau_2)\psi^* \tag{2.75}$$

It seems Eq.(2.75) is identical to Eq.(2.59), which means T and R_{spin} are identical. This is obviously wrong, the difference here lies in the fact that T is anti-linear but R_{spin} is linear.

In terms of 4-component Dirac fermion $\tilde{\psi}$:

$$R_{spin} : \tilde{\psi} = \mathbf{R}^\dagger\psi \rightarrow \mathbf{R}^\dagger(i\tau_2)\psi^* = (i\tau_2)\mathbf{R}\mathbf{R}^*\tilde{\psi}^* = (i\tau_2)(-\gamma_1\gamma_5)\tilde{\psi}^* \tag{2.76}$$

The transformation rule above is in real space. In momentum space,

$$\begin{aligned} R_{spin} : \tilde{\psi}_k &= \frac{1}{\sqrt{N}}\sum_j e^{-ikj}\tilde{\psi}_j \\ &\rightarrow (-i\tau_2)(\gamma_1\gamma_5)\frac{1}{\sqrt{N}}\sum_j e^{-ikj}\tilde{\psi}_j^* \\ &= (-i\tau_2)(\gamma_1\gamma_5)\tilde{\psi}_{-k}^* \end{aligned} \tag{2.77}$$

i.e., the spin rotation transformation R_{spin} also flip the sign of momentum!

Now think about how $\hat{U}_{ij}$ transforms under R_{spin}. The form of Eq.(2.62) is explicitly R_{spin} invariant, so $\hat{U}_{ij}$ is R_{spin} invariant. This is expected since we have spin rotation invariant $\hat{\chi}$ and $\hat{\eta}$. This is actually the point of this slave-boson mean-field approach. We choose the mean-field variables to be spin rotation singlets, such that even it acquires non-zero average value, it doesn't break spin-rotation symmetry, which describes spin liquid states. Moreover, since R_{spin} is a linear operator, we know that the average value of $\hat{U}_{ij}$ is also R_{spin} invariant.

$$R_{spin} : U_{ij} \rightarrow R_{spin}U_{ij}R_{spin}^{-1} = U_{ij} \tag{2.78}$$

This is consistent with the usual property of linear operator: it commutes with c-numbers.

What is the transformation on mean-field Hamiltonian? We should put transfor-

PSG element	Transformation on fermion
$T_x^{PSG} = W_{T_x} \circ T_x$	γ_3
$T_y^{PSG} = W_{T_y} \circ T_y$	γ_5
$P_x^{PSG} = W_{P_x} \circ P_x$	γ_1
$P_y^{PSG} = W_{P_y} \circ P_y$	γ_2
$P_{xy}^{PSG} = W_{P_{xy}} \circ P_{xy}$	$\frac{1}{2}(\gamma_1 - \gamma_2)(\gamma_3 + \gamma_5)$
$T^{PSG} = W_T \circ T$	$\tilde{\psi} \to (i\tau_2)\gamma_0\tilde{\psi}^*$ (anti-linear)
$C^{PSG} = W_C \circ C$	$\tilde{\psi} \to -(i\tau_2)\gamma_1\gamma_5\tilde{\psi}^*$ (linear)

Table 2.1: Transformations of Dirac fermion $\tilde{\psi}$, here C is R_{spin} and W_C is identity.

mations on fermion Eq.(2.75) and U_{ij} Eq.(2.78) together:

$$\begin{aligned} R_{spin} : \psi_i^\dagger U_{ij} \psi_j \to & \psi_i^T (i\tau_2)^\dagger U_{ij} (i\tau_2) \psi_j^* \\ \text{using Eq.(2.67)} \quad = & \psi_i^T (-U_{ij}^*) \psi_j^* \\ = & \psi_j^\dagger U_{ij}^\dagger \psi_i = \psi_j^\dagger U_{ji} \psi_i \end{aligned}$$

This is just another term in the original mean-field Hamiltonian. We conclude that H_{mean} is invariant under R_{spin}. This again is expected since our spin-liquid states should not break R_{spin}. So R_{spin} is also an element of PSG.

Here we point out that the form of R_{spin} transformation Eq.(2.76) is very similar to the charge-conjugation transformation C in usual Dirac field theory. In fact we can denote R_{spin} as C in our later discussion. We summarize the transformations on Dirac fermion in Table 2.1.

2.5.5 Transformations of fermion bilinears

Let us focus on $SU(2)$-linear state. We know that the mean-field Hamiltonian is characterized by a $SU(2)$ doublet of massless Dirac fermions. But can the mass gap be generated after including quantum fluctuations? If yes then the mean-field theory cannot describe the real physical system at all since the low energy behavior is completely different. In this section we will show that this is not the case.

We know that for a certain mean-field state, it has a certain PSG, which is the symmetry of the mean-field hamiltonian. After we include fluctuation, this symmetry will still be respected. Suppose we go through an renormalization group process to find the low energy theory, any counter-term explicitly breaking PSG will not be generated when taking care of fluctuations.

This can be viewed in the following way: let $L(\psi_i, U_{ij}, a^l_{0i})$ in Eq.(2.7) be the Lagrangian describing the dynamics of fermion and gauge fields. In the original theory, we have a huge "symmetry" group leaving L invariant, for example, the translation along x-axis by one lattice site T_x:

$$L(\psi_i, \hat{U}_{ij}) = L(T_x \psi_i T_x^{-1}, T_x \hat{U}_{ij} T_x^{-1}) = L(\psi_{i-x}, \hat{U}_{i-x,j-x}) \tag{2.79}$$

or an arbitrary local $SU(2)$ gauge "symmetry" transformation W (here the meaning of quotion mark is that gauge "symmetry" is not a physical symmetry, instead it is just a many-to-one bad labelling.):

$$L(\psi_i, \hat{U}_{ij}) = L(W_i \psi_i, W_i \hat{U}_{ij} W_j^\dagger) \tag{2.80}$$

But after $\hat{U}_{ij}$ condense, things are different. The above huge "symmetry" group will be "spontaneously" broken (the unbroken state must have $U_{ij} = 0$). PSG is the remaining unbroken "symmetry" group after this symmetry breaking. PSG is defined as the collection of all transformations leaving the Lagrangian $L(\psi_i, \hat{U}_{ij}, a^l_{0i})$ invariant and also leaving average value U_{ij} invariant. Let P be an element of PSG, then

$$L(\psi_i, \hat{U}_{ij}) = L(P\psi_i P^{-1}, P\hat{U}_{ij} P^{-1}) \tag{2.81}$$

$$U_{ij} = P U_{ij} P^{-1} \tag{2.82}$$

We can consider fluctuation around the average value U_{ij}:

$$\hat{U}_{ij} = U_{ij} + \delta\hat{U}_{ij} \tag{2.83}$$

Plugging into Eq.(2.81)

$$\begin{aligned} L(\psi_i, U_{ij} + \delta\hat{U}_{ij}) &= L(P\psi_i P^{-1}, P(U_{ij} + \delta\hat{U}_{ij})P^{-1}) \\ &= L(P\psi_i P^{-1}, U_{ij} + P\delta\hat{U}_{ij} P^{-1}) \end{aligned} \tag{2.84}$$

So the Lagrangian for the fluctuations $L(\psi_i, \delta\hat{U}_{ij})$ must be invariant under PSG transformations.

We want to find out the transformations of fermion bilinears under PSG. Because if they all transform non-trivially under PSG, they will be all forbidden. That is why the fermions remain to be massless after including fluctuations.

Here we will consider only the fermion bilinears of form $\tilde{\psi}^\dagger\tilde{\psi}$. The bilinears of

	T_x^{PSG}	T_y^{PSG}	P_x^{PSG}	P_y^{PSG}	P_{xy}^{PSG}	T^{PSG}	C^{PSG}
$\bar{\tilde{\psi}}\tilde{\psi}$	-1	-1	-1	-1	$+1$	-1	-1
$\bar{\tilde{\psi}}\gamma_0\tilde{\psi}$	$+1$	$+1$	$+1$	$+1$	$+1$	-1	-1
$i\bar{\tilde{\psi}}\gamma_3\gamma_5\tilde{\psi}$	$+1$	$+1$	-1	-1	-1	-1	$+1$
$i\bar{\tilde{\psi}}\gamma_1\gamma_2\tilde{\psi}$	-1	-1	$+1$	$+1$	-1	-1	$+1$
$\begin{pmatrix} i\bar{\tilde{\psi}}\gamma_1\tilde{\psi} \\ i\bar{\tilde{\psi}}\gamma_2\tilde{\psi} \end{pmatrix}$	$+1$	$+1$	$\begin{pmatrix} -1 & \\ & +1 \end{pmatrix}$	$\begin{pmatrix} +1 & \\ & -1 \end{pmatrix}$	$\begin{pmatrix} & +1 \\ +1 & \end{pmatrix}$	-1	-1
$\begin{pmatrix} \bar{\tilde{\psi}}\gamma_0\gamma_1\tilde{\psi} \\ \bar{\tilde{\psi}}\gamma_0\gamma_2\tilde{\psi} \end{pmatrix}$	-1	-1	$\begin{pmatrix} +1 & \\ & -1 \end{pmatrix}$	$\begin{pmatrix} -1 & \\ & +1 \end{pmatrix}$	$\begin{pmatrix} & +1 \\ +1 & \end{pmatrix}$	$+1$	$+1$
$\begin{pmatrix} i\bar{\tilde{\psi}}\gamma_3\tilde{\psi} \\ i\bar{\tilde{\psi}}\gamma_5\tilde{\psi} \end{pmatrix}$	$\begin{pmatrix} -1 & \\ & +1 \end{pmatrix}$	$\begin{pmatrix} +1 & \\ & -1 \end{pmatrix}$	$+1$	$+1$	$\begin{pmatrix} & -1 \\ -1 & \end{pmatrix}$	$+1$	$+1$
$\begin{pmatrix} \bar{\tilde{\psi}}\gamma_0\gamma_3\tilde{\psi} \\ \bar{\tilde{\psi}}\gamma_0\gamma_5\tilde{\psi} \end{pmatrix}$	$\begin{pmatrix} +1 & \\ & -1 \end{pmatrix}$	$\begin{pmatrix} -1 & \\ & +1 \end{pmatrix}$	-1	-1	$\begin{pmatrix} & -1 \\ -1 & \end{pmatrix}$	$+1$	-1
$\begin{pmatrix} i\bar{\tilde{\psi}}\gamma_1\gamma_3\tilde{\psi} \\ i\bar{\tilde{\psi}}\gamma_2\gamma_5\tilde{\psi} \end{pmatrix}$	$\begin{pmatrix} +1 & \\ & -1 \end{pmatrix}$	$\begin{pmatrix} -1 & \\ & +1 \end{pmatrix}$	$\begin{pmatrix} +1 & \\ & -1 \end{pmatrix}$	$\begin{pmatrix} -1 & \\ & +1 \end{pmatrix}$	$\begin{pmatrix} & -1 \\ -1 & \end{pmatrix}$	-1	-1
$\begin{pmatrix} i\bar{\tilde{\psi}}\gamma_1\gamma_5\tilde{\psi} \\ i\bar{\tilde{\psi}}\gamma_2\gamma_3\tilde{\psi} \end{pmatrix}$	$\begin{pmatrix} -1 & \\ & +1 \end{pmatrix}$	$\begin{pmatrix} +1 & \\ & -1 \end{pmatrix}$	$\begin{pmatrix} +1 & \\ & -1 \end{pmatrix}$	$\begin{pmatrix} -1 & \\ & +1 \end{pmatrix}$	$\begin{pmatrix} & -1 \\ -1 & \end{pmatrix}$	-1	-1

Table 2.2: Transformations of 16 fermion bilinears. All transform non-trivially.

forms $\tilde{\psi}\tilde{\psi}$ and $\tilde{\psi}^\dagger\tilde{\psi}^\dagger$ are not invariant under the spin S_z rotation and are not allowed in the effective Lagrangian. Since we are using 4-component fermion, there should be $4 \times 4 = 16$ different fermion bilinears of form $\tilde{\psi}^\dagger\tilde{\psi}$. From Table 2.1, it is quite easy to find the transformations of all fermion bilinears under PSG. It turns out that among these 16 bilinears, as shown in Table 2.2, there are four 1-dimensional representations and six 2-dimensional representations of PSG. All the fermion bilinears transform non-trivially under the PSG. So perturbatively, the fermions remain massless after inclusion of fluctuations.

Now let us consider the fermion bi-linear terms that also contain a single spatial derivative. Those terms represent marginal perturbations when $N_f = \infty$. From the table 2.2, we see that the only term that is allowed by the PSG is $\bar{\tilde{\psi}}\partial_x\gamma_1\tilde{\psi} + \bar{\tilde{\psi}}\partial_y\gamma_2\tilde{\psi}$. All other terms are forbiden. The reason is as follows: The 1-dimensional representations together with a spatial derivative cannot be Lorentz singlet, so are ruled out. Among 2-dimensional representations together with a spatial derivative, only $\bar{\tilde{\psi}}\partial_x\gamma_1\tilde{\psi}+\bar{\tilde{\psi}}\partial_y\gamma_2\tilde{\psi}$ is invariant under translation T_x^{PSG} (in fact, it is invariant under full PSG); all others are ruled out. But the term $\bar{\tilde{\psi}}\partial_1\gamma_1\tilde{\psi} + \bar{\tilde{\psi}}\partial_2\gamma_2\tilde{\psi}$, which is already present in Eq.(2.40), only changes the velocity of the fermions. In a RG study, this counter-term means a wavefunction renormalization. The low-energy effective theory Eq.(2.40) remains valid.

The next question is, will there be 4-fermion interaction terms? The answer is yes. For example, we choose a certain 1-dimension representation in Table 2.2, say $\bar{\tilde{\psi}}\tilde{\psi}$, then couple this term to itself to make a 4-fermion interaction. It is obvious that this 4-fermion term is PSG invariant, which is allowed in the Lagrangian. Will this kind of 4-fermion term change the low energy behavior drastically? The answer is no. This is because we are in 2+1 space-time dimension, and by power counting 4-fermion terms are of dimension 4, so they are irrelevant couplings. Same argument can be done for fermion bilinear terms with second order derivatives; those terms are also irrelevant.

In summary, we have discussed the possible fermion self-interactions. Our conclusion is that in perturbative sense, these fermion self-interactions will not change the low energy behavior from the mean-field result. We may say that the $SU(2)$-linear mean-field state is stable under fermion self-interactions.

2.5.6 Emergent $Sp(4)$ physical symmetry

In this section we will discuss the emergent symmetry for $SU(2)$-linear phase whose low energy effective theory is Eq.(2.40). We already know that there are two fermion-chiral symmetry generators γ_3 and γ_5, and they are anticommuting. (Here please note that we are talking about fermion-chiral symmetry, which is different from the spin-chirality in the later discussion about chiral spin liquid.) Therefore the symmetry of $SU(2)$-linear phase contains at least a global $SU(2)$ fermion-chiral Lie group whose generators are γ_3, γ_5 and $i\gamma_3\gamma_5$.

We also know that the theory should be global $SU(2)$ spin-rotation invariant, since we are talking about a spin liquid phase here. Thus there should be at least another $SU(2)$ spin-rotation symmetry group. However after the particle-hole transformation we made in Eq.(2.8), this spin-rotation symmetry was hidden in our formalism.

The full physical symmetry group of $SU(2)$-linear phase should contain both the $SU(2)$ fermion-chiral and $SU(2)$ spin-rotation as its subgroups. The naive guess for the full group is $SU(2) \times SU(2)$ but it turns out to be wrong. We will show in this section that the correct full symmetry group is $Sp(4)$. We noticed that the same $Sp(4)$ symmetry was found earlier by Tanaka and Hu[42] by viewing the π-flux state as a fermionic mean field state, i.e., ignoring the effect of $SU(2)$ gauge field. Here we clarified the gauge field effect and obtained the same global flavor symmetry. Then we can classify all the fermion bilinears according to their transformation rules under $Sp(4)$ group.

Later, we will show that after including the $SU(2)$ gauge fluctuations, the $SU(2)$-linear state remains gapless and the correlations between various operators remain algebraic. But the exponents of algebraic correlations may be modified by the $SU(2)$ gauge interaction. Classifying fermion bilinears according to their transformation under the $Sp(4)$ group is very important in understanding the scaling properties of those operators. The operators that belong to the same irreducible $Sp(4)$ representation will have the same scaling dimension.

First we consider the spin rotation group; basically it will mix ψ and ψ^*. To make the spin rotation transformation explicit, it is convenient to reintroduce the $\widehat{\psi}$ formalism in Eq.(2.10):

$$\widehat{\psi} = i\sigma_2\psi^* = \begin{pmatrix} f_\downarrow \\ -f_\uparrow^\dagger \end{pmatrix} \tag{2.85}$$

Let us look at lattice fermion ψ at certain site. If we put ψ (2-component, corresponding to spin up and down) and $\widehat{\psi}$ (2-component) together to form a 4-component vector:

$$\Psi = \begin{pmatrix} \psi \\ \widehat{\psi} \end{pmatrix} \tag{2.86}$$

then it is straightforward to write down the spin rotation transformation. For example, the rotation around z-axis:

$$\psi \to \begin{pmatrix} e^{i\theta/2} & 0 \\ 0 & e^{i\theta/2} \end{pmatrix} \psi \qquad\qquad \widehat{\psi} \to \begin{pmatrix} e^{-i\theta/2} & 0 \\ 0 & e^{-i\theta/2} \end{pmatrix} \widehat{\psi} \tag{2.87}$$

Therefore

$$\Psi \to 1 \otimes e^{i\theta\sigma_3/2}\Psi \tag{2.88}$$

where the identity matrix labels the internal space of ψ (spin up and down), while $e^{i\theta\sigma_3/2}$ acts on the space mixing ψ and $\widehat{\psi}$.

What about rotation along y-axis? Suppose we do an infinitesimal transformation

$$f_\uparrow \to f_\uparrow + \frac{\theta}{2} f_\downarrow \qquad\qquad f_\downarrow \to f_\downarrow - \frac{\theta}{2} f_\uparrow \tag{2.89}$$

it implies:

$$\psi_1 \to \psi_1 + \frac{\theta}{2}\psi_2^* \qquad\qquad \psi_2 \to \psi_2 - \frac{\theta}{2}\psi_1^* \tag{2.90}$$

thus

$$\psi \to \psi + \frac{\theta}{2}\widehat{\psi} \qquad\qquad \widehat{\psi} \to \widehat{\psi} - \frac{\theta}{2}\psi \tag{2.91}$$

in terms of Ψ:

$$\Psi \to \mathbf{1} \otimes e^{i\theta\sigma_2/2}\Psi \tag{2.92}$$

Similarly the rotation along x-axis is:

$$\Psi \to \mathbf{1} \otimes e^{i\theta\sigma_1/2}\Psi \tag{2.93}$$

To summarize, we know that the spin rotation is acting on the space mixing ψ and $\widehat{\psi}$.

Let us go to continuous limit, and consider the 4-component Dirac fermion $SU(2)$ doublet $\tilde{\psi}$ in Eq.(2.36). Again we write it together with $\widehat{\tilde{\psi}}$:

$$\widetilde{\Psi} = \begin{pmatrix} \tilde{\psi} \\ \widehat{\tilde{\psi}} \end{pmatrix} \tag{2.94}$$

Note that actually $\widetilde{\Psi}$ has 16 components and $16 = 4 \times 2 \times 2$ where 4 is the number of Dirac components, the first 2 is for $SU(2)$ gauge doublet and the second 2 is for the space mixing $\tilde{\psi}$ and $\widehat{\tilde{\psi}}$. From the above discussion, the space mixing $\tilde{\psi}$ and $\widehat{\tilde{\psi}}$ is actually spin rotation space. A generic transformation G on fermion field can be written as a transformation on $\widetilde{\Psi}$:

$$G = G_{Dirac} \otimes G_{gauge} \otimes G_{spin} \tag{2.95}$$

where the transformations with subscripts act on each corresponding space.

The three spin rotation generators are, from above discussion:

$$\mathbf{1} \otimes \mathbf{1} \otimes \sigma_1, \qquad \mathbf{1} \otimes \mathbf{1} \otimes \sigma_2, \qquad \mathbf{1} \otimes \mathbf{1} \otimes \sigma_3 \tag{2.96}$$

The fermion-chiral generator γ_3 is acting on $\tilde{\psi}$. One can easily check that while

acting on $\widetilde{\Psi}$, since $\widehat{\tilde{\psi}} = i\sigma_2\tilde{\psi}^*$, the generator has the form: $\gamma_3 \otimes \mathbf{1} \otimes \sigma_3$. Similarly one can find the other two generators of fermion-chiral transformation. In summary, they are:

$$\gamma_3 \otimes \mathbf{1} \otimes \sigma_3, \qquad \gamma_5 \otimes \mathbf{1} \otimes \sigma_3, \qquad i\gamma_3\gamma_5 \otimes \mathbf{1} \otimes \mathbf{1} \tag{2.97}$$

Now if we do commutations between Eq.(2.96) and Eq.(2.97), the full set of symmetry generators can be found:

$$\mathbf{1} \otimes \mathbf{1} \otimes \boldsymbol{\sigma}, \qquad \gamma_3 \otimes \mathbf{1} \otimes \boldsymbol{\sigma}, \qquad \gamma_5 \otimes \mathbf{1} \otimes \boldsymbol{\sigma}, \qquad i\gamma_3\gamma_5 \otimes \mathbf{1} \otimes \mathbf{1} \tag{2.98}$$

Totally $3 + 3 + 3 + 1 = 10$ elements, which satisfy $Sp(4)$ algebraic relation.

Here one thing we need to mention is that the three gauge transformation generators:

$$\mathbf{1} \otimes \boldsymbol{\tau} \otimes \mathbf{1} \tag{2.99}$$

will also keep the Lagrangian Eq.(2.40) invariant. But they are gauge transformations and should not be taken as physical symmetries.

We just showed the emergent $Sp(4)$ global symmetry. Can the emergent continuous symmetry group larger than $Sp(4)$? The answer is no, as one can see in the following. We have totally 8 components of fermions, and they form four $SU(2)$ gauge doublets. For global symmetry we should only consider transformations invariant in the gauge sector, which means we should consider the transformation between the 4 doublets only (i.e., in flavor space but not in gauge space), including the mixing between ψ and $\psi^\dagger$. In Majorana fermion representation, it is obvious that the allowed flavor transformations form $SO(8)$ group. The Lorentz transformations $i\gamma_0\gamma_1, i\gamma_0\gamma_2, i\gamma_1\gamma_2$ generate $SO(3)$ group in Euclidean space, and we also know that $Sp(4) = SO(5)$. The flavor symmetry $SO(5)$ and Lorentz symmetry $SO(3)$ actually commute. This $SO(5)$ is the largest continuous subgroup of $SO(8)$ which can commute with $SO(3)$ and has no common element with $SO(3)$ except for identity. Therefore $Sp(4)$ is the largest continuous global symmetry.

If we introduce N_f flavors of fermions, it turns out that the emergent symmetry group is $Sp(4N_f)$. We should also include the Lorentz symmetry. Here by Lorentz Group we mean the continuous group $SO(2,1)$, generated by $\gamma_1\gamma_2, \gamma_0\gamma_1, \gamma_0\gamma_2$. Note that the physical lattice rotation is not identical to the rotation element in this emergent Lorentz group. For example, according to Table 2.1, the rotation on lattice

$R_{90} = P_{xy} \circ P_x$ is given by

$$R_{90} = \frac{1}{2}(\gamma_1 - \gamma_2)(\gamma_3 + \gamma_5)\gamma_1 = \frac{1}{2}(1 + \gamma_1\gamma_2)(\gamma_3 + \gamma_5)$$
$$= e^{\frac{\pi}{4}\gamma_1\gamma_2}\frac{1}{\sqrt{2}}(\gamma_3 + \gamma_5) = \text{Dirac } 90^\circ \text{ Rotation } \cdot \frac{1}{\sqrt{2}}(\gamma_3 + \gamma_5) \qquad (2.100)$$

in the continuum limit. We can see that the physical rotation on lattice is a combination of the Dirac rotation and an element in the $Sp(4)$: $\frac{1}{\sqrt{2}}(\gamma_3 + \gamma_5)$. This element actually exchanges γ_3 and γ_5.

We should also include certain discrete symmetries such as time-reversal T, spatial reflections P_x, P_y, P_{xy}, total parity $-\mathbf{1}$ and charge conjugation. But we know that charge conjugation is related to the spin rotation, which is included in the $Sp(4)$; P_{xy} is related to Dirac rotation, P_x and element $\frac{1}{\sqrt{2}}(\gamma_3 + \gamma_5)$ in $Sp(4)$; and $-\mathbf{1}$ is included in $Sp(4)$ as well, namely $e^{i\pi\gamma_3}$. Therefore the full symmetry group of the low energy effective theory for the $SU(2)$-linear state is $Sp(4N_f) \times$ Lorentz Group $\times\, T \times P_x \times P_y$. Such a symmetry group is certainly much larger than the symmetry group of the lattice model. (The effective theory for the $SU(2)$-linear state does contain terms that violate the $Sp(4N_f) \times$ Lorentz Group. But all those terms are irrelevant and have vanishing effects at low energies.)

One can classify the fermion bilinears according to their transformation rules under $Sp(4)$ and Lorentz group. It is convenient to rewrite the 16 bilinears in terms of $\widehat{\tilde{\psi}}$, then in terms of $\widehat{\Psi}$:

$$\overline{\tilde{\psi}}\tilde{\psi} = -\overline{\widehat{\tilde{\psi}}}\widehat{\tilde{\psi}}$$
$$\overline{\tilde{\psi}}\gamma_0\tilde{\psi} = -\overline{\widehat{\tilde{\psi}}}\gamma_0\widehat{\tilde{\psi}}$$
$$\overline{\tilde{\psi}}i\gamma_3\gamma_5\tilde{\psi} = \overline{\widehat{\tilde{\psi}}}i\gamma_3\gamma_5\widehat{\tilde{\psi}}$$
$$\overline{\tilde{\psi}}i\gamma_1\gamma_2\tilde{\psi} = \overline{\widehat{\tilde{\psi}}}i\gamma_1\gamma_2\widehat{\tilde{\psi}}$$
$$\overline{\tilde{\psi}}i\gamma_1\tilde{\psi} = -\overline{\widehat{\tilde{\psi}}}i\gamma_1\widehat{\tilde{\psi}}$$
$$\overline{\tilde{\psi}}i\gamma_2\tilde{\psi} = -\overline{\widehat{\tilde{\psi}}}i\gamma_2\widehat{\tilde{\psi}}$$
$$\overline{\tilde{\psi}}\gamma_0\gamma_1\tilde{\psi} = \overline{\widehat{\tilde{\psi}}}\gamma_0\gamma_1\widehat{\tilde{\psi}}$$

$$
\begin{aligned}
\overline{\tilde{\psi}}\gamma_0\gamma_2\tilde{\psi} &= \overline{\hat{\tilde{\psi}}}\gamma_0\gamma_2\hat{\tilde{\psi}} \\
\overline{\tilde{\psi}}i\gamma_3\tilde{\psi} &= \overline{\hat{\tilde{\psi}}}i\gamma_3\hat{\tilde{\psi}} \\
\overline{\tilde{\psi}}i\gamma_5\tilde{\psi} &= \overline{\hat{\tilde{\psi}}}i\gamma_5\hat{\tilde{\psi}} \\
\overline{\tilde{\psi}}\gamma_0\gamma_3\tilde{\psi} &= -\overline{\hat{\tilde{\psi}}}\gamma_0\gamma_3\hat{\tilde{\psi}} \\
\overline{\tilde{\psi}}\gamma_0\gamma_5\tilde{\psi} &= -\overline{\hat{\tilde{\psi}}}\gamma_0\gamma_5\hat{\tilde{\psi}} \\
\overline{\tilde{\psi}}i\gamma_1\gamma_3\tilde{\psi} &= -\overline{\hat{\tilde{\psi}}}i\gamma_1\gamma_3\hat{\tilde{\psi}} \\
\overline{\tilde{\psi}}i\gamma_2\gamma_5\tilde{\psi} &= -\overline{\hat{\tilde{\psi}}}i\gamma_2\gamma_5\hat{\tilde{\psi}} \\
\overline{\tilde{\psi}}i\gamma_1\gamma_5\tilde{\psi} &= -\overline{\hat{\tilde{\psi}}}i\gamma_1\gamma_5\hat{\tilde{\psi}} \\
\overline{\tilde{\psi}}i\gamma_2\gamma_3\tilde{\psi} &= -\overline{\hat{\tilde{\psi}}}i\gamma_2\gamma_3\hat{\tilde{\psi}}
\end{aligned}
\tag{2.101}
$$

Here if there is no minus sign, it transforms as singlet under spin rotation. If there is a minus sign after the equal sign, it means the fermion bilinear has a σ_3 in spin space, which in turn means the fermion bilinear transforms as triplet under spin rotation. Triplet should have 3 components, but in our 16 bilinears we only included one of them (the one along z-axis). And the other two are fermion bilinears of form $\tilde{\psi}\tilde{\psi}$ and $\tilde{\psi}^\dagger\tilde{\psi}^\dagger$.

One can express all the fermion bilinears in terms of $\widetilde{\Psi}$. In summary, one can organize them as in Table 2.3. Notice that there are 10 conserved currents of $Sp(4)$, so they all have zero anomalous dimension.

In Table 2.3, we enumerate all the fermion bilinears. But what do they correspond to in our original spin model? For example, let us look at a particular fermion bilinear $\overline{\widetilde{\Psi}}\gamma_0\gamma_3 \otimes \mathbf{1} \otimes \boldsymbol{\sigma}\widetilde{\Psi}$. We will show that this term corresponds to the spin triplet bond order: $(-)^{i_y}\mathbf{S}_{\boldsymbol{i}} \times \mathbf{S}_{\boldsymbol{i}+\boldsymbol{x}}$. Let us write this fermion bilinear interaction in terms of the lattice fermion operators in a unit cell ψ_i $(i = 0, 1, 2, 3)$, as shown in Fig.2-2:

$$
H_1 = \overline{\widetilde{\Psi}}\gamma_0\gamma_3 \otimes \mathbf{1} \otimes \boldsymbol{\sigma}\widetilde{\Psi} = \left(\psi_0^\dagger, \psi_1^\dagger, \psi_2^\dagger, \psi_3^\dagger\right) \begin{pmatrix} 0 & -1 & 0 & 0 \\ -1 & 0 & 0 & 0 \\ 0 & 0 & 0 & 1 \\ 0 & 0 & 1 & 0 \end{pmatrix} \begin{pmatrix} \psi_0 \\ \psi_1 \\ \psi_2 \\ \psi_3 \end{pmatrix} \tag{2.102}
$$

Now we can write down the Hamiltonian $H_{\text{SU(2)-linear}} + \theta H_1$ on lattice. For example,

Dirac Scalar (5 elements)	$\bar{\tilde{\Psi}}1\otimes 1\otimes\boldsymbol{\sigma}\tilde{\Psi}$, $\bar{\tilde{\Psi}}i\gamma_3\otimes 1\otimes 1\tilde{\Psi}$, $\bar{\tilde{\Psi}}i\gamma_5\otimes 1\otimes 1\tilde{\Psi}$
Dirac Scalar (1 element)	$\bar{\tilde{\Psi}}i\gamma_3\gamma_5\otimes 1\otimes 1\tilde{\Psi}$
Dirac Vector (30 elements)	$\bar{\tilde{\Psi}}\gamma_0\otimes 1\otimes\boldsymbol{\sigma}\tilde{\Psi}$, $\bar{\tilde{\Psi}}\gamma_0\gamma_3\otimes 1\otimes\boldsymbol{\sigma}\tilde{\Psi}$, $\bar{\tilde{\Psi}}\gamma_0\gamma_5\otimes 1\otimes\boldsymbol{\sigma}\tilde{\Psi}$, $\bar{\tilde{\Psi}}i\gamma_1\gamma_2\otimes 1\otimes 1\tilde{\Psi}$ $\bar{\tilde{\Psi}}i\gamma_1\otimes 1\otimes\boldsymbol{\sigma}\tilde{\Psi}$, $\bar{\tilde{\Psi}}i\gamma_1\gamma_3\otimes 1\otimes\boldsymbol{\sigma}\tilde{\Psi}$, $\bar{\tilde{\Psi}}i\gamma_1\gamma_5\otimes 1\otimes\boldsymbol{\sigma}\tilde{\Psi}$, $\bar{\tilde{\Psi}}\gamma_0\gamma_2\otimes 1\otimes 1\tilde{\Psi}$ $\bar{\tilde{\Psi}}i\gamma_2\otimes 1\otimes\boldsymbol{\sigma}\tilde{\Psi}$, $\bar{\tilde{\Psi}}i\gamma_2\gamma_3\otimes 1\otimes\boldsymbol{\sigma}\tilde{\Psi}$, $\bar{\tilde{\Psi}}i\gamma_2\gamma_5\otimes 1\otimes\boldsymbol{\sigma}\tilde{\Psi}$, $\bar{\tilde{\Psi}}\gamma_0\gamma_1\otimes 1\otimes 1\tilde{\Psi}$

Table 2.3: Under $Sp(4)$ and Lorentz group, all fermion bilinears can be classified into 3 groups. A group of Dirac scalar and $Sp(4)$ 5-dimenion representation, a group of Dirac scalar and $Sp(4)$ singlet, and a group with Dirac vectors in it. For a given group of bilinears, they are connected by $Sp(4)$ transformation in each row, and connected by Lorentz group in each column. Totally there are 36 bilinears. All elements in a given group have the same scaling dimension. In the group of Dirac vector, we actually have conserved current corresponding to each column, totally 10 conserved currents. Those are the conserved $Sp(4)$ currents, and they all have zero anomalous dimension after inclusion of the $SU(2)$ gauge interaction.

the interaction between site-0 and site-1, in terms of f-operator, is

$$i\chi f^\dagger_{0\alpha}f_{1\alpha}+\theta f^\dagger_{0\alpha}\sigma^3_{\alpha\beta}f_{1\beta}+h.c. \tag{2.103}$$

which basically tells us that $\left\langle f^\dagger_{0\uparrow}f_{1\uparrow}\right\rangle = i\chi+\theta$, and $\left\langle f^\dagger_{0\downarrow}f_{1\downarrow}\right\rangle = i\chi-\theta$.

On the other hand, we can write down the spin operator $\mathbf{S}_0\times\mathbf{S}_1$ in terms of f operators. Focusing on the z-component:

$$\begin{aligned}\langle(\mathbf{S}_0\times\mathbf{S}_1)_z\rangle &= -2i\langle(f^\dagger_{0\uparrow}f_{1\uparrow}f^\dagger_{1\downarrow}f_{0\downarrow}-f^\dagger_{0\downarrow}f_{1\downarrow}f^\dagger_{1\uparrow}f_{0\uparrow})\rangle \\ &= -2i\left(\left\langle f^\dagger_{0\uparrow}f_{1\uparrow}\right\rangle\left\langle f^\dagger_{0\downarrow}f_{1\downarrow}\right\rangle^*-\left\langle f^\dagger_{0\downarrow}f_{1\downarrow}\right\rangle\left\langle f^\dagger_{0\uparrow}f_{1\uparrow}\right\rangle^*\right)=-8\chi\theta\neq 0\end{aligned} \tag{2.104}$$

Similarly one can show that $\langle(\mathbf{S}_2\times\mathbf{S}_3)_z\rangle = 8\chi\theta$, and our correspondence is established.

In Table 2.4 we list the correspondence between the field theory operators and original spin operators. From this table we know that ferromagnetic order, triplet VBS order and staggered spin chirality order all have zero anomalous dimension and their correlation function all scale as $\frac{1}{x^4}$ even after the inclusion of the $SU(2)$ gauge interaction. We also know that the Neel order and VBS order have the same anomalous dimension which turns out to be non-zero after inclusion of the $SU(2)$ gauge interaction. We noticed that the same $Sp(4)$ emergent group for π-flux state

Dirac Scalar	$\bar{\tilde{\Psi}}\mathbf{1}\otimes\mathbf{1}\otimes\boldsymbol{\sigma}\tilde{\Psi}$	Neel Order: $(-)^i\mathbf{S}_i$
	$\bar{\tilde{\Psi}}i\gamma_3\otimes\mathbf{1}\otimes\mathbf{1}\tilde{\Psi}$	VBS: $(-)^{i_y}\mathbf{S}_i\cdot\mathbf{S}_{i+x}$
	$\bar{\tilde{\Psi}}i\gamma_5\otimes\mathbf{1}\otimes\mathbf{1}\tilde{\Psi}$	VBS: $(-)^{i_x}\mathbf{S}_i\cdot\mathbf{S}_{i+y}$
Dirac Scalar	$\bar{\tilde{\Psi}}i\gamma_3\gamma_5\otimes\mathbf{1}\otimes\mathbf{1}\tilde{\Psi}$	Uniform Spin Chirality: $\mathbf{S}_i\cdot(\mathbf{S}_{i+x}\times\mathbf{S}_{i+x+y})$
Dirac Vector	$\bar{\tilde{\Psi}}\gamma_0\otimes\mathbf{1}\otimes\boldsymbol{\sigma}\tilde{\Psi}$	Ferromagnetic Order: $\mathbf{S}_i$
	$\bar{\tilde{\Psi}}\gamma_0\gamma_3\otimes\mathbf{1}\otimes\boldsymbol{\sigma}\tilde{\Psi}$	Triplet VBS Order: $(-)^{i_y}\mathbf{S}_i\times\mathbf{S}_{i+x}$
	$\bar{\tilde{\Psi}}\gamma_0\gamma_5\otimes\mathbf{1}\otimes\boldsymbol{\sigma}\tilde{\Psi}$	Triplet VBS Order: $(-)^{i_x}\mathbf{S}_i\times\mathbf{S}_{i+y}$
	$\bar{\tilde{\Psi}}i\gamma_1\gamma_2\otimes\mathbf{1}\otimes\mathbf{1}\tilde{\Psi}$	Staggered Spin Chirality: $(-)^i\mathbf{S}_i\cdot(\mathbf{S}_{i+x}\times\mathbf{S}_{i+x+y})$

Table 2.4: The correspondence between fermion field operators and original spin operators. In the group of Dirac vector, only the density components of each current is presented, since the other components correspond to the flow of these densities. From this table, we know that ferromagnetic order, triplet VBS order and staggered spin chirality order all have zero anomalous dimension and their correlation functions all scale as $\frac{1}{x^4}$. We also know that the Neel order and VBS order have same anomalous dimension.

which rotates Neel order into VBS order was found[42] when ignoring the $SU(2)$ gauge field effect.

Here we should mention the work done by Hermele et.al[43], where the $U(1)$-linear spin liquid was discussed and the emergent symmetry is $SU(4)$, and similar classification of totally 64 fermion bilinears was done. One can recover their result from our formalism. From our formulation of $SU(2)$-linear phase, the $U(1)$-linear phase can be regarded as a Higgs phase where $SU(2)$ gauge field is broken down to $U(1)$. Let us assume the remaining $U(1)$-gauge symmetry is along τ_3 direction. The only things one should add to recover their result are: first the gauge invariant transformations not only include those in Eq.(2.98); we should also include

$$\gamma_3\otimes\tau_3\otimes\mathbf{1},\gamma_5\otimes\tau_3\otimes\mathbf{1},i\gamma_3\gamma_5\otimes\tau_3\otimes\boldsymbol{\sigma}. \tag{2.105}$$

So totally 15 elements, and they form a $SU(4)$ algebra. Secondly the bilinear with a τ_3 in the gauge sector is also gauge invariant, as shown in Table 2.5.

2.5.7 The effect of $SU(2)$ gauge interaction on $SU(2)$-linear spin liquid

We know that in the continuous limit, the full lagrangian should be Eq.(2.40). The question is, will the $SU(2)$ gauge interaction change the low energy behavior of mean-field theory drastically? The answer is complicated. There are two main concerns:

Dirac Scalar (15 elements)	$\bar{\tilde{\Psi}}1\otimes 1\otimes\sigma\tilde{\Psi}$, $\bar{\tilde{\Psi}}i\gamma_3\otimes 1\otimes 1\tilde{\Psi}$, $\bar{\tilde{\Psi}}i\gamma_5\otimes 1\otimes 1\tilde{\Psi}$ $\bar{\tilde{\Psi}}1\otimes\tau_3\otimes 1\tilde{\Psi}$, $\bar{\tilde{\Psi}}i\gamma_3\otimes\tau_3\otimes\sigma\tilde{\Psi}$, $\bar{\tilde{\Psi}}i\gamma_5\otimes\tau_3\otimes\sigma\tilde{\Psi}$ $\bar{\tilde{\Psi}}i\gamma_3\gamma_5\otimes\tau_3\otimes\sigma\tilde{\Psi}$
Dirac Scalar (1 element)	$\bar{\tilde{\Psi}}i\gamma_3\gamma_5\otimes 1\otimes 1\tilde{\Psi}$
Dirac Vector (45 elements)	$\bar{\tilde{\Psi}}\gamma_0\otimes 1\otimes\sigma\tilde{\Psi}$, $\bar{\tilde{\Psi}}\gamma_0\gamma_3\otimes 1\otimes\sigma\tilde{\Psi}$, $\bar{\tilde{\Psi}}\gamma_0\gamma_5\otimes 1\otimes\sigma\tilde{\Psi}$, $\bar{\tilde{\Psi}}i\gamma_1\gamma_2\otimes 1\otimes 1\tilde{\Psi}$ $\bar{\tilde{\Psi}}i\gamma_1\otimes 1\otimes\sigma\tilde{\Psi}$, $\bar{\tilde{\Psi}}i\gamma_1\gamma_3\otimes 1\otimes\sigma\tilde{\Psi}$, $\bar{\tilde{\Psi}}i\gamma_1\gamma_5\otimes 1\otimes\sigma\tilde{\Psi}$, $\bar{\tilde{\Psi}}\gamma_0\gamma_2\otimes 1\otimes 1\tilde{\Psi}$ $\bar{\tilde{\Psi}}i\gamma_2\otimes 1\otimes\sigma\tilde{\Psi}$, $\bar{\tilde{\Psi}}i\gamma_2\gamma_3\otimes 1\otimes\sigma\tilde{\Psi}$, $\bar{\tilde{\Psi}}i\gamma_2\gamma_5\otimes 1\otimes\sigma\tilde{\Psi}$, $\bar{\tilde{\Psi}}\gamma_0\gamma_1\otimes 1\otimes 1\tilde{\Psi}$ $\bar{\tilde{\Psi}}\gamma_0\gamma_3\otimes\tau_3\otimes 1\tilde{\Psi}$, $\bar{\tilde{\Psi}}\gamma_0\gamma_5\otimes\tau_3\otimes 1\tilde{\Psi}$, $\bar{\tilde{\Psi}}i\gamma_1\gamma_2\otimes\tau_3\otimes\sigma\tilde{\Psi}$ $\bar{\tilde{\Psi}}i\gamma_1\gamma_3\otimes\tau_3\otimes 1\tilde{\Psi}$, $\bar{\tilde{\Psi}}i\gamma_1\gamma_5\otimes\tau_3\otimes 1\tilde{\Psi}$, $\bar{\tilde{\Psi}}\gamma_0\gamma_2\otimes\tau_3\otimes\sigma\tilde{\Psi}$ $\bar{\tilde{\Psi}}i\gamma_2\gamma_3\otimes\tau_3\otimes 1\tilde{\Psi}$, $\bar{\tilde{\Psi}}i\gamma_2\gamma_5\otimes\tau_3\otimes 1\tilde{\Psi}$, $\bar{\tilde{\Psi}}\gamma_0\gamma_1\otimes\tau_3\otimes\sigma\tilde{\Psi}$
Dirac Vector (3 elements)	$\bar{\tilde{\Psi}}i\gamma_0\otimes\tau_3\otimes 1\tilde{\Psi}$, $\bar{\tilde{\Psi}}i\gamma_1\otimes\tau_3\otimes 1\tilde{\Psi}$, $\bar{\tilde{\Psi}}i\gamma_2\otimes\tau_3\otimes 1\tilde{\Psi}$

Table 2.5: Under $SU(4)$ and Lorentz group, the total 64 bilinears can be classified into 4 groups: A group of Dirac scalars and $SU(4)$ adjoint representation with 15 elements, a group of Dirac scalar and $SU(4)$ singlet with one element, a group of Dirac vectors and $SU(4)$ 12-dimension representation with $3\times 15 = 45$ elements, and group of Dirac vectors and $SU(4)$ singlets with 3 elements.

spontaneous chiral symmetry breaking (SCSB) and confinement. SCSB means that fermion mass is generated dynamically. And confinement means that no excitation with gauge charge can show up in the spectrum, and gauge interaction is linearly confining. If any of these happens, the low energy behavior of the system is changed drastically and we say that the mean-field state is unstable under gauge fluctuation. In this case, the mean-field $SU(2)$-linear state does not lead to a stable algebraic spin liquid. (Actually, we do not know the low energy properties of the model beyond the mean-field theory.)

This problem is a famous and difficult problem in QCD, since both effects are non-perturbative. And these two effects are related: if there is a mass gap generated for the fermion, then below the mass gap there is effectively no fermion to screen the gauge interaction and we only have pure gauge field. We know that pure gauge interaction is confining. So logically SCSB will induce confinement. The other way, whether confinement will induce SCSB, is not clear yet.

Usually it is believed that for a $SU(N)$ gauge theory coupled to N_f flavor of massless fermions, there is a critical N_f^c[44, 45, 46]. If N_f is smaller than N_f^c, the system have both SCSB and confinement. However if N_f is larger than N_f^c, there is

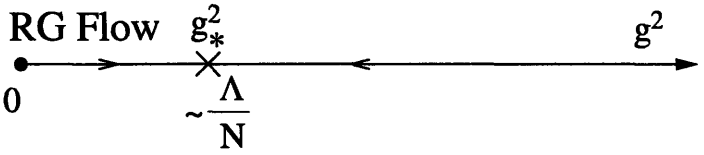

Figure 2-4: The fixed point of many Dirac fermions coupling to $SU(2)$ gauge field

a conformal invariant IR fixed point.

In particular, in 2+1 dimension, QCD always has a stronger interaction at low energies. But if N_f is large enough, the fermion screening effect is dominant and the renormalization group flow will terminate at an IR fixed point $g_*^2 \sim \frac{1}{N_f}$. The low energy behavior is governed by that fixed point, which is deconfined and has no SCSB. When $N_f \to \infty$, $g_* \to 0$, we are in the perturbative region.

To have a quantitative study, we need work within large N_f limit[47]. Before we study the $SU(2)$ gauge fluctuation, it is worthwhile to mention the $U(1)$ case[23]. The main result there was that in the large N_f expansion, the model remains gapless and the spin-spin correlation function is a power law with an anomalous dimension γ. This anomalous dimension γ is calculable in large N_f expansion, and up to the $1/N_f$ (leading) order, γ is found to be $-\frac{32}{3\pi^2 N_f}$.

Now we look at the $SU(2)$ case in detail. We will study the $SU(2)$-linear state in particular. The low energy effective theory is Eq.(2.40). Technically there are two ways to do large-N_f limit. The first way is a complete renormalization group analysis. To have an controlled calculation, one first does an ϵ-expansion, then studies the renormalization group flow, finds out the IR fixed point, and the scaling dimension of operators at that fixed point, finally sets N_f to be large. This way is generally accepted and the result is thought to be reliable. However the calculation is complicated.

Here we do the large-N_f calculation in a different way[47]. Taking large-N_f limit:

$$N_f \to \infty, \quad N_f g^2 \to \text{const.} \tag{2.106}$$

The fermion contribution to any physical quantity can be expanded in $\frac{1}{N_f}$ systematically. This is just a way to organize the summation of Feynman diagrams. For example, the leading order term usually corresponds to summation of fermion one-loop diagrams. The IR fixed point can be found by cancellation of leading correction to scaling. We will discuss this in detail soon. Here we want to discuss whether this approach and the first approach are equivalent. There is no general proof that these two approaches are equivalent, but in [47] quite a lot of examples are presented and it

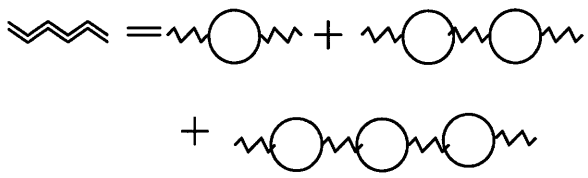

Figure 2-5: Gauge propagator at leading order of $1/N_f$ expansion

was found that these two approaches are equivalent, for example, in the case of Dirac fermions coupling to $U(1)$ gauge field, the scaling dimension and fixed point found in the two approaches are consistent. Gracey et al.[48, 49] calculated large-N_f expansion of anomalous dimensions of many quantities in QED_3 and QCD_3, including fermion mass, which is gauge invariant. Then they compared the results with results from usual MS renormalization+dimensional regularization, and found they are consistent.

First let us take a look at the gauge interaction. From Eq.(2.106), g^2 is of order $\frac{1}{N_f}$. In Figure 2-5, all leading order contributions to gauge propagator are summed together. The double line represents the leading order dressed gauge propagator.

One can calculate the gauge-gauge two point function in Fig.2-5. The result is:

$$-\frac{1}{2g^2}A^a_\mu(k^2\delta_{\mu\nu}-k_\mu k_\nu)A^a_\nu - N_f\mathrm{Tr}\mathbf{1}\mathrm{Tr}(\tau^a\tau^b)A^a_\mu(k^2\delta_{\mu\nu}-k_\mu k_\nu)\left(\frac{1}{64k}-\frac{1}{48\pi\Lambda}\right)A^b_\nu \tag{2.107}$$

Here $\mathbf{1}$ is the identity matrix in Dirac spinor space. In our $SU(2)$-linear example, $\mathrm{Tr}\mathbf{1}=4$. And τ^a are usual $SU(2)$ Pauli matrices. Note that the term $\frac{1}{64k}$ is independent of regularization scheme, but $-\frac{1}{48\pi\Lambda}$ is dependent. In different regularization schemes, the coefficients in front of $\frac{1}{\Lambda}$ are different. The result here $-\frac{1}{48\pi\Lambda}$ is from the Pauli-Villar regularization.

One immediately sees that at low energy ($k\to 0$), the term $\frac{1}{64k}$ dominates. The low energy two point function of gauge field is:

$$N_f\mathrm{Tr}\mathbf{1}\frac{1}{2}A^a_\mu(k^2\delta_{\mu\nu}-k_\mu k_\nu)\frac{1}{64k}A^a_\nu = A^a_\mu\frac{N_f}{32k}(k^2\delta_{\mu\nu}-k_\mu k_\nu)A^a_\nu \tag{2.108}$$

The IR fixed point is found by cancellation of the leading correction to scaling. Here it means that the $-\frac{1}{2g^2}$ term and the $-\frac{1}{48\pi\Lambda}$ term should cancel:'

$$\frac{1}{2g_*^2}=\frac{N_f\mathrm{Tr}\mathbf{1}}{2}\frac{1}{48\pi\Lambda} \qquad \Rightarrow \qquad g_*^2=\frac{12\pi\Lambda}{N_f} \tag{2.109}$$

The dimensionless coupling g^*/Λ describes the strength of gauge interaction at the energy scale Λ. We see that dimensionless coupling $g^*/\Lambda \to 0$ as the cut-off energy scale $\Lambda \to 0$ and $N_f \to \infty$, as we expected in the renormalization group flow diagram Fig. 2-4. Remember that if the number of flavors of fermions is small, confinement will happen, renormalization group flow will go to some fixed point of $g_*^2/\Lambda \sim 1$ as $\Lambda \to 0$ and perturbation theory breaks down. The message is that the fermion screening effect in our large N_f model drives the gauge interaction to weak limit at low energies.

From Eq.(2.107), we know that the gauge field remains massless, and in deconfined phase. So the $SU(2)$-linear state is also stable under gauge fluctuation. We can also see that the scaling dimension of gauge field A is $d_A = 1$ at leading order. With $1/N_f$ correction, we expect to have $d_A = 1 + O\left(\frac{1}{N}\right)$. Now we can understand why the fixed point g_*^2 is IR stable. Suppose we are slightly away from the fixed point:

$$L = \sum_{i=1}^{N_f} \bar{\psi}_i \left(\partial_\mu - i a_\mu^l \tau^l\right) \gamma_\mu \psi_i + \frac{1}{2g_*^2} \mathrm{Tr}\left[f_{\mu\nu}^l f_{\mu\nu}^l\right] + \delta g \mathrm{Tr}\left[f_{\mu\nu}^l f_{\mu\nu}^l\right] \tag{2.110}$$

By power counting, the scaling dimension of δg is $4 + O(\frac{1}{N_f})$, so it is irrelevant. Therefore at low energy δg flows to zero and g_*^2 is IR stable.

In the above discussion, we have shown that the $SU(2)$-linear mean-field state is stable under fermion self-interaction and gauge fluctuation in large N_f limit. So it is a stable phase. Here by "stable" we mean that the low energy behavior does not change drastically from mean-field result. When $N_f = \infty$ we are back to the mean-field result, but if N_f large but finite, the low energy behavior is changed from the mean-field result, but not drastically. Below we will see what this change is.

2.6 Spin-spin correlation function in $SU(2)$-linear phase

In this section we investigate the spin-spin correlation function. In a frustrated spin liquid, there is always a strong trend to antiferromagnetic long range order. To describe this trend, we can calculate the staggered spin-spin correlation function in fermion $\tilde{\psi}$ formalism:

$$\langle (-1)^x S^z(x) S^z(0) \rangle = \frac{1}{64} \left(\langle \bar{\tilde{\psi}} \tilde{\psi}(x) \bar{\tilde{\psi}} \tilde{\psi}(0) \rangle - \langle \bar{\tilde{\psi}} \tilde{\psi} \rangle^2 \right) \tag{2.111}$$

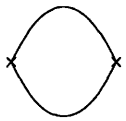

Figure 2-6: Spin-spin correlation function at zeroth order. Cross means spin operator insertion.

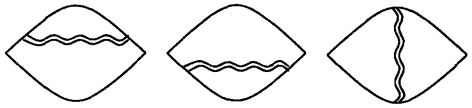

Figure 2-7: Contribution to spin-spin correlation function at order of $\frac{1}{N_f}$

Here $\tilde{\psi}$ is actually an 8-component fermion operator, with both spinor indices and $SU(2)$ gauge indices.

One can see that in field theory language, staggered spin-spin correlation function is nothing but the mass operator correlation function. At zeroth order, we have the free fermion Feynman diagram (Fig. 2-6). The staggered spin-spin correlation function in momentum space at zeroth order is

$$< S_s^z(q) S_s^z(-q) \rangle_0 = -\frac{1}{64} \int \frac{dp^3}{(2\pi)^3} \mathrm{Tr}\left[G_{\alpha\beta}(p) G_{\beta\alpha}(q-p)\right] = -\frac{\sqrt{q_0^2+\vec{q}^2}}{128} \qquad (2.112)$$

The first order in $\frac{1}{N_f}$ expansion involves diagrams in Fig.2-7. Note that the double line represents the dressed gauge field propagator:

$$D_{\mu\nu}^{ab} = \frac{16}{N_f} \frac{1}{k} \left(\delta_{\mu\nu} - \frac{k_\mu k_\nu}{k^2}\right) \delta^{ab} \qquad (2.113)$$

These diagrams will give the spin-spin correlation function an anomalous dimension. According to Eq.(2.112), the spin-spin correlation function in momentum space scales like $\sim |k|$. With $1/N_f$ correction, the correlation function scales like $\sim |k|^{1+2\gamma}$. Here γ is called the anomalous dimension. The contributions from the three diagrams in Fig.2-7 give (See Appendix A):

$$\gamma = -\frac{16}{\pi^2 N_f} \qquad (2.114)$$

We see that in the SU(2)-linear state, spin-spin correlation function remains gapless and algebraic, but the scaling dimensions of physical operators, for example spin operator, are unusual due to the gapless gauge interaction. Actually there is no

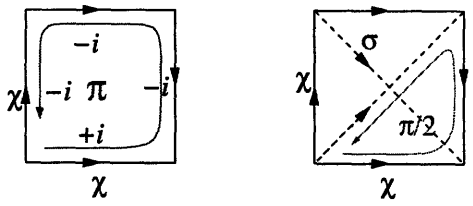

Figure 2-8: $SU(2)$-linear phase$SU(2)$-chiral phase

quasi-particle in this phase.

2.7 Phase transition between spin liquids

2.7.1 Phase transition between $SU(2)$-linear phase and $SU(2)$-chiral phase

The effective field theory for phase transition

In this section we study the phase transition between $SU(2)$-linear phase (A in phase diagram Fig.2-1) and $SU(2)$-chiral phase (D in Fig.2-1).

We have argued that the $SU(2)$-linear state is a stable phase. What about the $SU(2)$-chiral state in Eq.(2.25)? One can check that the fermion spectrum is gapped at mean-field level. As for gauge field, because time-reversal symmetry is broken in the $SU(2)$-chiral state, a Chern-Simons term is generated after integrating out the fermions. And that will also give gauge field a mass gap. So the $SU(2)$-chiral state is a fully gapped state. We know quantum fluctuation cannot kill a gapped system perturbatively, so $SU(2)$-chiral state is also a stable phase.

Now we have two stable phases. According to phase diagram Fig.2-1, there is a phase transition between the two phases around $J_2 = 0.35$. It also seems that the energies of the two phases connect smoothly on the same diagram, which indicates the phase transition may be continuous. We will study this phase transition in this section.

Fig.2-8 shows the plot of the ansatzs of the two phases on lattice. Our notation

here is

$$\begin{array}{ll} SU(2)\text{-linear phase:} & SU(2)\text{-chiral phase:} \\ & u_{i,i+x} = i\chi, \\ u_{i,i+x} = i\chi, & u_{i,i+y} = i\chi(-)^{i_x}, \\ u_{i,i+y} = i(-)^{i_x}\chi. & u_{i,i+x+y} = -i\sigma(-)^{i_x}, \\ & u_{i,i+x-y} = i\sigma(-)^{i_x}. \end{array} \tag{2.115}$$

In Fig.2-8, we also show the phases one fermion gains after hopping around a plaquette. In $SU(2)$-linear case, this phase for the square plaquette is π; while in $SU(2)$-chiral case, this phase for the triangle plaquette is $\frac{\pi}{2}$. Those phases indicate the fluxes through the plaquettes. After a time-reversal transformation, the flux will change sign. For $SU(2)$-linear case, we have $-\pi$ flux, and $-\pi$ differs from π by 2π, thus equivalent. This indicates the $SU(2)$-linear phase respects time-reversal symmetry. However for the $SU(2)$-chiral phase, we have $-\frac{\pi}{2}$, which is physically different from $\frac{\pi}{2}$. So the $SU(2)$-chiral phase breaks time-reversal symmetry and the parity symmetry. Other than that, one can show that $SU(2)$-chiral phase has full translation and rotation symmetry:

$$\text{Physical symmetry of } SU(2)\text{-chiral phase} = \{T_x, T_y, R_{90^\circ}, C\} \tag{2.116}$$

The two phases involved in the phase transition, $SU(2)$-linear and $SU(2)$-chiral states, have different PSGs, because even their physical symmetries are different. The phase transition breaks time-reversal symmetry.

The low energy physics at mean-field level of the systems can be derived by taking the lattice model into continuous limit:

$$SU(2)\text{-linear phase: } L_{mean} = \bar{\psi}\partial_\mu\gamma_\mu\psi \tag{2.117}$$

$$SU(2)\text{-chiral phase: } L_{mean} = \bar{\psi}\partial_\mu\gamma_\mu\psi + \sigma\bar{\psi}[i\gamma_3\gamma_5]\psi \tag{2.118}$$

To save notation, we dropped the tilde above the fermion operator ψ.

Here we see that the σ boson field is driving the phase transition. In $SU(2)$-linear phase, $\langle\sigma\rangle = 0$; in $SU(2)$-chiral phase, $\langle\sigma\rangle \neq 0$. Therefore to understand the phase transition, we need to know the dynamics of the σ field. Let us include quantum

fluctuations of all fields, the low energy effective theory is:

$$L = \sum_{i=1}^{N_f} \bar{\psi}_i \left(\partial_\mu - i a_\mu^l \tau^l\right) \gamma_\mu \psi_i + \frac{1}{2g^2} \mathrm{Tr}\left[f_{\mu\nu}^l f_{\mu\nu}^l\right] + \sigma \bar{\psi} [i\gamma_3\gamma_5] \psi + \frac{1}{2\rho^2} (\partial_\mu \sigma)^2 + V(\sigma) \tag{2.119}$$

Here to have a controlled calculation, we again introduced N_f flavors of fermion. The first line is the Dirac fermion coupling to $SU(2)$ gauge field. The second line is the coupling between the fermion and σ boson, and the dynamics of σ boson field. The potential $V(\sigma)$ is not known yet. Nevertheless we know in $SU(2)$-linear phase, the dynamics of σ boson gives $\langle\sigma\rangle = 0$; while in $SU(2)$-chiral phase, $\langle\sigma\rangle \neq 0$, and the time-reversal symmetry is broken. This is similar to the usual formalism of the phase transition of symmetry breaking, except for the fact that we have gauge field involved here.

The correct effective theory from PSG consideration

Eq. (2.119) is the effective Lagrangian for both phases. What is the symmetry that the lagrangian should respect? It should respect the full symmetry of the lattice model. Before the symmetry breaking the $SU(2)$-linear phase has a symmetry described by the $SU(2)$-linear PSG. Thus, the effective theory for the phase transition should respect the symmetry described by the $SU(2)$-linear PSG.

We have shown that, under the $SU(2)$-linear PSG, the fermion bilinears transform in the way described by Table 2.2. For example, the transformation P_x^{PSG}:

$$P_x^{PSG} : i\bar{\psi}[\gamma_3\gamma_5]\psi \to -i\bar{\psi}[\gamma_3\gamma_5]\psi \tag{2.120}$$

and

$$P_x^{PSG} : \sigma \to -\sigma \tag{2.121}$$

In fact, σ is the average of $i\bar{\psi}[\gamma_3\gamma_5]\psi$ and transforms in the same way as $i\bar{\psi}[\gamma_3\gamma_5]\psi$ under the $SU(2)$-linear PSG (see Table 2.2), thus the term $\sigma\bar{\psi}[i\gamma_3\gamma_5]\psi$ is invariant under the full $SU(2)$-linear PSG. We also see that the other three possible couplings $\sigma\bar{\psi}\psi$, $\sigma\bar{\psi}\gamma_0\psi$, and $\sigma\bar{\psi}\gamma_1\gamma_2\psi$ are not invariant under the $SU(2)$-linear PSG and hence are not allowed the effective theory.

Similarly, the potential $V(\sigma)$ should also respect $\sigma \to -\sigma$ symmetry and take a

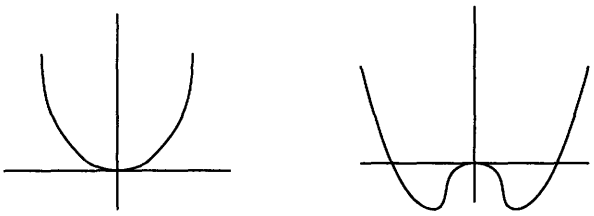

Figure 2-9: The behavior of potential $V(\sigma)$ before(left) and after(right) the phase transition from $SU(2)$-linear phase to $SU(2)$-chiral phase.

form

$$V(\sigma) = \frac{m^2}{2}\sigma^2 + \lambda\sigma^4 \tag{2.122}$$

up to quartic order. There is no cubic term since it breaks the P_x^{PSG}.

Here we see that PSG tells us the correct form of low energy effective theory:

$$\begin{aligned} L = &\sum_{i=1}^{N_f} \bar{\psi}_i \left(\partial_\mu - i a_\mu^l \tau^l\right) \gamma_\mu \psi_i + \frac{1}{2g^2}\mathrm{Tr}\left[f_{\mu\nu}^l f_{\mu\nu}^l\right] \\ &+ \sigma\bar{\psi}[i\gamma_3\gamma_5]\psi + \frac{1}{2\rho^2}(\partial_\mu\sigma)^2 + \frac{m^2}{2}\sigma^2 + \lambda\sigma^4 \end{aligned} \tag{2.123}$$

At the mean-field level, we already have the picture for this phase transition, as shown in Fig. 2-9. We see that when $m^2 > 0$, $\langle\sigma\rangle = 0$, we are in the $SU(2)$-linear phase; when $m^2 < 0$, $\langle\sigma\rangle \neq 0$, we are in the $SU(2)$-chiral phase. $m^2 = 0$ is the phase transition point.

At this level the phase transition is second-order, $\langle\sigma\rangle$ changes continuously from zero to nonzero. The next question is, will this transition be second-order after including quantum fluctuations?

The T breaking phase transition does not belong to the Ising class

To answer the above question, we need to count the number of relevant coupling constants at the phase transition fixed point in the renormalization group sense. If there is only one relevant coupling m^2, that means the phase transition is indeed second-order, and $m^2 = 0$ is the critical point.

We can estimate the scaling dimension d_σ of σ field. In tree level, power counting gives us $d_\sigma = \frac{1}{2}$. But in large-N_f limit, the fermion dressing changes d_σ strongly. The leading order σ propagator in $\frac{1}{N_f}$ expansion is shown in Fig.2-10. the σ boson two

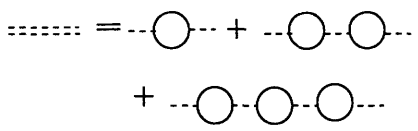

Figure 2-10: The leading order σ boson propagator in $\frac{1}{N_f}$ expansion

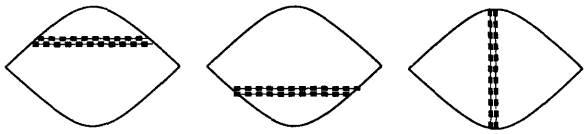

Figure 2-11: σ boson contribution to spin-spin correlation function at critical point at the first order of $\frac{1}{N_f}$ expansion

point function at leading order is

$$\frac{N_f}{16}\sigma\sqrt{\partial^2}\sigma \tag{2.124}$$

which indicates that the scaling dimension $d_\sigma = 1 + O(\frac{1}{N_f})$. Therefore the scaling dimension of $(\partial\sigma)^2$ and σ^4 are both $4 + O(\frac{1}{N_f})$, which is larger than space-time dimension 3 and thus irrelevant. As for the gauge coupling g, the argument in the end of section 2.5.7 is still valid. So δg is also irrelevant. Now we can safely say that the only relevant coupling is $\frac{m^2}{2}\sigma^2$, whose scaling dimension is $2 + O(\frac{1}{N_f})$.

We can calculate the scaling behavior at the critical point where σ boson is also massless. For example, we again compute the staggered spin-spin correlation function. At the critical point, apart from the contribution from massless gauge field in Fig.2-7, we have the contribution from massless σ boson in Fig.2-11 as well.

So at the critical point, the staggered spin-spin correlation function not only receives an anomalous dimension from gauge field $\gamma = -\frac{16}{\pi^2 N_f}$ (Eq.(2.114)), but also receives an anomalous dimension from the gapless σ boson γ'. Detailed calculation shows that at order of $\frac{1}{N_f}$, $\gamma' = \frac{4}{3\pi^2 N_f}$ (See Appendix A).

The total anomalous dimension γ_{total} is the sum of γ and γ':

$$\gamma_{total} = \gamma + \gamma' = -\frac{44}{3\pi^2 N_f} \tag{2.125}$$

Fig.2-12 shows the change of scaling dimension of staggered spin-spin correlation function during the phase transition. Note that in terms of symmetry breaking, this phase transition is quite normal: it simply breaks the time-reversal, which is

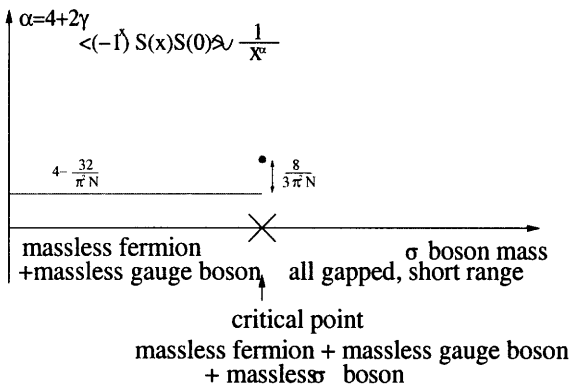

Figure 2-12: Change of scaling dimension of staggered spin-spin correlation function during phase transition

a Z_2-like symmetry. In our usual understanding of phase transition, the Landau-Ginzburg paradigm, the symmetry determines the universality of the phase transition. Therefore our usual understanding for this phase transition should be a Z_2-like or Ising-like phase transition. However, our study shows it is not the case. Although the phase transition is characterized by the breaking of a Z_2-like symmetry, it is obviously not Ising-like. For example, an Ising like transition is gapless only at the critical point, whereas in our transition the $SU(2)$-linear phase is also gapless. The scaling behavior is very different from the Ising-universality. Actually with different value of N_f, the scaling exponent can have infinite number of values, which indicates infinite number of universalities.

The above discussion is at zero temperature, but in experiments, people can only measure the system at finite temperature. What people can see in experiments actually should be crossover behavior between disordered phase and quantum critical region, as shown in Fig.2-13.

2.7.2 Phase transition between $SU(2)$-linear phase and Z_2-linear phase.

Z_2-linear phase.

In this section we study the phase transition between $SU(2)$-linear phase (A in phase diagram Fig.2-1) and Z_2-linear phase (G in Fig.2-1). The following is the ansatz of the Z_2-linear state (Fig.2-14).

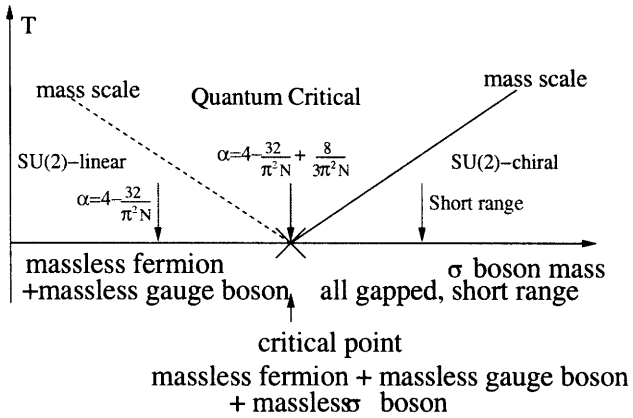

Figure 2-13: At finite temperature T, system shows crossover behavior between $SU(2)$-linear phase and quantum critical region (dashed line). But the $SU(2)$-chiral phase and quantum critical region are still separated by a phase transition since there is a physical symmetry breaking (solid line).

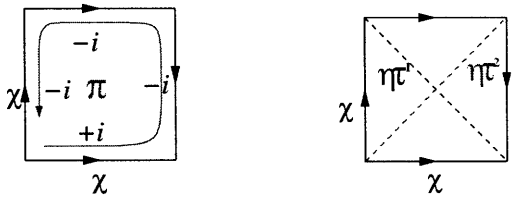

Figure 2-14: $SU(2)$-linear phaseZ_2-linear phase

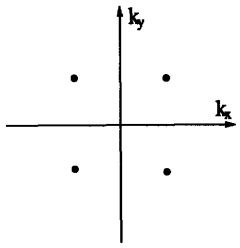

Figure 2-15: The 4 fermi points of Z_2-linear state

$$\begin{aligned} u_{i,i+x} &= i\chi, \\ u_{i,i+y} &= i(-)^{i_x}\chi \\ u_{i,i+x+y} &= \eta\tau^1, \\ u_{i,i-x+y} &= \eta\tau^2. \end{aligned} \tag{2.126}$$

The fermion energy spectrum of Z_2-linear state at mean-field level is characterized by 4 fermi points as shown in Fig.2-15.

The low energy effective theory is the massless fermion coupling to Z_2 gauge field. At mean-field level where we do not include gauge fluctuation yet, after taking continuous limit, we have

$$L_{mean} = \bar{\psi}\partial_\mu\gamma_\mu\psi + \bar{\psi}\left[\eta\tau^1 i\gamma_1\gamma_5 + \eta\tau^2 i\gamma_2\gamma_3\right]\psi \tag{2.127}$$

Once again we need to argue that the Z_2-linear state is a stable phase. Here by stable we still mean that the low energy behavior is not changed after including quantum fluctuations. Similar to what we did in Section 2.5, we can discuss the stability of Z_2-linear state.

Through a PSG analysis we can show that the fermion bilinear term is not allowed and the fermions remain massless after including quantum fluctuation[27]. Therefore the PSG protects the masslessness of fermion in the Z_2-linear state. In addition, Z_2 gauge fluctuation is always gapped. For pure Z_2 gauge theory on lattice in 2+1 dimension, it can be in deconfined phase or confined phase[50]. Here we have massless fermion coupling to Z_2 gauge field, fermion dressing effect should drive the system even more likely to be deconfined. We assume that the gauge field is deconfined, then the gapped Z_2 gauge fluctuation should be irrelevant. Therefore Z_2-linear state is also a stable phase.

In Eq.(2.127), $\eta\tau^1$ and $\eta\tau^2$ describe the fluxes through the red and blue triangle plaquettes in Fig.2-14. Since the two fluxes are not colinear, the $SU(2)$ gauge group

breaks down to Z_2 gauge group. In Eq.(2.127), one can say that the η field is driving the phase transition. When $\langle\eta\rangle = 0$, we go back to $SU(2)$-linear phase, and when $\langle\eta\rangle \neq 0$, we are in Z_2-linear phase.

We notice that η field is not gauge invariant. After a local $SU(2)$ gauge transformation, the direction of τ^1 and τ^2 in Eq.(2.127) will be rotated. Thus we should use a vector field $\vec{n}$ to describe the fluctuations of η. Furthermore, since the η in front of $\gamma_1\gamma_5$ and the η in front of $\gamma_2\gamma_3$ should be able to fluctuate independently, we should have two vector fields, say $\vec{n}_1$ and $\vec{n}_2$, to describe them. So the gauge invariant way to write Eq.(2.127) would be:

$$L_{mean} = \bar{\psi}\partial_\mu\gamma_\mu\psi + \bar{\psi}\left[(\vec{n}_1\cdot\vec{\tau})\, i\gamma_1\gamma_5 + (\vec{n}_2\cdot\vec{\tau})\, i\gamma_2\gamma_3\right]\psi \tag{2.128}$$

where $\vec{n}_1$ and $\vec{n}_2$ transform as the adjoint representation of $SU(2)$ gauge group. Now we include dynamics of $\vec{n}$ fields. To have controlled calculation, we introduce N_f flavors of fermions, too. The following is the low energy effective theory of the system:

$$\begin{aligned} L = &\sum_{i=1}^{N_f} \bar{\psi}_i\partial_\mu\gamma_\mu\psi_i + \frac{1}{2\kappa^2}\left((D_\mu\vec{n}_1)^2 + (D_\mu\vec{n}_2)^2\right) \\ &+ \sum_{i=1}^{N_f} \bar{\psi}_i\left[(\vec{n}_1\cdot\vec{\tau})\, i\gamma_1\gamma_5 + (\vec{n}_2\cdot\vec{\tau})\, i\gamma_2\gamma_3\right]\psi_i + V(\vec{n}_1,\vec{n}_2) \end{aligned} \tag{2.129}$$

where D_μ is the covariant derivative of $SU(2)$ gauge theory, and the form of potential $V(\vec{n}_1,\vec{n}_2)$ is unknown yet. The phase transition is described by a Higgs mechanism, $\vec{n}_1$ and $\vec{n}_2$ are Higgs bosons. When $\langle\vec{n}_1\rangle = \langle\vec{n}_2\rangle = 0$, we are in the $SU(2)$-linear phase; when $\langle\vec{n}_1\rangle \neq 0$, $\langle\vec{n}_2\rangle \neq 0$ and $\langle\vec{n}_1\rangle \perp \langle\vec{n}_2\rangle$, we are in the Z_2-linear phase.

The low energy effective theory from PSG consideration

What is the symmetry that the low energy effective Lagrangian Eq.(2.129) should respect? Again it should be the full symmetry described by the PSG of the $SU(2)$-linear state. We simply need to review Table 2.2 again to see how $\vec{n}$ fields transform

under PSG. For example:

$$T_x^{PSG}: \begin{array}{lcl} \bar{\psi}[\gamma_1\gamma_5]\psi & \to & -\bar{\psi}[\gamma_1\gamma_5]\psi \\ \bar{\psi}[\gamma_2\gamma_3]\psi & \to & \bar{\psi}[\gamma_2\gamma_3] \end{array} \tag{2.130}$$

$$T_y^{PSG}: \begin{array}{lcl} \bar{\psi}[\gamma_1\gamma_5]\psi & \to & \bar{\psi}[\gamma_1\gamma_5]\psi \\ \bar{\psi}[\gamma_2\gamma_3]\psi & \to & -\bar{\psi}[\gamma_2\gamma_3] \end{array} \tag{2.131}$$

$$P_{xy}^{PSG}: \begin{array}{lcl} \bar{\psi}[\gamma_1\gamma_5]\psi & \to & -\bar{\psi}[\gamma_2\gamma_3] \\ \bar{\psi}[\gamma_2\gamma_3]\psi & \to & -\bar{\psi}[\gamma_1\gamma_5] \end{array} \tag{2.132}$$

To have the term $\bar{\psi}\left[(\vec{n}_1\cdot\vec{\tau})\, i\gamma_1\gamma_5 + (\vec{n}_2\cdot\vec{\tau})\, i\gamma_2\gamma_3\right]\psi$ in Eq.(2.129) invariant under PSG, we should have:

$$T_x^{PSG}: \begin{array}{lcl} \vec{n}_1 & \to & -\vec{n}_1 \\ \vec{n}_2 & \to & \vec{n}_2 \end{array} \tag{2.133}$$

$$T_y^{PSG}: \begin{array}{lcl} \vec{n}_1 & \to & \vec{n}_1 \\ \vec{n}_2 & \to & -\vec{n}_2 \end{array} \tag{2.134}$$

$$P_{xy}^{PSG}: \begin{array}{lcl} \vec{n}_1 & \to & -\vec{n}_2 \\ \vec{n}_2 & \to & -\vec{n}_1 \end{array} \tag{2.135}$$

In summary, the following three transformations of $\vec{n}$ should be the symmetry of the potential $V(\vec{n}_1, \vec{n}_2)$:

$$\vec{n}_1 \to -\vec{n}_1 \qquad \vec{n}_2 \to -\vec{n}_2 \qquad \vec{n}_1 \leftrightarrow \vec{n}_2 \tag{2.136}$$

which strongly constrains the form of potential $V(\vec{n}_1, \vec{n}_2)$. The only allowed gauge invariant form of $V(\vec{n}_1, \vec{n}_2)$ up to quartic order is:

$$\begin{aligned} V(\vec{n}_1, \vec{n}_2) =& \frac{1}{2}m^2(\vec{n}_1^2 + \vec{n}_2^2) + a(\vec{n}_1^4 + \vec{n}_2^4) + b(\vec{n}_1^2\vec{n}_2^2) \\ &+ c(\vec{n}_1\cdot\vec{n}_2)^2 \end{aligned} \tag{2.137}$$

Terms like $\vec{n}_1\cdot\vec{n}_2$ and $(\vec{n}_1\cdot\vec{n}_2)(\vec{n}_1)^2$ are forbidden since they break PSG.

A phase transition with no breaking symmetry.

One can show that the two phases involved in the phase transition, the $SU(2)$-linear phase and the Z_2-linear phase, have different PSGs. In [27], PSG of the $SU(2)$-linear phase was labelled as $SU2Bn0$, whereas PSG of Z_2-linear phase was labelled

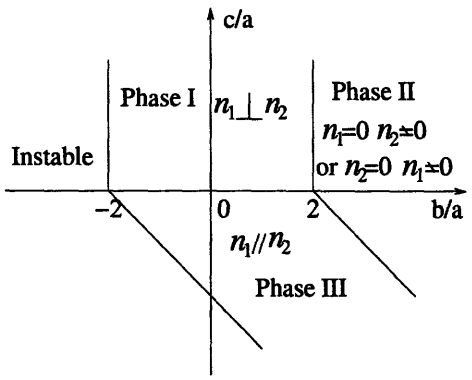

Figure 2-16: Various Higgs condensed phases with different values of a, b and c. In phase I, $|\langle \vec{n}_1 \rangle| = |\langle \vec{n}_2 \rangle|$ and $\langle \vec{n}_1 \rangle \perp \langle \vec{n}_2 \rangle$, it is the Z_2-linear phase. In phase II, $\langle \vec{n}_1 \rangle = 0$ and $\langle \vec{n}_2 \rangle \neq 0$ or vice versa. It is a $U(1)$-linear phase which breaks translation and rotation symmetry. In phase III, $|\langle \vec{n}_1 \rangle| = |\langle \vec{n}_2 \rangle|$ and $\langle \vec{n}_1 \rangle \parallel \langle \vec{n}_2 \rangle$. It is another $U(1)$-linear phase which breaks rotation and translation symmetry.

as $Z2Azz13$. But after projection, the physical symmetries of the two phases are identical. They both have the full symmetry of translation, rotation and time-reversal:

$$\begin{aligned} &\text{Physical symmetry of } SU(2)\text{-linear and } Z_2\text{-linear states} \\ &= \{T_x, T_y, P_x, P_y, P_{xy}, T, C\} \end{aligned} \tag{2.138}$$

We are investigating a phase transition with no breaking of physical symmetry. Here the introduction of quantum order, or PSG is inevitable. Otherwise we do not know what is changed during the phase transition.

At mean-field level, we already have the picture for the phase transition. With different values of coupling constant in potential $V(\vec{n}_1, \vec{n}_2)$, the Higgs bosons $\vec{n}_1, \vec{n}_2$ may or may not condense. If they do not condense, we are in the $SU(2)$-linear phase. If they condense in such a fashion that $\langle \vec{n}_1 \rangle \perp \langle \vec{n}_2 \rangle$, we are in the Z_2-linear phase. Detailed study of the potential shows that if $m^2 > 0$, Higgs bosons do not condense. If $m^2 < 0$, Higgs bosons do condense, and the way of condensation is determined by the value of parameters a, b and c as shown in Fig. 2-16. There are three different Higgs condensed phases, labelled by I, II and III.

Our Z_2-linear phase is phase I. On the mean-field level, the phase transition from the $SU(2)$-linear phase to the Z_2-linear phase can be described by changing m^2 from positive to negative, and $m^2 = 0$ is the phase transition point.

The next question is whether this mean-field picture survives after inclusion of quantum fluctuations. If there is only one relevant coupling constant m^2, our mean-

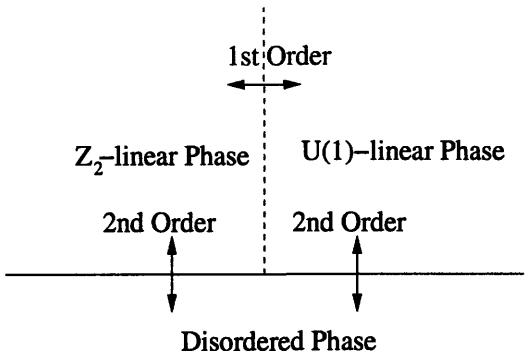

Figure 2-17: The critical theories are the same along the whole solid line.

field picture remains valid, otherwise it would fail.

We now estimate the scaling dimension of $\vec{n}$ field. Again the fermion dressing is strong in the large-N_f limit. Similar to our argument for σ boson in section 2.7.1, we know that the scaling dimension of $\vec{n}$ field is $d_{\vec{n}} = 1 + O(\frac{1}{N_f})$. Therefore by power counting, the terms $(\partial_\mu \vec{n})^2$ and $\vec{n}^4$(those a, b, c terms) are both of scaling dimension $4 + O(\frac{1}{N_f})$, which are irrelevant. However since the Lagrangian Eq.(2.129) is not Lorentz invariant, calculating the $\frac{1}{N_f}$ correction to $d_{\vec{n}}$ would be complicated.

We have just concluded that there is only one relevant coupling m^2, so the phase transition is second-order and $m^2 = 0$ is the critical point. Although a, b, c couplings are irrelevant at the critical point, they are important to determine which Higgs condensed phase the system would end up. Therefore they are dangerous irrelevant couplings. This can be seen from Fig.2-17. Although the critical theories for the phase transition from the $SU(2)$-linear phase to Higgs condensed phases are the same, the system may change into different Higgs condensed phases depending the values of couplings a, b, c. Different Higgs phases separate from each other by first order transition boundaries.

The transition from the $SU(2)$-linear state to the Z_2-linear state is a phase transition without breaking of any symmetry. What are the changes in physically measurable quantities during the phase transition? Let us think about the staggered spin-spin correlation function again. On both sides of the phase transition, the fermions are massless so the spin-spin correlation functions are of power law. But the values of power are different. As shown in Fig.2-18, in the Z_2-linear phase, since Z_2 gauge field is gapped, spin-spin correlation does not receive anomalous dimension. At the critical point, due to the existence of the massless Higgs fields, the correlation function will have another scaling exponent.

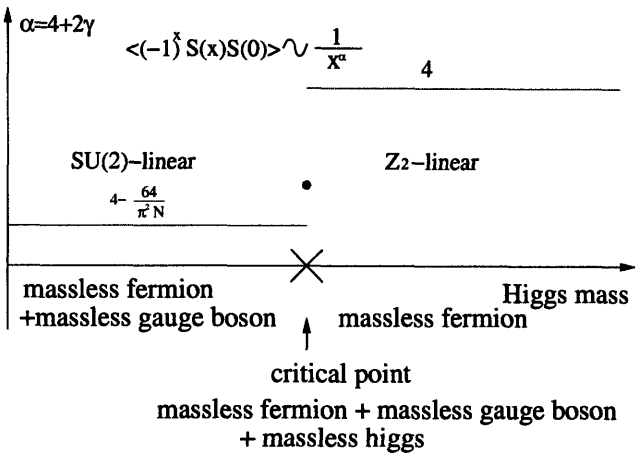

Figure 2-18: The change of scaling exponent of staggered spin-spin correlation function during the phase transition from $SU(2)$-linear phase to Z_2-linear phase

Phase transition from spin liquids to ordered phases

Spin liquids phases can also experience phase transitions into ordered phases. Our discussion of phase transition between $SU(2)$-linear phase and chiral spin liquid is an example where the time-reversal is broken, but no space translation or spin rotation symmetries are broken. Here we focus on the phase transition from spin liquids to phases breaking space translation or spin rotation symmetries. For example, it can go into ferromagnetic phase, anti-ferromagnetic phase or VBS phase.

Suppose our starting point is the $SU(2)$-linear phase (or π-flux phase). Table 2.4 is very useful. For example, a phase transition from $SU(2)$-linear phase to Neel phase can be easily understood as the opening of a mass gap $\overline{\psi}\psi$. Then because at energy scale below the mass gap there is no fermion, we are left with a pure $SU(2)$ gauge field which is confined in 2+1 dimension. This phase transition then have two ingredients in it: fermion-chiral symmetry breaking and confinement. Because of the confinement effect the spinons are always bounded together and do not appear in physical excitations.

Similarly one can study the phase transition from $SU(2)$-linear phase to VBS order and ferromagnetic order. The features for these phase transitions are all similar: opening of a mass gap and the confinement.

2.8 Conclusion

In this article, we studied the stability of various spin liquids, including gapless spin liquid (also called algebraic spin liquid). Spin liquids are defined as the disordered phases of a spin system. They have the full space-time translation and spin rotation symmetries. Different spin liquids may have the same physical symmetry. To understand the physics of these phases, first one needs to understand why they are different despite they have the same symmetry. That means we have to classify quantum states in greater detail than those achieved through usual symmetry group. This is the main motivation to introduce the idea of quantum order. The PSG is just one attempt to characterize quantum order mathematically.

We find that PSG is very important in understanding the stability of algebraic spin liquid. Without PSG, it is hard to understand why fermions can remain massless after including fluctuations around the mean-field state. After considering certain PSG transformations originated from lattice symmetry, we find that such PSG transformations turns into chiral symmetry in continuous limit, which guarantees the masslessness of fermions. Using this idea, we show the existence of an algebraic spin liquid – $SU(2)$-linear state – whose low energy effective theory is a QCD_3 with $SU(2)$ gauge group. The spin-spin correlation function is also calculated. We find that the $SU(2)$-linear state has a large emergent symmetry – $Sp(4) \times$ Lorentz Group $\times T \times P_x \times P_y$ (or $Sp(4N) \times$ Lorentz Group $\times T \times P_x \times P_y$ for the large N model) – at low energies. The lattice model does contain terms that violate the $Sp(4) \times$ Lorentz Group symmetry. But all those terms are shown to be irrelevant with the help of the PSG analysis.

We also discussed the continuous quantum phase transition between spin liquids. Again, the PSG plays a key role here. The first transition we studied is a quantum phase transition that breaks time reversal and parity symmetries, which is the transition between the $SU(2)$-linear state and the $SU(2)$-chiral state. Such a Z_2 symmetry breaking transition has a well defined order parameter. However, as one can see from the calculated critical exponents, the critical point at the transition does not belong to the Ising universality class. It is interesting to see that even some symmetry breaking continuous phase transitions are beyond Landau's symmetry breaking paradigm in the sense that critical properties are different for those obtained from Ginzburg-Landau theory.

The second transition that we studied is a continuous quantum phase transition between the $SU(2)$-linear state and the Z_2-linear state. The two states have the same symmetry. Hence we show that continuous phase transitions even exist between two

phases with the *same* symmetry[34, 35, 36, 37, 38].

The third transition that we studied is a continuous quantum phase transition between the $SU(2)$-linear state and a $U(1)$-linear state. Such a transition breaks the lattice translation and lattice rotation symmetry. Amazingly, we found that the third transition and the second transition are described by the same critical theory with the same set of critical exponents. So it is possible for transitions between very different states to have the same critical point.

All above phenonmena are beyond Landau-Ginzburg paradigm for phase and phase transition. Those discoveries suggest that we need rethink Landau-Ginzburg symmetry breaking approach to phase and phase transition. We know that stable phases and critical points can all be viewed as fixed point in the renormalization group sense. If a fixed point has no relevant operator that is allowed by the symmetry (or PSG), the fixed point will represent a stable phase. If a fixed point has only one relevant operator that is allowed by the symmetry (or PSG), the fixed point will represent a critical point between two phases. In this chapter, we found that one cannot use symmetry to characterize all the possible fixed points. New kind of order beyond the symmetry description exists. We showed that how to use the PSG analysis to capture the new physics beyond Landau-Ginzburg symmetry breaking paradigm.

The phase transitions studied here are characterized by a change of quantum order in addition to a possible change of symmetry. This is why those phases and phase transitions are beyond Landau-Ginzburg paradigm of breaking symmetry. We emphasize that quantum order, or PSG, is necessary to understand the correct low energy effective theory and the critical phenomena. Also, an experimental discovery of a new critical point (with unusual critical exponents) implies a discovery of new quantum orders. Thus it is very important to measure critical exponents even for seemingly ordinary symmetry breaking transitions.

Chapter 3

Spin-1/2 Kagome lattice

Recent experimental studies of a spin-1/2 Kagome system $ZnCu_3(OH)_6Cl_2$[51, 52, 53] show that the system is in a non-magnetic ground state. The Kagome lattice can be viewed as corner-sharing triangles in two-dimension(Fig.3-1(a)). The compound shows no magnetic order down to very low temperature (50mK) compared with the Curie-Weiss temperature (>200K). The spin susceptibility rises with decreasing temperature, but saturates to a finite value below 0.3 K. The specific heat is consistent with a linear T behavior below 0.5 K. There is no sign of a spin gap in dynamical neutron scattering. These observations led us to re-examine the issue of the ground state of the spin-1/2 Kagome lattice.

Based on Monte Carlo studies of Gutzwiller projected wavefunctions, we propose the ground state to be a U(1)-Dirac spin-liquid state which has relativistic Dirac spinons. The low energy effective theory is a U(1) gauge field coupled to four flavors of two-component Dirac fermions in 2+1 dimension. This state was studied earlier in the mean-field approximation[54]. However, that study focused on an instability toward a Valence Bond Solid (VBS) state which breaks translation symmetry[54]; it was not appreciated that the U(1)-Dirac state can be a stable phase. Using the Projective Symmetry Group[55, 56, 13] (PSG) technique, we reconsider the stability of the U(1)-Dirac state and find it can be stable. Our numerical calculations confirm that neighbor states like the VBS states and chiral spin-liquid state all have higher energies.

One way to construct spin-liquid states is to introduce fermionic spinon operators [7, 57] $f_\uparrow$ and $f_\downarrow$ to represent the bosonic spin operator: $\vec{\mathbf{S}}_i = \frac{1}{2} f^\dagger_{i\alpha} \vec{\sigma}_{\alpha\beta} f_{i\beta}$. This representation enlarges the Hilbert space, and a local constraint is needed to go back to the physical Hilbert space: $f^\dagger_\uparrow f_\uparrow + f^\dagger_\downarrow f_\downarrow = 1$. For the nearest neighbor Heisenberg

model (with antiferromagnetic exchange $J > 0$)

$$H = J \sum_{\langle ij \rangle} \vec{\mathbf{S}}_i \cdot \vec{\mathbf{S}}_j, \tag{3.1}$$

we can substitute the spin operator by the spinon operators, so that the spin interaction is represented as a four-fermion interaction. The four-fermion interaction can be decomposed via a Hubbard-Stratonovich transformation by introducing the complex field χ_{ij} living on the links. The path integral of the spin model is then $Z = \int d\chi d\lambda df df^\dagger e^{-S}$, where the action is

$$S = \int d\tau \Big[\sum_i f_{i\alpha}^\dagger \partial_\tau f_{i\alpha} + i\lambda_i (f_{i\alpha}^\dagger f_{i\alpha} - 1) + \sum_{ij} 2J \left|\chi_{ij}\right|^2 + J(\chi_{ij} f_{j\alpha}^\dagger f_{i\alpha} + h.c.) \Big] \tag{3.2}$$

Here λ is the Lagrangian multiplier to ensure the local constraint, and it can be viewed as the time component of a compact U(1) gauge field, whereas the phase of χ_{ij} can be viewed as the space components of the same gauge field. Only when the full gauge field fluctuations are included can one go back to the physical Hilbert space.

With this fermionic representation, one can do a mean-field study of the spin-liquid states by taking χ_{ij} as mean-field parameters. For the Kagome lattice, the mean-field states are characterized by the fluxes through the triangles and the hexagons. Controlled mean-field studies were done by generalizing the $SU(2)$ spin model to $SU(N)$ spin model via introducing $N/2$ flavors of fermions[58, 54], and several candidate states were found:

(i) Valence Bond Solid (VBS) states which break translation symmetry.

(ii) a spin liquid state (SL-$\left[\frac{\pi}{2}, 0\right]$) with a flux $+\pi/2$ through each triangle on Kagome lattice and zero-flux through the hexagons. This is a chiral spin liquid which breaks time-reversal symmetry.

(iii) a spin liquid state (SL-$\left[\pm\frac{\pi}{2}, 0\right]$) with staggered $\pi/2$-flux through the triangles ($+\frac{\pi}{2}$ through up triangles and $-\frac{\pi}{2}$ through down triangles) and zero-flux through the hexagons.

(iv) a spin liquid state (SL-$\left[\frac{\pi}{2}, \pi\right]$) with $+\pi/2$-flux through the triangles and π-flux through the hexagons.

(v) a uniform RVB spin liquid state (SL-[0, 0]) with zero-flux through both triangles and hexagons. This state has a spinon Fermi surface.

(vi) a U(1)-Dirac spin liquid state (SL-$[0,\pi]$) with zero-flux through the triangles and π-flux through the hexagons. This state has four flavors of two-component Dirac fermions.

Among the states (ii)-(v), the chiral spin liquid SL-$\left[\frac{\pi}{2},0\right]$ has the lowest mean-field energy [58]. But numerical calculations[59] do not support a large chirality-chirality correlation, and Hastings[54] found SL-$[0,\pi]$ to be the state with the lowest mean-field energy among the non-chiral spin liquid states. However its mean-field energy is still higher than that of (ii). The above arguments are based on the $\frac{1}{N}$ expansion treatment of gauge fluctuations, which may fail when $N=2$ in the physical case. To clarify which candidate is the lowest energy spin liquid state, we do a Monte Carlo study on the trial projected wavefunctions[60].

As we mentioned, fermionic representation enlarges the Hilbert space. One way to treat the unphysical states is to do a projection by hand. Given a mean-field ground state wavefunction $|\Psi_{mean}(\chi_{ij})\rangle$ with mean-field parameters χ_{ij}, the projected wavefunction $|\Psi_{prj}(\chi_{ij})\rangle = P_D|\Psi_{mean}(\chi_{ij})\rangle$ is a physical state; here $P_D = \prod_i(1 - n_{i\uparrow}n_{i\downarrow})$ is the projection operator ensuring one fermion per site. The calculation of energy $\langle\Psi_{prj}|H|\Psi_{prj}\rangle$ can be implemented by a Monte Carlo approach with power law complexity, which means that one can do a fairly large lattice.[60] We note that states related by a global transformation $\chi_{ij} \rightarrow -\chi_{ij}^*$ represent the same spin wavefunction after projection. This is a special case of the $SU(2)$ gauge symmetry[61].

For the model of Eq.(3.1), we did the Monte Carlo calculation for energies of projected spin liquid states on lattices with 8x8 and 12x12 unit cells (each unit cell has 3 sites). We chose mixed boundary conditions; i.e., periodic along one Bravais lattice vector, and anti-periodic along the other Bravais lattice vector. The results are summarized in Table 3.1.

We found that the U(1)-Dirac state [the *projection* of the mean-field state (vi)] has the lowest energy, which is $-0.429J$ per site. Note that these results change the order of mean-field energies of the spin liquids (ii)-(vi), where the chiral spin liquid (ii) was found to be of the lowest energy. In Table 3.2 we list the estimates of the ground state energy by various methods. It is striking that even though the projected U(1)-Dirac state has *no variational parameter*, it has an energy which is even lower than some numerical estimates of ground state energy. Furthermore its energy is very close to the exact diagonalization result when extrapolated to large sample size. Thus we propose it to be the ground state of the spin-1/2 nearest neighbor Heisenberg model on the Kagome lattice.

Hastings[54] proposed a neighboring VBS ordered state as an instability of the

Spin liquid	8x8x3 lattice	12x12x3 lattice
SL-$[\frac{\pi}{2},0]$	-0.4010(1)	-0.4010(1)
SL-$[\pm\frac{\pi}{2},0]$	-0.3907(1)	-0.3910(1)
SL-$[\frac{\pi}{2},\pi]$	-0.3814(1)	-0.3822(1)
SL-$[0,0]$	-0.4115(1)	-0.4121(1)
SL-$[0,\pi]$	-0.42866(2)	-0.42863(2)

Table 3.1: For all candidate projected spin-liquids, we list the energy per site in unit of J. The U(1)-Dirac state SL-$[0,\pi]$ is the lowest energy state, and its energy is even lower than some numerical estimates of the ground state energy(see Table 3.2).

Method	energy per site
Exact Diagonalization[59]	-0.43
Coupled Cluster Method[62]	-0.4252
Spin-wave Variational method[63]	-0.419

Table 3.2: We list the previous estimates for ground state energy in unit of J.

U(1)-Dirac state. This state can be obtained by giving the fermions non-chiral masses. In particular, he proposed a VBS state with with a 2×2 expansion of the unit cell. The 12 hopping parameters on the boundary of the star of David (six triangles surounding the hexagon) have amplitude χ_1, while all other hoppings have amplitude χ_2. Our numerical calculations show that this VBS ordered state has higher energy (see Table 3.3), so the U(1)-Dirac state is stable against VBS ordering. Another neighbor state of the U(1)-Dirac spin liquid discussed by Hastings[54] is obtained by giving the fermions chiral masses. The resulting state is a chiral spin liquid with broken time-reversal symmetry, and has θ-flux through the triangles and $(\pi - 2\theta)$-flux through the hexagons (if $\theta = 0$ the state goes back to the U(1)-Dirac state). In Table 3.3 we also show that non-zero θ increases the energy.

To determine whether the U(1)-Dirac state is a stable phase, we start with its effective theory

$$S = \int dx^3 [\frac{1}{g^2}(\varepsilon_{\lambda\mu\nu}\partial_\mu a_\nu)^2 + \sum_\sigma \bar{\psi}_{+\sigma}(\partial_\mu - ia_\mu)\tau_\mu\psi_{+\sigma} + \sum_\sigma \bar{\psi}_{-\sigma}(\partial_\mu - ia_\mu)\tau_\mu\psi_{-\sigma}] + \cdots, \quad (3.3)$$

where the first term comes from integrating out some higher energy fermions, and $\cdots$ represents other terms that are generated by interaction. The massless Dirac fermions in the effective theory come from the gapless nodal spinons in the mean-field theory.

State	8x8x3 lattice	12x12x3 lattice
U(1)-Dirac spin liquid	-0.42866(2)	-0.42863(2)
VBS state($\lvert\chi_1/\chi_2\rvert = 1.05$)	-0.42848(2)	-0.42844(2)
VBS state($\lvert\chi_1/\chi_2\rvert = 0.95$)	-0.42846(2)	-0.42846(2)
Chiral spin liquid($\theta = 0.05$)	-0.42857(2)	-0.42853(2)

Table 3.3: We list the energy per site in unit of J for possible instabilities of the U(1)-Dirac spin liquid, which were discussed in Ref[54](see text). Both VBS order and chiral spin liquid increase the energy. Note that both the VBS and chiral spin liquid states are obtained by continuous deformations of the U(1)-Dirac wavefunction; because we are checking local stability, the parameters used here correspond to small deformations, and the energy differences are rather small.

The two-component Dirac spinor fields are denoted by $\psi_{\pm\sigma}$, where $\pm$ label the two inequivalent nodes and σ the up/down spins. Also, $\bar{\psi}_{\pm\sigma} = \psi^\dagger_{\pm\sigma}\tau^3$, and the τ_μ are Pauli matrices. The massless fermions lead to an algebraic spin liquid [55, 56]. The stability of the U(1)-Dirac state can now be determined by examining the $\cdots$ terms: If $\cdots$ terms contain no relevant perturbations – that is, if all relevant perturbations are forbidden by microscopic symmetries – then the U(1)-Dirac state can be stable.

The potential relevant terms are the 16 gauge-invariant, spin-singlet bilinears of $\psi_{\pm\sigma}$. To see if those bilinears are generated by interaction or not, we need to study how lattice symmetries are realized in the effective theory (3.3). Because spinons are not gauge invariant, lattice symmetry is realized in the effective theory as a projective symmetry, described by a PSG. This means that the realization of lattice symmetry includes nontrivial gauge transformations. For example, translation $T_{\boldsymbol{R}}$ by a Bravais lattice vector $\boldsymbol{R}$ acts on the spinons by $T_{\boldsymbol{R}} : f_{i\alpha} \to g(i, \boldsymbol{R}) f_{i'\alpha}$, where i' is the image of the site i, and $g(i, \boldsymbol{R}) = \pm 1$ is a position-dependent gauge transformation. Upon diagonalizing the mean-field Hamiltonian for the U(1)-Dirac state and focusing on the low-energy excitations near the Dirac nodes (see below), the action of $T_{\boldsymbol{R}}$ (and other symmetries) on the fermions $\psi_{\pm\sigma}$ of the effective theory can be worked out. This in turn determines how the bilinears transform under microscopic symmetries. The details of this analysis for the U(1)-Dirac state, which do not differ substantially from similar analyses of other spin liquids[55, 56, 13], will appear in an upcoming paper; here, we simply give the results.

We find that 15 of 16 bilinears are forbidden by translation symmetry and time-reversal alone. The remaining bilinear, which is allowed by symmetry, is $\sum_{\pm,\sigma} \psi^\dagger_{\pm\sigma}\psi_{\pm\sigma}$. This term shifts the spinon Fermi level to make the ground state to have exactly one spinon per site. In this case, the lower three of six spinon bands are filled and the

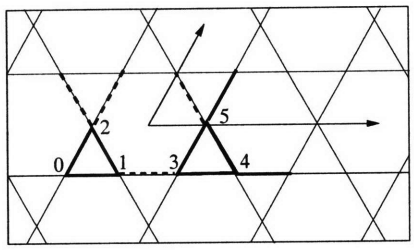

(a)

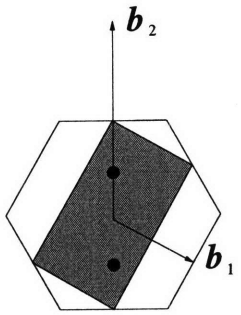

(b)

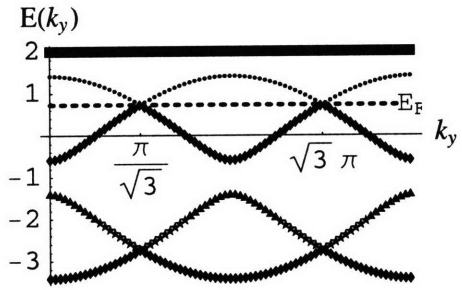

(c)

Figure 3-1: (a): We choose a six-site unit cell for the Kagome lattice. The sites are labeled $0, \ldots, 5$ as shown. Only those bonds depicted as bold solid lines (positive hopping) and bold dashed lines (negative hopping) are contained within the unit cell. (b): The Brillouin zone for the doubled unit cell (gray area), with reciprocal lattice basis vectors $\boldsymbol{b}_i$ shown. The outer hexagon is the Brillouin zone for the 3-site unit cell of a single up-pointing triangle. The positions of the Dirac nodes are denoted by the black circles. (c): Plot of the band structure of the $U(1)$-Dirac state on the line from $\boldsymbol{k} = 0$ to $\boldsymbol{k} = \boldsymbol{b}_2$ with energy in units of χJ(see text). The flat band is doubly-degenerate; all others are nondegenerate. The Fermi level corresponding to one spinon per site is indicated by the dashed line.

spinon Fermi level is exactly at the gapless nodal points. This analysis tells us that the U(1)-Dirac state is stable in mean-field theory (and also in a large-N treatment). Because not all scaling exponents are known in such an algebraic spin liquid, perturbations other than fermion bilinears could in principle lead to an instability. However, so far, the variational wavefunction analysis suggests that this is not the case and that the U(1)-Dirac state is stable.

Now we study the U(1)-Dirac spin liquid on the mean-field level. The U(1)-Dirac mean-field state is defined as the ground state of the following tight-binding spinon Hamiltonian: $H_{mean} = J \sum_{\langle ij \rangle} \chi_{ij} f^\dagger_{j\alpha} f_{i\alpha} + h.c.$. All χ_{ij} have the same magnitude and they produce zero-flux through the triangles and π-flux through the hexagons.

Although the U(1)-Dirac state does not break translation symmetry (because the translated state differs from the original state only by a gauge transformation), the

unit cell has to be doubled to work out the mean-field spinon band structure. One can fix a gauge in which all hoppings are real as shown in Fig. 3-1(a). In this gauge the Dirac nodes are found to be at $\boldsymbol{k} = (0, \pm\frac{\pi}{\sqrt{3}a})$ as shown in Fig. 3-1(b)(c), where a is the Kagome unit cell spacing, i.e., twice the nearest neighbor distance. These are isotropic Dirac nodes; i.e., the Fermi velocity is the same in all directions. In the extended zone scheme, the Dirac nodes form a triangular lattice in momentum space with lattice spacing $\frac{2\pi}{\sqrt{3}a}$. The positions of the Dirac nodes are gauge dependent, but the momentum vectors connecting any two Dirac nodes are gauge invariant. Because the spinon excitations are gapless at the nodal points, we expect the spin-1 excitations of the U(1)-Dirac spin liquid are also gapless at zero momentum and those momenta connecting two Dirac nodes.

For the $ZnCu_3(OH)_6Cl_2$ compound, the Heisenberg coupling was estimated to be $J \approx 300$K[51], and one can calculate the Fermi velocity at mean-field level. We find $v_F = \frac{a\chi J}{\sqrt{2}\hbar}$, where χ is the magnitude of the self-consistent mean-field parameter. Hastings[54] found $\chi = 0.221$. χ describes the renormalization of the spinon bandwidth and is not expected to be given quantitatively by the mean-field theory. Hence in the formulae below we retain χ as a parameter. We find $v_F = \frac{a\chi J}{\sqrt{2}\hbar} = 19\chi \cdot 10^3$ m/s.

We can also calculate the specific heat at the mean-field level. At low temperature ($k_B T \ll \chi J$), one expects a $C \propto T^2$ law because of the Dirac nodes. The coefficient is related to v_F:

$$\frac{C}{T^2} = \frac{72\zeta(3)\pi k_B^3 A}{(2\pi\hbar v_F)^2} = 1.1\chi^{-2} \cdot 10^{-3} \text{ Joule/mol K}^3, \tag{3.4}$$

where A is the area of the 2-D system. (Note that for $ZnCu_3(OH)_6Cl_2$ compound, the unit cell spacing $a = 6.83$Å, so $A = 2.4 \cdot 10^5$ m^2/mol, where mole refers to one formula unit. We also used the fact that there are four two-component Dirac fermions.)

The gauge field also gives a T^2 contribution to the specific heat. However, in a large-N treatment this will be down by a factor of $1/N$ compared to the fermion contribution. Furthermore, the self energy correction due to gauge fluctuations does not lead to singular corrections to the Fermi velocity[64], so the T^2 dependence of C is a robust prediction.

We notice that experiment observed that the specific heat of Kagome compound $ZnCu_3(OH)_6Cl_2$ behaves as $C \propto T^{2/3}$ in zero magnetic field over the temperature window 106 mK $< T <$ 600 mK[51], which is enhanced from $C \propto T^2$ law. This enhancement is suppressed by a modest magnetic field[51]. Furthermore, over a large temperature range (10K to 100K), the spin susceptibility is consistent with Curie's law

with 6% impurity local moment[53]. We propose that these impurity spins (possibly due to Cu located on the Zn sites) may be coupled to the spinons to form a Kondo type ground state with a Kondo temperature $\lesssim$ 1K, thus accounting for the large C/T and the saturation of the spin susceptibility below 0.3K. The Kondo physics of impurities coupled to Dirac spinons is in itself a novel problem worthy of a seperate study. Meanwhile it appears to dominate the low temperature properties and obscure the true excitations of the Kagome system. We propose that a better place to look for the Dirac spectrum may be at higher temperature (above 10K) and as a function of magnetic field, where the impurity contributions may be suppressed and the unique signature of Eq.(3.4) may be tested. On the other hand, we caution that from Fig.3-1(c), the spinon spectrum deviates from linearity already at a relatively low energy scale($\sim 0.5\chi J$). Our theory also predicts a linear T spin susceptibility of $k_B T \ll \chi J$. Knight shift measured by Cu NMR is the method of choice to seperate this from the impurity contribution.

Finally we remark on a possible comparison with exact diagonalization studies which found a small spin gap of $\sim \frac{J}{20}$ and a large number of low energy singlets[59]. It is not clear whether these results can be reconciled with a $U(1)$-Dirac spin liquid. Here we simply remark that in a finite system the Dirac nodes can easily produce a small triplet gap and that the gauge fluctuations may be responsible for low energy singlet excitations.

We thank J. Helton and Y. S. Lee for helpful discussions. This research is supported by NSF grant No. DMR-0433632 and DMR-0517222.

Chapter 4

Dichotomy in Doped Mott Insulator

4.1 Introduction

One powerful experimental technique to study high-T_c material is the Angular Resolved Photoemission Spectroscopy (ARPES)[65]. ARPES study for the pseudogap region showed a strong anisotropy of the electron spectral function in momentum space[66, 67]. Basically it was found that in the nodal direction, excitations are more quasi-particle like; while in the anti-nodal direction, excitations have no quasi-particle peak. This is the so-called dichotomy. If one lowers the temperature to let the material to go into superconducting phase, it was found that anti-nodal direction also has a small quasi-particle peak. Tunneling experiments show that the underdoped samples are inhomogeneous[68, 69, 70]. Due to this inhomogeneity, it is possible that the underdoped sample can be separated into optimal doped regions and underdoped regions, and the quasi-particle peak only comes from the optimal doped region. With such a point of view, it is possible that even the superconducting phase can have a very anisotropic electron spectral function in momentum space.

Exact diagonalization on t-t'-t''-J model (t' and t'' stand for next nearest neighbor and next next nearest neighbor, respectively) with 32 sites has been done[71, 72] for hole-doped case (one hole doped). It was found that if $t' = t'' = 0, J = 0.3t$, then the quasiparticle weight Z_- is almost a constant along the direction $(\pi, 0)$-$(0, \pi)$: $Z_- = 0.311$ at $(\pi/2, \pi/2)$, and $Z_- = 0.342$ at $(\pi, 0)$. However if one put in $t' = -0.3t, t'' = 0.2t, J = 0.3t$, which is an optimal parameter fitting for $Sr_2CuO_2Cl_2$, then there is a strong dichotomy feature: $Z_- = 0.353$ at $(\pi/2, \pi/2)$, and $Z_- = 0.029$

at $(\pi, 0)$. This suggests that the dichotomy can be a result of t' and t'' hopping.

Exact diagonalization was also done for the electron doped case (a few electrons doped on 32 sites)[72], where Z_+ was measured. Due to the particle-hole symmetry at half-filling, we know that if $t' = t'' = 0$, Z_+ and Z_- are equal up to a momentum shift of (π, π). Therefore Z_+ are also flat along the direction $(\pi, 0)$-$(0, \pi)$ in pure t-J model. But when we put in $t' = -0.3t, t'' = 0.2t, J = 0.3t$, the particle-hole symmetry was broken. Z_+ was found to develop a strong anisotropy along $(\pi, 0)$-$(0, \pi)$: $Z_+ = 0.005$ at $(\pi/2, \pi/2)$, and $Z_+ = 0.636$ at $(\pi, 0)$.

What mechanism can destroy the quasi-particle coherence in the anti-nodal region? The simplest thing comes into one's mind is that we need some other things to destroy it. For example, neutron scattering experiments indicate that there are some low energy magnetic fluctuations[73, 74, 75, 76], and it was proposed[66, 67] that magnon scattering process can destroy the quasi-particle coherence in anti-nodal region. In this chapter, however, we propose a physically different scenario: The dichotomy is due to the t' and t'' hopping terms. The quasiparticle spectral weight Z_k is naturally suppressed in some region in k-space to lower the t' and t" hopping energy. This contradicts a naive thinking that hopping always enhance Z_k. Using the t-t'-t''-J model, we will show that the new scenario can explain the distribution of Z_k for both hole-doped and electron-doped samples in a unified way.

If we believe that the dichotomy is driven by the t' and t'' hopping terms, then there is an important issue: Is there a mean-field theory and the corresponding trial wavefunction that captures this mechanism?

One way to understand high-T_c superconductors is to view them as doped Mott-insulators. Under Zhang-Rice singlet mapping[77], the minimal model which includes the essential Mott physics is t-J model on square lattice. On the analytical side, a powerful mean-field theory for t-J model, the slave-boson approach, was developed[7, 57, 61]. This approach emphasizes the fractionalization picture of the doped Mott insulator: electron is splited into a spinon (a fermion with spin and no charge) and a holon (a boson with charge and no spin), which characterize the low energy excitations of the doped Mott insulator. This mean-field approach also successfully predicted the pseudogap metal for underdoped samples. On the numerical side, the same physics picture gives rise to the projected BCS wavefunction[78](pBCSwf), which turns out to be a very good trial wavefunction for t-J model. However, more detailed studies of pBCSwf[79, 80] indicate that the slave-boson approach fail to explain the dichotomy. So a momentum dependent quasiparticle weight Z_k remains to be a big challenge for slave-boson theory.

In this chapter, we will use a new spinon-dopon approach[81] and the corresponding trial wavefunction to study the underdoped samples. Instead of using spinons and holons, in the new approach, we use the spinons and the bond states of spinons and holons to describe the low energy excitations. The bond states of spinons and holons are called dopons which are charge-e spin-$\frac{1}{2}$ fermions. The spinon-dopon approach leads to a new trial wavefunction, the projected spinon-dopon wave function (pSDwf). The new trial wave function turns out to be an improvement over the old projected BCS wavefunction (pBCSwf).

The holon condensation in slave-boson approach correspond to spinon-dopon mixing. However, in the spinon-dopon approach, the mixing can have a momentum dependence, which is beyond the mean-field slave-boson approach. If we set the mixing to have no momentum dependence, then the pSDwf turns out to be identical to the old pBCSwf. So the pSDwf is a generalization of the pBCSwf.

Now the question is, why the mixing wants to have strong momentum dependence? The answer is that the wavefunction with momentum dependent mixing can make the hopping more coherent, and therefore gain hopping energy. Roughly speaking, the pSDwf with momentum dependent mixing is the summation of the old projected BCS wavefunction together with hopping terms $c_i^\dagger c_j$ acting on it. Here one should notice that the old pBCSwf, with uniform mixing, already has a pretty good t hopping energy. But to have a good t' and t'' hopping energy, the mixing needs to have a momentum dependence, along the direction from $(\pi, 0)$ to $(0, \pi)$. Our Monte Carlo calculation shows that pSDwf with momentum dependent mixing is indeed a better trial wavefunction in energetic sense. To get a quantitative sense how big is the improvement, we find that the energy of a doped hole in pSDwf is about $0.4t$ lower than that of a doped hole in pBCSwf. This is a very big improvement, indicating that the spin-charge correlation (or more precisely, the spin configuration near a doped hole) is much better described by pSDwf than pBCSwf.

Can one measure the momentum dependence of mixing? The answer is yes. In this article we will show that the mixing is directly related to Z_-, the quasi-particle weight, which is measurable in ARPES. Roughly speaking, mixing is proportional to Z_-. We have also developed a Monte Carlo technique to calculate Z_-. The calculation shows that momentum dependent mixing pSDwf indeed has strong anisotropy in momentum space, and consistent with the observed dichotomy.

Comparing pBCSwf and pSDwf, we like to point out two wave functions have similar background spin-spin correlation and similar spin energy. However, that pBCSwf does not capture the detailed charge dynamics. The new trial wavefunction, pS-

Dwf, contains more correct spin-charge correlation. As a result, the energy of doped holes/electrons is much lower in the pSDwf. The holes/electrons in the pSDwf reproduce the correct momentum dependence of quasi-particle spectral weight. We also expect our pSDwf to have a strong momentum dependence in quasi-particle current, which may explain the temperature dependence of superfluid density of High T_c superconductors[82].

4.2 Spinon-dopon Approach and pSDwf

4.2.1 Slave-boson Approach and Projected BCS Wavefunction – Why the approach fails to capture k-dependent features?

Why would we want to introduce the spinon-dopon approach to t-J model? Let us firstly look into the previous mean field approach, more specifically, slave-boson approach. The general t-J model can be written in terms of electron operator:

$$H_{tJ} = J \sum_{\langle ij\rangle \in NN} \left(\mathbf{S}_i \cdot \mathbf{S}_j - \frac{1}{4} n_i n_j \right) - \sum_{ij} t_{ij} \mathbf{P} \left(c_i^\dagger c_j + c_j^\dagger c_i \right) \mathbf{P}. \tag{4.1}$$

Here the projection operator $\mathbf{P}$ is to ensure the Hamiltonian is acting within the physical Hilbert space: one each site, the physical states are $|\uparrow\rangle$, $|\downarrow\rangle$ or $|0\rangle$, i.e., no double occupancy.

Slave-boson approach[7, 57] emphasizes the spin-charge separation picture. In that approach, one splits electron operator into spinon and holon operators:

$$c_{i\sigma} = f_{i\sigma} b_i^\dagger, \tag{4.2}$$

where f is spinon, carrying spin 1/2 and charge 0, i labels site and σ labels spin; b is holon, carrying spin 0 and charge 1. This splitting enlarges the Hilbert space. To go back to physical Hilbert space, a local constraint is needed:

$$f_{i\uparrow}^\dagger f_{i\uparrow} + f_{i\downarrow}^\dagger f_{i\downarrow} + b_i^\dagger b_i = 1. \tag{4.3}$$

Due to spin interaction, spinons form a d-wave paired state. The superconducting phase is realized through an additional holon condensation at momentum $k = 0$. Within such a construction, the quasi-particle weight Z is proportional to doping x

everywhere in k-space, in both nodal and anti-nodal region. To see this, one can simply look at the mean-field Green function of electron:

$$\langle c_k c_k^\dagger \rangle = \langle b_{k=0}^\dagger b_{k=0} f_k f_k^\dagger \rangle = x \langle f_k f_k^\dagger \rangle. \tag{4.4}$$

Therefore x is the residue of quasi-particle pole and $Z = x$ is independent of k.

Slave-boson approach is supposed to capture the physics of spin-charge separation. It has successfully generated the phase diagram of High-T_c superconductor. But this approach, at least at mean-field level, could not capture some more detailed features, such as momentum dependence of quasi-particle weight or the quasi-particle current. One can argue that including gauge fluctuation, those detailed features may be reproduced, but here we will try to develop another approach which can capture these features at mean-field level.

Before we go into the new spinon-dopon approach, let us see how far one can go using slave-boson approach. One can actually try to build a trial wavefunction based on slave-boson mean-field approach. We know that the mean-field approach enlarged the Hilbert space, and the resulting wavefunction lies outside the physical Hilbert space. Only when one includes the full gauge fluctuations can one go back to the physical Hilbert space.

So one way to include the full gauge fluctuations, is to build the mean-field ground state first, and then do a projection from the enlarged Hilbert space to the physical Hilbert space. The wavefunction after projection would serve as a trial wavefunction for the physical Hamiltonian. This projected wavefunction is supposed to incorporate the effect of gauge fluctuation of the slave-boson approach, and may answer the question that, after including gauge fluctuation, whether slave-boson approach can capture the detailed features like dichotomy.

The mean-field ground state for underdoped case can be constructed as follows. Let N_h be the number of holes, N_f is the number of spinons, and $N = N_h + N_f$ is the total number of sites. The slave-boson mean-field ground state is then given by

$$|\Phi_{SB,mean}\rangle = (b_{k=0}^\dagger)^{N_h} \prod_k (u_k + v_k f_{k\uparrow}^\dagger f_{-k\downarrow}^\dagger)|0\rangle, \tag{4.5}$$

where the spinon part of the wavefunction is a standard d-wave pairing state:

$$\frac{v_k}{u_k} = \frac{\Delta(k)}{\xi_k + \sqrt{\xi_k^2 + \Delta(k)^2}}, \tag{4.6}$$

where

$$\xi_k = -2\chi(\cos k_x + \cos k_y) - \mu$$
$$\Delta(k) = \Delta(\cos k_x - \cos k_y) \qquad \text{(d-wave)}. \tag{4.7}$$

Here μ is the chemical potential to give the correct average number of spinon $\langle \sum_i f^\dagger_{i\sigma} f_{i\sigma} \rangle = N_f$; χ and Δ are mean-field parameters which have been found to be $\frac{\Delta}{\chi} = 2$ [83] at half-filling, and $\frac{\Delta}{\chi}$ decreases to zero at doping around J/t.

Now one can do a projection to go back to the physical Hilbert space. The constraint for physical Hilbert space is Eq.(4.3). This constraint ensures that the total number of spinon must be N_f and there is no double occupancy of spinon: spinon number $n_{f,i}$ at site i has to be either 0 or 1. One can easily see that the resulting wavefunction is the usual Projected d-wave BCS Wavefunction (pBCSwf):

$$|\Phi_{PBCS}\rangle = P_D^{SB} P_N^{SB} |\Phi_{SB,mean}\rangle \tag{4.8}$$
$$= P_D P_N \prod_k (u_k + v_k c^\dagger_{k\uparrow} c^\dagger_{-k\downarrow})|0\rangle \tag{4.9}$$
$$\propto P_D \left(\sum_k a(k) c^\dagger_{k\uparrow} c^\dagger_{-k\downarrow} \right)^{N_f/2} |0\rangle, \tag{4.10}$$

where in the first line, P_N^{SB} is the projection into fixed total number of particles, i.e., N_h holons and N_f spinons; while P_D^{SB} is the projection into physical Hilbert space, i.e., removing all states not satisfying constraint Eq.(4.3). In the second line, P_N is the projection into fixed total number of electrons, which has to be N_f, P_D is the projection which removes all double occupancies. $a(k)$ is defined as $a(k) = \frac{v_k}{u_k}$.

Projected BSC wavefunction turned out to be a surprisingly good trial wavefunction for t-J model[78]. However numerical studies[79, 80] showed that the quasi-particle weight is almost a constant along the direction from $(\pi, 0)$ to $(0, \pi)$, i.e., it fails to reproduce the dichotomy. The quasi-particle current of pBCSwf is also pretty smooth in the k space[79]. It is because pBCSwf is unable to capture the momentum dependence properties that we need a new approach to underdoped high T_c superconductors.

4.2.2 How to capture k-dependence features? – Spinon-dopon approach and projected spinon-dopon wavefunction

Rebeiro and Wen[81] developed this new mean-field approach trying to capture the spinon-holon recombination physics. In the following we briefly review their work. We know that at low temperature, spinon and holon recombine pretty strongly to give electron-like quasi-particle. So it is natural to introduce dopon operator – a bound state between a spinon and a holon – to describe low energy excitations. Note that a dopon has the same quantum number as an electron and describes a doped electron (or hole). But the Mott and spin-liquid physics at half filling should also be addressed. So one should also keep the spinon operator. As a result, two types of fermions are introduced here: spinon f and dopon d. Spinon carries spin $1/2$ and no charge, and dopon carries spin $1/2$ and charge 1. By introducing these two types of fermions one enlarges the Hilbert space: now there are 16 states per site, among them only three are physical. The three physical states on site i can be represented in terms of spinon and dopon fermions as:

$$|\uparrow\rangle = |\uparrow_f\rangle, \qquad |\downarrow\rangle = |\downarrow_f\rangle, \qquad |0\rangle = \frac{1}{\sqrt{2}}|\uparrow_f\downarrow_d - \downarrow_f\uparrow_d\rangle. \tag{4.11}$$

Here please notice that the constraints are two-fold: firstly there must be one f spinon per site, secondly d dopon has to form a local singlet with the spinon.

One can do a self-consistent mean-field study. The mean-field Hamiltonian takes the form:

$$\begin{aligned} H_{mean} = & (-2\chi(\cos k_x + \cos k_y) - \mu) f^\dagger_{k\alpha} f_{k\alpha} \\ & + \Delta(\cos k_x - \cos k_y) f^\dagger_{k\uparrow} f^\dagger_{-k\downarrow} + \epsilon_k d^\dagger_{k\alpha} d_{k\alpha} \\ & + \beta_k f^\dagger_{k\alpha} d_{k\alpha} + h.c.. \end{aligned} \tag{4.12}$$

Here H_{mean} can be divided into three parts: spinon part, dopon part and spinon-dopon interaction. The spinon part describes the usual d-wave paired ansatz: $\chi = J\langle f^\dagger_{k\alpha} f_{k\alpha}\rangle$, $\Delta = J\langle f_{k\uparrow} f_{-k\downarrow}\rangle$. The dopon part is simply a free dopon band, with ϵ_k determined by high energy ARPES measurement. Note that ϵ_k is not taken as tunable mean-field parameter. Finally the spinon-dopon interaction is described by a k-dependent hybridization, roughly speaking $\beta_k = \epsilon_k\langle d^\dagger_i f_i\rangle$. One can see that $d^\dagger_i f_i$ is a bosonic field carrying charge 1 and spin 0. Its non-zero average value corresponds to holon

condensation in slave-boson approach, which leads to superconductivity. μ is the chemical potential required to tune the doping.

Along this line Rebeiro and Wen did a mean-field phase diagram, and successfully fit to ARPES data and tunneling data[84, 85]. Here we try to emphasize that the main lesson we learned from this new mean-field approach is that one can have a k-dependent hybridization at mean-field level (in Eq.(4.12) this hybridization is controlled by β_k and energy spectrum of spinon band and dopon band.), which is roughly the counterpart of holon condensation in slave-boson approach. This is why one can study detailed features like dichotomy in this new approach.

Several open questions naturally arise in this new approach. It seems there are two types of excitations, spinon and dopon, what do they look like? We also know that mean-field approach is not very reliable, so it would be nice to understand the physical trial wavefunction corresponding to the new mean-field approach, from where we would know exactly what we are doing. In the following we try to answer these questions.

Let us construct trial wavefunctions based on this spinon-dopon mean-field approach. One can simply take a mean-field ground state wavefunction, then do a projection back into the physical Hilbert space, just like the way we did in the slave boson case:

$$|\Phi_{PSD}\rangle = P_{SD} P_N |\Phi_{SD,mean}\rangle. \tag{4.13}$$

Here P_N is the projection into fixed number of spinon and dopon, which gives the correct doping; and P_{SD} is the projection into to physical Hilbert space Eq.(4.11). $|\Phi_{SD,mean}\rangle$ is the ground state wavefunction of some mean-field Hamiltonian in the form of Eq.(4.12). Suppose we know how to do this projection numerically, one can do a variational study of the these Projected Spinon-Dopon Wavefunctions (pSDwf), to see what is the lowest-energy ansatz. In general, however, the full projection is not doable, so we develop a simple numerical technique to do a local projection to have some rough idea about what kind of wavefunction is energetically favorable (See Appendix B). What we found is that the best trial wavefunction for underdoped case

has the following form:

$$|\Phi^{SC}_{PSD}\rangle = P_{SD}P_N|\Phi^{SC}_{SD,mean}\rangle \tag{4.14}$$

$$= P_{SD}P_N \exp\left(\sum_k b(k)\tilde{f}^\dagger_{k\uparrow}\tilde{f}^\dagger_{-k\downarrow}\right)|0\rangle \tag{4.15}$$

$$\propto P_{SD}\left(\sum_k b(k)\tilde{f}^\dagger_{k\uparrow}\tilde{f}^\dagger_{-k\downarrow}\right)^{\frac{N+N_h}{2}}|0\rangle, \tag{4.16}$$

where

$$\tilde{f}^\dagger_{k\alpha} = \sqrt{1-\beta_k^2}f^\dagger_{k\alpha} + \beta_k d^\dagger_{k\alpha}. \tag{4.17}$$

Here $\tilde{f}$ form a d-wave paired state and the superscript SC means this wavefunction is superconducting. $b(k)$ and β_k are some real functions and we assume $\beta_k = \beta_{-k}$ to respect time reversal symmetry. For this particular ansatz, full projection is doable in low doping limit. In section 4.4 we develop the numerical method to do the full projection and we will see that this wavefunction is a even better trial wavefunction than pBCSwf.

Note that the total number of f and d fermions is $N + N_h$. Also P_{SD} requires one f-fermion per site, so totally N f-fermions. Therefore we must have N_h d-fermions, which gives the correct doping.

4.2.3 How does pSDwf capture the k-dependent features? – properties of wavefunction before projection $|\Phi^{SC}_{SD,mean}\rangle$: Z_k at mean-field level.

The form of $|\Phi^{SC}_{PSD}\rangle$ looks very similar to pBCSwf, basically we are constructing a pairing wavefunction based on hybridized fermion $\tilde{f}_k$. In the next section we will see that $|\Phi^{SC}_{PSD}\rangle$ and pBCSwf are indeed closely related. For the moment let us have a closer look at the wavefunction $|\Phi^{SC}_{SD,mean}\rangle$ before projection. The idea is that physical properties may not change drastically after the projection. In this case the mean-field level understanding will give us insight of the wavefunction after the projection.

First of all it is obvious that this wavefunction is superconducting. That is because the nonzero β_k signals the mixing between spinon and dopon $\langle f^\dagger_{k\alpha}d_{k\alpha}\rangle \neq 0$, and thus signals breaking of charge conservation. It is natural to believe the superconductivity survives after projection.

Let us introduce the other combination of f and d fermions:

$$\tilde{d}^{\dagger}_{k\alpha} = -\beta_k f^{\dagger}_{k\alpha} + \sqrt{1-\beta_k^2} d^{\dagger}_{k\alpha}, \tag{4.18}$$

and the quasi-particle operators:

$$\gamma^{\dagger}_{k\uparrow} = \tilde{u}_k \tilde{f}^{\dagger}_{k\uparrow} - \tilde{v}_k \tilde{f}_{-k\downarrow} \tag{4.19}$$

$$\gamma_{-k\downarrow} = \tilde{u}_k \tilde{f}_{-k\downarrow} + \tilde{v}_k \tilde{f}^{\dagger}_{k\uparrow}, \tag{4.20}$$

where

$$\tilde{u}_k = \frac{1}{\sqrt{1+b(k)^2}} \qquad\qquad \tilde{v}_k = \frac{b(k)}{\sqrt{1+b(k)^2}}, \tag{4.21}$$

are the coherent factors for a d-wave paired state. We can show that

$$|\Phi^{SC}_{SD,mean}\rangle = \exp\left(\sum_k b(k) \tilde{f}^{\dagger}_{k\uparrow} \tilde{f}^{\dagger}_{-k\downarrow}\right)|0\rangle,$$

satisfies:

$$\tilde{d}_{k\alpha}|\Phi^{SC}_{SD,mean}\rangle = 0, \tag{4.22}$$

and

$$\gamma_{k\alpha}|\Phi^{SC}_{SD,mean}\rangle = 0. \tag{4.23}$$

The mean-field Hamiltonian which can generate $|\Phi^{SC}_{SD,mean}\rangle$ as ground state is simply:

$$H_{mean} = \sum_k \left(\epsilon_{\tilde{f}}(k)\gamma^{\dagger}_{k\alpha}\gamma_{-k\alpha} + \epsilon_{\tilde{d}}(k)\tilde{d}^{\dagger}_{k\alpha}\tilde{d}_{k\alpha}\right), \tag{4.24}$$

with $\epsilon_{\tilde{f}}(k), \epsilon_{\tilde{d}}(k) \geqslant 0$. Later we will see that there are physical reasons that $\epsilon_{\tilde{d}}(k) > \epsilon_{\tilde{f}}(k)$, meaning $\tilde{f}$ band is lowest energy excitation, and $\tilde{d}$ band is fully gapped, $\epsilon_{\tilde{d}}(k) > 0$ for any k.

We can express f and d fermions in terms of γ and $\tilde{d}$ fermions:

$$f_{k\alpha} = \sqrt{1-\beta_k^2}(\tilde{u}_k\gamma_{k\alpha} + \tilde{v}_k\epsilon_{\alpha\delta}\gamma^{\dagger}_{-k\delta}) - \beta_k\tilde{d}_{k\alpha} \tag{4.25}$$

$$d_{k\alpha} = \beta_k(\tilde{u}_k\gamma_{k\alpha} + \tilde{v}_k\epsilon_{\alpha\delta}\gamma^{\dagger}_{-k\delta}) + \sqrt{1-\beta_k^2}\tilde{d}_{k\alpha}. \tag{4.26}$$

Based on Eq.(4.25) and (4.26), it is easy to obtain:

$$\frac{\langle \Phi^{SC}_{SD,mean}|f^{\dagger}_{k\alpha}f_{k\alpha}|\Phi^{SC}_{SD,mean}\rangle}{\langle \Phi^{SC}_{SD,mean}||\Phi^{SC}_{SD,mean}\rangle} = (1-\beta_k^2)\tilde{v}_k^2 \tag{4.27}$$

$$\frac{\langle \Phi^{SC}_{SD,mean}|d^{\dagger}_{k\alpha}d_{k\alpha}|\Phi^{SC}_{SD,mean}\rangle}{\langle \Phi^{SC}_{SD,mean}||\Phi^{SC}_{SD,mean}\rangle} = \beta_k^2\tilde{v}_k^2. \tag{4.28}$$

We know that the mean-field wavefunction should give one f-fermion and $x = \frac{N_h}{N}$ d-fermion per site on average:

$$\sum_k (1-\beta_k^2)\tilde{v}_k^2 = N \tag{4.29}$$

$$\sum_k \beta_k^2\tilde{v}_k^2 = N_h \tag{4.30}$$

In the low doping limit $x \to 0$, it is clear from the above relations that $\beta_k^2 \propto x$.

Now let us understand how to calculate Z_- and Z_+ on this mean-field wavefunction. Z_+ and Z_- are defined to be:

$$Z_{-,k} = \frac{|\langle N-1,k|c_k|\Phi^N_{GS}\rangle|^2}{\langle N-1,k|N-1,k\rangle\langle\Phi^N_{GS}|\Phi^N_{GS}\rangle}, \tag{4.31}$$

$$Z_{+,k} = \frac{|\langle N+1,k|c^{\dagger}_k|\Phi^N_{GS}\rangle|^2}{\langle N+1,k|N+1,k\rangle\langle\Phi^N_{GS}|\Phi^N_{GS}\rangle}, \tag{4.32}$$

where $|N-1,k\rangle$ ($|N+1,k\rangle$) are the lowest-energy $N-1$ ($N+1$) electron states which have nonzero overlap with $c_k|\Phi^N_{GS}\rangle$ ($c^{\dagger}_k|\Phi^N_{GS}\rangle$).

In our mean-field wavefunction, the lowerest energy excited states are given by creating γ_k-quasi-particle. Note that now $d^{\dagger}_k$ is the hole creation operator, so at mean-field level the Z_k for spinon-dopon wavefunction are:

$$Z^{SD}_{-,k\uparrow} = \frac{|\langle \Phi^{SC}_{SD,mean}|\gamma_{k\uparrow}d^{\dagger}_{k\uparrow}|\Phi^{SC}_{SD,mean}\rangle|^2}{\langle \Phi^{SC}_{SD,mean}|\gamma_{k\uparrow}\gamma^{\dagger}_{k\uparrow}|\Phi^{SC}_{SD,mean}\rangle\langle\Phi^{SC}_{SD,mean}|\Phi^{SC}_{SD,mean}\rangle}, = \beta_k^2\tilde{u}_k^2 \tag{4.33}$$

$$Z^{SD}_{+,k\uparrow} = \frac{|\langle \Phi^{SC}_{SD,mean}|\gamma_{-k\downarrow}d_{k\uparrow}|\Phi^{SC}_{SD,mean}\rangle|^2}{\langle \Phi^{SC}_{SD,mean}|\gamma_{-k\downarrow}\gamma^{\dagger}_{-k\downarrow}|\Phi^{SC}_{SD,mean}\rangle\langle\Phi^{SC}_{SD,mean}|\Phi^{SC}_{SD,mean}\rangle} = \beta_k^2\tilde{v}_k^2. \tag{4.34}$$

At this moment, let us compare spinon-dopon wavefunction (SDwf) with BCS wavefunction (BCSwf), both before projection (In Section 4.2.4 we will compare them after projection).

In Section 4.2.1 we view pBCSwf as the projected slave-boson mean-field state

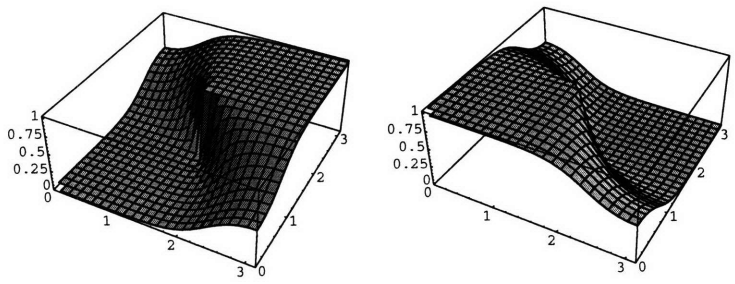

Figure 4-1: Plot of u_k^2 (left) and v_k^2 (right) within one quarter Brillouin Zone, k_x and k_y range from 0 to π.

into physical Hilbert space. We may also view pBCSwf as projected BCSwf with all double occupancies removed:

$$|\Phi_{PBCS}\rangle = P_D P_N |\Phi_{BCS}\rangle \tag{4.35}$$

$$= P_D P_N \exp(\sum_k a(k) c_{k\uparrow}^\dagger c_{-k\downarrow}^\dagger)|0\rangle \tag{4.36}$$

$$\propto P_D \left(\sum_k a(k) c_{k\uparrow}^\dagger c_{-k\downarrow}^\dagger\right)^{N_f/2} |0\rangle, \tag{4.37}$$

where

$$|\Phi_{BCS}\rangle = \exp(\sum_k a(k) c_{k\uparrow}^\dagger c_{-k\downarrow}^\dagger)|0\rangle \tag{4.38}$$

$$\propto \prod_k (u_k + v_k c_{k\uparrow}^\dagger c_{-k\downarrow}^\dagger)|0\rangle. \tag{4.39}$$

Before the projection, the spectral weight of the electron operator c_k can be calculated easily:

$$Z_{-,k}^{BCS} = v_k^2 = n_k \qquad\qquad Z_{+,k}^{BCS} = u_k^2 = 1 - n_k, \tag{4.40}$$

where $n_k = \langle c_k^\dagger c_k \rangle_{BCS}$. For a d-wave BCSwf Eq.(4.6), we can plot the Z_k in Fig.4-1. In low doping limit, parameters are taken as $\mu = 0$, $\chi = 1$, $\Delta = 0.55$. Such choice of parameters leads to a pBCSwf with lowest average energy at half filling.

The $Z_{+,k}$ and $Z_{-,k}$ for the pBCSwf after the projection were also calculated[79]. Roughly speaking what was found is that the Z_k profile after projection is similar to that before the projection. There is a quasi fermi surface, which is roughly along

the diagonal direction, $Z_{-,k}$ is large inside the fermi surface and decreases very fast when you go outside fermi surface; while $Z_{+,k}$ is large outside fermi surface, and decreases fast when you go into fermi surface. But there is one big difference, which is a reduction factor. For the $Z_{+,k}$, this reduction factor was found to be proportional to x. But for $Z_{-,k}$, this reduction factor depends on k and is finite (around 0.2) for $k = (0, 0)$ even at low-doping limit. From slave-boson approach Eq.(4.4), we already see that $Z \propto x$ at mean field level. Basically at half filling, $Z = 0$ and we have a Mott insulator instead of a band insulator.

Notice that along diagonal direction $(\pi, 0) - (0, \pi)$, the Z_k^{BCS} is dispersionless: $Z_k^{BCS} = 0.5$, which does not have dichotomy feature; After projection, there is a factor x reduction, but Z_k is still almost a constant along the diagonal direction[80, 79].

To compare the calculated Z from the BSCwf and SDwf, we note that the projected wave functions, pBCSwf and pSDwf, are closely related (see section 4.2.4). More precisely:

$$|\Phi_{PSD}^{SC}\rangle = |\Phi_{PBCS}\rangle \text{ if:}$$
$$\tilde{u}_k = v_k,\ \tilde{v}_k = u_k, \text{ and } \beta_k = \beta_0 \text{ (constant)} \tag{4.41}$$

It is easy to understand this identification at half-filling, since both wavefunctions simply give the same spin-liquid (usually referred to as staggered flux spin liquid in literatures), characterized by χ and Δ. Now in the pSDwf $\tilde{f} = f$, with no mixing with d-fermion. It is simply a particle-hole transformed pBCSwf, by which u_k transformed into $\tilde{v}_k$ and vice versa. The important message is that u_k, v_k and $\tilde{u}_k, \tilde{v}_k$ characterize the spin dynamics, but β_k characterizes the charge dynamics.

With this identification in mind, from Eq.(4.33,4.34) and (4.40) we immediately know that when $\beta_k = \beta_0$ these two wavefunctions give the same mean-field Z_k profile except that SDwf has an extra x factor, because $\beta_k^2 = \beta_0^2 \propto x$ in low doping limit. However, when β_k has a strong k-dependence, Z_k from the two approaches can be very different.

Let us think about whether or not these wavefunctions can capture dichotomy in low doping limit. What did we learn from these mean-field result? We learned that it is impossible to capture dichotomy by BCSwf, because in order to capture the k-dependence along $(0, \pi)$–$(\pi, 0)$, one has to tune u_k, v_k. Because d-wave u_k, v_k are constant along $(0, \pi)$–$(\pi, 0)$, one has to destroy the d-wave ansatz to have a k-dependent u_k, v_k along $(0, \pi)$–$(\pi, 0)$. This leads to a higher J energy. On the other hand, it is possible to capture dichotomy by SDwf, because one can tune β_k to have a

strong k-dependence while keeping $\tilde{u}_k, \tilde{v}_k$ to be d-wave ansatz. This will not destroy the spin background. Based on our experience of projection, we expect that even after projection, the above statement is qualitatively true.

4.2.4 Why mixing β_k has a strong k-dependence? –Relation between pBCSwf and pSDwf

In the last section we see that pSDwf can potentially capture the dichotomy through a k dependent β_k. Now the issue is, why does the β_k want to have a k dependence that can explain the dichotomy in Z_k? Why does such k-dependent β_k lead to a pSDwf which is energetically more favorable? To understand this, we need to know what a pSDwf looks like in real space.

The discussion below for identifying the relation between pSDwf and pBCSwf is rather long. The result, however, is simple. Let us present the result here first. We introduce $\tilde{\beta}_k = \beta_k/\sqrt{1-\beta_k^2}$. In low doping limit, $\tilde{\beta}_k \approx \beta_k$. For the simplest one-hole case, if $\tilde{\beta}_k$ has the simplest modulation in k-space $\tilde{\beta}_k = \tilde{\beta}_0 + 2\tilde{\beta}_1(\cos k_x + \cos k_y)$, then the pSDwf can be viewed as pBCSwf mixed with the wavefunction generated by the nearest neighbor hopping operators (see Eq.(4.56)). For more complicated $\tilde{\beta}_k = \tilde{\beta}_0 + 2\tilde{\beta}_1(\cos k_x + \cos k_y) + 4\tilde{\beta}_2 \cos k_x \cos k_y + 2\tilde{\beta}_3(\cos 2k_x + \cos 2k_y)$, the pSDwf can be viewed as pBCSwf mixed with the wavefunction generated by the nearest neighbor, next nearest neighbor and third nearest neighbor hopping operators (see Eq.(4.59)). Therefore to lower the hopping energy, finite β_i's are naturally developed. This is why β_k with a proper k dependence is more energetically favorable.

Before we look into pSDwf, let us review what a pBCSwf looks like in real space. One can do a Fourier transformation:

$$
\begin{aligned}
|\Phi_{PBCS}\rangle &= P_D \left(\sum_k a(k) c^\dagger_{k\uparrow} c^\dagger_{-k\downarrow} \right)^{N_f/2} |0\rangle \\
&= P_D \left(\sum_{\mathbf{R}_{i\uparrow}, \mathbf{R}_{j\downarrow}} a(\mathbf{R}_{j\downarrow} - \mathbf{R}_{i\uparrow}) c^\dagger_{\mathbf{R}_{i\uparrow},\uparrow} c^\dagger_{\mathbf{R}_{j\downarrow},\downarrow} \right)^{N_f/2} |0\rangle, \qquad (4.42)
\end{aligned}
$$

where $a(\mathbf{r}) = \sum_k a(k)\cos(k\cdot\mathbf{r})$. If we have a spin basis $\{\mathbf{R}_{i\uparrow}, \mathbf{R}_{j\downarrow}\}$, where $\mathbf{R}_{i\uparrow}$ labels

the positions of spin up electrons and $\mathbf{R}_{j\downarrow}$ labels the positions of spin down electrons:

$$\langle\{\mathbf{R}_{i\uparrow},\mathbf{R}_{j\downarrow}\}|\Phi_{PBCS}\rangle = \begin{vmatrix} a(\mathbf{R}_{1\downarrow}-\mathbf{R}_{1\uparrow}) & a(\mathbf{R}_{1\downarrow}-\mathbf{R}_{2\uparrow}) & \cdots & a(\mathbf{R}_{1\downarrow}-\mathbf{R}_{\frac{N_f}{2}\uparrow}) \\ a(\mathbf{R}_{2\downarrow}-\mathbf{R}_{1\uparrow}) & a(\mathbf{R}_{2\downarrow}-\mathbf{R}_{2\uparrow}) & \cdots & a(\mathbf{R}_{2\downarrow}-\mathbf{R}_{\frac{N_f}{2}\uparrow}) \\ \vdots & \vdots & \ddots & \vdots \\ a(\mathbf{R}_{\frac{N_f}{2}\downarrow}-\mathbf{R}_{1\uparrow}) & a(\mathbf{R}_{\frac{N_f}{2}\downarrow}-\mathbf{R}_{2\uparrow}) & \cdots & a(\mathbf{R}_{\frac{N_f}{2}\downarrow}-\mathbf{R}_{\frac{N_f}{2}\uparrow}) \end{vmatrix}. \tag{4.43}$$

We see that the overlap between a spin basis and pBCSwf is simply a single slater determinant of a two-particle wavefunction. This is why pBCSwf can be numerically simulated on a fairly large lattice.

Now we go back to pSDwf. Up to a normalization constant, one can express pSDwf as:

$$|\Phi_{PSD}^{SC}\rangle = P_{SD}\left(\sum_k b(k)(f_{k\uparrow}^\dagger + \tilde{\beta}_k d_{k\uparrow}^\dagger)(f_{-k\downarrow}^\dagger + \tilde{\beta}_k d_{-k\downarrow}^\dagger)\right)^{\frac{N+N_h}{2}}|0\rangle \tag{4.44}$$

where $\tilde{\beta}_k = \beta_k/\sqrt{1-\beta_k^2}$. Since $\beta_k \propto \sqrt{x}$, in the low doping limit, $\tilde{\beta}_k = \beta_k$.

One can also do a Fourier transformation into the real space:

$$\begin{aligned}|\Phi_{PSD}^{SC}\rangle = P_{SD}\cdot\Bigg(&\sum_{\mathbf{R}_{i\uparrow},\mathbf{R}_{j\downarrow}} b(\mathbf{R}_{j\downarrow}-\mathbf{R}_{i\uparrow})(f_{\mathbf{R}_{i\uparrow}\uparrow}^\dagger + \tilde{\beta}_0 d_{\mathbf{R}_{i\uparrow}\uparrow}^\dagger + \sum_\delta \tilde{\beta}_\delta d_{\mathbf{R}_{i\uparrow}+\delta,\uparrow}^\dagger) \\ &\cdot (f_{\mathbf{R}_{j\downarrow}\downarrow}^\dagger + \tilde{\beta}_0 d_{\mathbf{R}_{j\downarrow}\downarrow}^\dagger + \sum_\delta \tilde{\beta}_\delta d_{\mathbf{R}_{j\downarrow}+\delta,\downarrow}^\dagger)\Bigg)^{\frac{N+N_h}{2}}|0\rangle,\end{aligned} \tag{4.45}$$

where $\tilde{\beta}_\delta$'s are the Fourier components of $\tilde{\beta}_k$:

$$\tilde{\beta}_k = \tilde{\beta}_0 + \tilde{\beta}_{\mathbf{x}}e^{ik_x} + \tilde{\beta}_{-\mathbf{x}}e^{-ik_x} + \tilde{\beta}_{\mathbf{y}}e^{ik_y} + \tilde{\beta}_{-\mathbf{y}}e^{-ik_y} + \cdots. \tag{4.46}$$

We should only consider the rotation invariant $\tilde{\beta}_k$, and let us only keep the first three Fourier components:

$$\begin{aligned}\tilde{\beta}_k =& \tilde{\beta}_0 + 2\tilde{\beta}_1(\cos k_x + \cos k_y) + 4\tilde{\beta}_2 \cos k_x \cos k_y \\ &+ 2\tilde{\beta}_3(\cos 2k_x + \cos 2k_y).\end{aligned} \tag{4.47}$$

We claimed that if $\tilde{\beta}_k = \tilde{\beta}_0$, then pSDwf is identical to pBCSwf if $b(k) = \frac{1}{a(k)}$. Let us see how that is true. Without $\beta_{1,2,3}$, Eq.(4.45) is:

$$|\Phi^{SC}_{PSD}(\tilde{\beta}_0)\rangle = P_{SD}\left(\sum_{\mathbf{R}_{i\uparrow},\mathbf{R}_{j\downarrow}} b(\mathbf{R}_{j\downarrow}-\mathbf{R}_{i\uparrow})(f^\dagger_{\mathbf{R}_{i\uparrow}\uparrow}+\tilde{\beta}_0 d^\dagger_{\mathbf{R}_{i\uparrow}\uparrow})(f^\dagger_{\mathbf{R}_{j\downarrow}\downarrow}+\tilde{\beta}_0 d^\dagger_{\mathbf{R}_{j\downarrow}\downarrow})\right)^{\frac{N+N_h}{2}}|0\rangle. \tag{4.48}$$

What does a pBCSwf look like? If one does a particle-hole transformation $c^\dagger_{i\uparrow} \to h_{i\downarrow}$, pBCSwf is:

$$|\Phi_{PBCS}\rangle = P_D\left(\sum_k \frac{1}{a(k)} h^\dagger_{k\uparrow}h^\dagger_{-k\downarrow}\right)^{\frac{N+N_h}{2}}|0\rangle \tag{4.49}$$

$$= P_D\left(\sum_{\mathbf{R}_{i\uparrow},\mathbf{R}_{j\downarrow}} b(\mathbf{R}_{j\downarrow}-\mathbf{R}_{i\uparrow})h^\dagger_{\mathbf{R}_{i\uparrow},\uparrow}h^\dagger_{\mathbf{R}_{j\downarrow},\downarrow}\right)^{\frac{N+N_h}{2}}|0\rangle, \tag{4.50}$$

where P_D is the projection forbidding any empty site.

If we consider a spin basis $\{\mathbf{R}_{i\uparrow},\mathbf{R}_{j\downarrow}\}$, with the empty sites $\{\mathbf{R}_{k,0}\}$, then after particle-hole transformation, we have single occupied sites $\{\mathbf{R}_{i\uparrow},\mathbf{R}_{j\downarrow}\}$, and double occupied sites $\{\mathbf{R}_{k,0}\}$. So the position of spin up and down sites in the hole representation are $\{\tilde{\mathbf{R}}_{i\uparrow},\tilde{\mathbf{R}}_{j\downarrow}\}_h$, where $\{\tilde{\mathbf{R}}_{i\uparrow}\}_h = \{\mathbf{R}_{i\uparrow}\}\cup\{\mathbf{R}_{k,0}\}$ and $\{\tilde{\mathbf{R}}_{j\downarrow}\}_h = \{\mathbf{R}_{j\downarrow}\}\cup\{\mathbf{R}_{k,0}\}$. The overlap of pBCSwf and the spin basis in hole representation is:

$$\begin{aligned}\langle\{\mathbf{R}_{i\uparrow},\mathbf{R}_{j\downarrow}\}|\Phi_{PBCS}\rangle &= \langle\{\tilde{\mathbf{R}}_{i\uparrow},\tilde{\mathbf{R}}_{j\downarrow}\}_h|\Phi_{PBCS}\rangle \\ &= \begin{vmatrix} b(\tilde{\mathbf{R}}_{1\downarrow}-\tilde{\mathbf{R}}_{1\uparrow}) & b(\tilde{\mathbf{R}}_{1\downarrow}-\tilde{\mathbf{R}}_{2\uparrow}) & \cdots & b(\tilde{\mathbf{R}}_{1\downarrow}-\tilde{\mathbf{R}}_{\frac{N+N_h}{2}\uparrow}) \\ b(\tilde{\mathbf{R}}_{2\downarrow}-\tilde{\mathbf{R}}_{1\uparrow}) & b(\tilde{\mathbf{R}}_{2\downarrow}-\tilde{\mathbf{R}}_{2\uparrow}) & \cdots & b(\tilde{\mathbf{R}}_{2\downarrow}-\tilde{\mathbf{R}}_{\frac{N+N_h}{2}\uparrow}) \\ \vdots & \vdots & \ddots & \vdots \\ b(\tilde{\mathbf{R}}_{\frac{N+N_h}{2}\downarrow}-\tilde{\mathbf{R}}_{1\uparrow}) & b(\tilde{\mathbf{R}}_{\frac{N+N_h}{2}\downarrow}-\tilde{\mathbf{R}}_{2\uparrow}) & \cdots & b(\tilde{\mathbf{R}}_{\frac{N+N_h}{2}\downarrow}-\tilde{\mathbf{R}}_{\frac{N+N_h}{2}\uparrow}) \end{vmatrix}.\end{aligned} \tag{4.51}$$

The equation works this way because if one simply expands the polynomial in Eq.(4.50), each sum will give you one term in the expansion of the determinant in Eq.(4.51), and Pauli statistics is accounted by the sign in determinant expansion.

Now we can do the same analysis on pSDwf Eq.(4.48). First of all $\tilde{\beta}_0$ is not relevant in the wavefunction, since we are projecting into a state with fixed number of d-fermion, which means that all $\tilde{\beta}_0$ does is to give an overall factor $\tilde{\beta}_0^{N_h}$ in front of

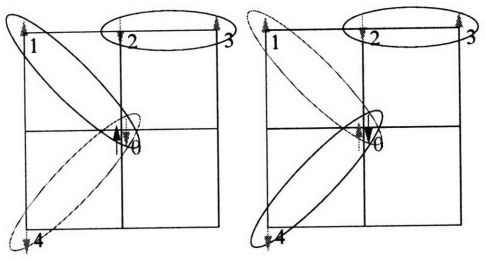

Figure 4-2: pSDwf with only $\tilde{\beta}_0$. The site 0 is empty. f-fermions are represented by green spin, and d-fermion is represented by red spin. Black valence bonds are bonds with of f-fermions, while red valence bond has a d-fermion. The two figures are two contributions of the overlap between pSDwf and a spin basis $|1_\uparrow 3_\uparrow 2_\downarrow 4_\downarrow 0_{emp}\rangle$, and they correspond to the same term in determinant Eq.(4.52). The two figures give rise to states: left: $|\uparrow_{1f}\downarrow_{0f}\uparrow_{3f}\downarrow_{2f}\uparrow_{0d}\downarrow_{4f}\rangle = |\uparrow_{1f}\uparrow_{3f}\downarrow_{2f}\downarrow_{4f}(\downarrow_{0f}\uparrow_{0d})\rangle$ and right: $|\uparrow_{1f}\downarrow_{0d}\uparrow_{3f}\downarrow_{2f}\uparrow_{0f}\downarrow_{4f}\rangle = -|\uparrow_{1f}\uparrow_{3f}\downarrow_{2f}\downarrow_{4f}(\uparrow_{0f}\downarrow_{0d})\rangle$ The minus sign means that the two figures contribute additively.

the wavefunction. To have an overlap with spin basis $\{\mathbf{R}_{i\uparrow}, \mathbf{R}_{j\downarrow}, \mathbf{R}_{k,0}\}$, we know that on empty site $\mathbf{R}_{k,0}$ the expansion of polynomial Eq.(4.48) should give either $|\uparrow_f\downarrow_d\rangle$ or $|\uparrow_d\downarrow_f\rangle$. After projection each case would contribute to $\frac{1}{\sqrt{2}}|0\rangle$ where $|0\rangle = \frac{1}{\sqrt{2}}(|\uparrow_f\downarrow_d\rangle + |\uparrow_d\downarrow_f\rangle)$

One immediately sees that the expansion of polynomial Eq.(4.48) gives similar terms as the expansion of Eq.(4.50); actually corresponding to one term in determinant Eq.(4.51), we have 2^{N_h} terms from Eq.(4.48), since we can either have $|\uparrow_f\downarrow_d\rangle$ or $|\uparrow_d\downarrow_f\rangle$ for each empty site. The details are visualized in Fig.4-2. Taking into account the factor$\frac{1}{\sqrt{2}}$ of projection, one has:

$$\begin{aligned}
&\langle\{\mathbf{R}_{i\uparrow}, \mathbf{R}_{j\downarrow}\}|\Phi^{SC}_{PSD}(\tilde{\beta}_0)\rangle \\
=&(\sqrt{2}\tilde{\beta}_0)^{N_h}\begin{vmatrix} b(\tilde{\mathbf{R}}_{1\downarrow}-\tilde{\mathbf{R}}_{1\uparrow}) & b(\tilde{\mathbf{R}}_{1\downarrow}-\tilde{\mathbf{R}}_{2\uparrow}) & \cdots & b(\tilde{\mathbf{R}}_{1\downarrow}-\tilde{\mathbf{R}}_{\frac{N+N_h}{2}\uparrow}) \\ b(\tilde{\mathbf{R}}_{2\downarrow}-\tilde{\mathbf{R}}_{1\uparrow}) & b(\tilde{\mathbf{R}}_{2\downarrow}-\tilde{\mathbf{R}}_{2\uparrow}) & \cdots & b(\tilde{\mathbf{R}}_{2\downarrow}-\tilde{\mathbf{R}}_{\frac{N+N_h}{2}\uparrow}) \\ \vdots & \vdots & \ddots & \vdots \\ b(\tilde{\mathbf{R}}_{\frac{N+N_h}{2}\downarrow}-\tilde{\mathbf{R}}_{1\uparrow}) & b(\tilde{\mathbf{R}}_{\frac{N+N_h}{2}\downarrow}-\tilde{\mathbf{R}}_{2\uparrow}) & \cdots & b(\tilde{\mathbf{R}}_{\frac{N+N_h}{2}\downarrow}-\tilde{\mathbf{R}}_{\frac{N+N_h}{2}\uparrow}) \end{vmatrix},
\end{aligned} \tag{4.52}$$

we found that $|\Phi_{PBCS}\rangle$ and $|\Phi^{SC}_{PSD}(\tilde{\beta}_0)\rangle$ are the same wavefunction.

Now let us put in the simplest k-dependence in $\tilde{\beta}_k$:

$$\tilde{\beta}_k = \tilde{\beta}_0 + 2\tilde{\beta}_1(\cos k_x + \cos k_y), \tag{4.53}$$

we try to write $|\Phi^{SC}_{PSD}(\tilde{\beta}_0, \tilde{\beta}_1)\rangle$ in real space. After the Fourier transformation into

real space:

$$|\Phi_{PSD}^{SC}(\tilde{\beta}_0,\tilde{\beta}_1)\rangle = P_{SD}\cdot\left(\sum_{\mathbf{R}_{i\uparrow},\mathbf{R}_{j\downarrow}} b(\mathbf{R}_{j\downarrow}-\mathbf{R}_{i\uparrow})(f^{\dagger}_{\mathbf{R}_{i\uparrow}\uparrow}+\tilde{\beta}_0 d^{\dagger}_{\mathbf{R}_{i\uparrow}\uparrow}+\tilde{\beta}_1\sum_{\delta=\pm\hat{x},\pm\hat{y}} d^{\dagger}_{\mathbf{R}_{i\uparrow}+\delta,\uparrow})\right.$$
$$\left.\cdot\,(f^{\dagger}_{\mathbf{R}_{j\downarrow}\downarrow}+\tilde{\beta}_0 d^{\dagger}_{\mathbf{R}_{j\downarrow}\downarrow}+\tilde{\beta}_1\sum_{\delta=\pm\hat{x},\pm\hat{y}} d^{\dagger}_{\mathbf{R}_{j\downarrow}+\delta,\downarrow})\right)^{\frac{N+N_h}{2}}|0\rangle. \tag{4.54}$$

If we expand this polynomial Eq.(4.54), of course we will still have contribution from $\tilde{\beta}_0$ terms which is nothing but the right hand side of Eq.(4.52). But apart from that, we also have contribution from $\tilde{\beta}_1$, which makes the problem more complicated. To start, let us consider the case of a single hole $N_h = 1$. To have an overlap with spin basis $\{\mathbf{R}_{i\uparrow},\mathbf{R}_{j\downarrow},\mathbf{R}_{k,0}\}$, the d-fermion on empty site $\mathbf{R}_{k,0}$ can also come from a bond connecting a spinful site and $\mathbf{R}_{k,0}+\delta$, which is the $\tilde{\beta}_1$ term effect. Let us consider the case $\delta = \hat{y}$. We can also assume the spin state on site $\mathbf{R}_{k,0}+\delta$ is spin down. Now it appears that we have two ways to construct the empty site on $\mathbf{R}_{k,0}$: $|\uparrow_f\downarrow_d\rangle$ or $|\uparrow_d\downarrow_f\rangle$. We study the two cases separately. Firstly if the empty site is constructed by $|\uparrow_f\downarrow_d\rangle$, shown in Fig.4-3, careful observation tells us that the contribution to the overlap is exactly cancelled by fermion statistics. On the other hand, if the empty site is constructed by $|\uparrow_d\downarrow_f\rangle$, we have the case in Fig.4-4. After careful observation, we know that this type of contribution is $-\frac{\tilde{\beta}_1}{2\tilde{\beta}_0}$ times the overlap between $|\Phi_{PSD}^{SC}(\tilde{\beta}_0)\rangle$ and the spin basis that differs from $\{\mathbf{R}_{i\uparrow},\mathbf{R}_{j\downarrow},\mathbf{R}_{k,0}\}$ by a hopping along $\hat{y}$. Considering the fact that the shift can also be $-\hat{y}$ and $\pm\hat{x}$, one has:

$$\langle\{\mathbf{R}_{i\uparrow},\mathbf{R}_{j\downarrow},\mathbf{R}_{k,0}\}|\Phi_{PSD}^{SC}(\tilde{\beta}_0,\tilde{\beta}_1)\rangle = \sqrt{2}\tilde{\beta}_0\langle\{\mathbf{R}_{i\uparrow},\mathbf{R}_{j\downarrow},\mathbf{R}_{k,0}\}|\Phi_{PBCS}\rangle$$
$$+\left(\frac{-\tilde{\beta}_1}{\sqrt{2}}\right)\langle\{\mathbf{R}_{i\uparrow},\mathbf{R}_{j\downarrow},\mathbf{R}_{k,0}\}|\sum_{\delta=\pm\hat{x},\pm\hat{y}} c^{\dagger}_{\mathbf{R}_{k,0}+\delta,\alpha}c_{\mathbf{R}_{k,0},\alpha}|\Phi_{PBCS}\rangle, \tag{4.55}$$

where the minus sign in the second terms comes from Fermi statistics.

Just by looking at Eq.(4.55), we arrive at the conclusion:

$$|\Phi_{PSD}^{SC}(\tilde{\beta}_0,\tilde{\beta}_1)\rangle = |\Phi_{PBCS}\rangle + \left(\frac{-\tilde{\beta}_1}{2\tilde{\beta}_0}\right)P_D\sum_{i,\delta=\pm\hat{x},\pm\hat{y}} c^{\dagger}_{i+\delta,\alpha}c_{i,\alpha}|\Phi_{PBCS}\rangle. \tag{4.56}$$

Let us study Eq.(4.55). With out $\tilde{\beta}_1$, one has a single Slater determinant for the overlap with a spin basis; with $\tilde{\beta}_1$, we have $1+n_{shift}=5$ Slater determinants, where

n_{shift} is the total number of ways that one hole can hop. Later we will see that for n_h holes, the number of Slater determinants for the overlap is $(1+n_{shift})^{n_h}$, which means numerically one can only do few holes.

The result (4.56) is obtained by studying one-hole case, and it is not hard to generalize the result for the multi-hole case. Basically, each hole may either not hop or hop once with a prefactor $\frac{-\tilde{\beta}_1}{2\tilde{\beta}_0}$, but not hop more than once. For example, for two-hole case, we have:

$$|\Phi^{SC}_{PSD}(\tilde{\beta}_0,\tilde{\beta}_1)\rangle$$
$$= \left(1 + P_D \sum_{i,\delta=\pm\hat{x},\pm\hat{y}} \frac{-\tilde{\beta}_1}{2\tilde{\beta}_0} c^\dagger_{i+\delta,\alpha} c_{i,\alpha} + P_D \frac{1}{2!} \sum_{\substack{\delta_1,\delta_2=\pm\hat{x},\pm\hat{y} \\ j,i\neq j+\delta_2}} \left(\frac{-\tilde{\beta}_1}{2\tilde{\beta}_0}\right)^2 c^\dagger_{j+\delta_2,\alpha_2} c_{j,\alpha_2} c^\dagger_{i+\delta_1,\alpha_1} c_{i,\alpha_1}\right) |\Phi_{PBCS}\rangle, \tag{4.57}$$

where the constraint $i \neq j+\delta_2$ makes sure no hole can hop twice, and the coefficient $\frac{1}{2!}$ comes from double counting.

We can also easily generalize it to the case with $\tilde{\beta}_2$ and $\tilde{\beta}_3$.... For two hole case, we have:

$$|\Phi^{SC}_{PSD}(\tilde{\beta}_0,\tilde{\beta}_\delta)\rangle$$
$$= \left(1 + P_D \sum_{i,\delta} \frac{-\tilde{\beta}_\delta}{2\tilde{\beta}_0} c^\dagger_{i+\delta,\alpha} c_{i,\alpha} + P_D \frac{1}{2!} \sum_{\substack{\delta_1,\delta_2 \\ j,i\neq j+\delta_2}} \left(\frac{-\tilde{\beta}_{\delta_1}}{2\tilde{\beta}_0}\right)\left(\frac{-\tilde{\beta}_{\delta_2}}{2\tilde{\beta}_0}\right) c^\dagger_{j+\delta_2,\alpha_2} c_{j,\alpha_2} c^\dagger_{i+\delta_1,\alpha_1} c_{i,\alpha_1}\right) |\Phi_{PBCS}\rangle. \tag{4.58}$$

In the end, the general formula for multi-hole pSDwf is:

$$|\Phi^{SC}_{PSD}(\tilde{\beta}_0,\tilde{\beta}_\delta)\rangle = P_D \exp_{n_{hop}=0,1}\left(1 + \sum_{i,\delta} \frac{-\tilde{\beta}_\delta}{2\tilde{\beta}_0} c^\dagger_{i+\delta,\alpha} c_{i,\alpha}\right) |\Phi_{PBCS}\rangle, \tag{4.59}$$

where $n_{hop} = 0, 1$ ensures that no hole can hop twice.

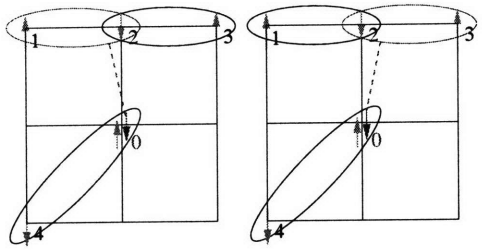

Figure 4-3: pSDwf with only $\tilde{\beta}_1$. The site 0 is empty. f-fermions are represented by green spin, and d-fermion is represented by red spin. Black valence bonds are bonds with of f-fermions, while red valence bond has a d-fermion. Notice that the position of d-fermion is shifted by $-\hat{y}$ by $\tilde{\beta}_1$ term effect (red dotted line). The two figures show the two contributions of the overlap between pSDwf and spin basis $|1_\uparrow 3_\uparrow 2_\downarrow 4_\downarrow 0_{emp}\rangle$, with *spin of f-fermion on site 2 and spin of d-fermion on site 0 are parallel.* They give rise to states: left: $|\uparrow_{1f}\downarrow_{0d}\uparrow_{3f}\downarrow_{2f}\uparrow_{0f}\downarrow_{4f}\rangle = |\uparrow_{1f}\uparrow_{3f}\downarrow_{2f}\downarrow_{4f}(\downarrow_{0d}\uparrow_{0f})\rangle$ and right: $|\uparrow_{1f}\downarrow_{2f}\uparrow_{3f}\downarrow_{0d}\uparrow_{0f}\downarrow_{4f}\rangle = -|\uparrow_{1f}\uparrow_{3f}\downarrow_{2f}\downarrow_{4f}(\downarrow_{0d}\uparrow_{0f})\rangle$ The minus sign means the two figures contribute subtractively, i.e., they cancel exactly.

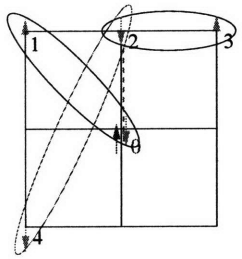

Figure 4-4: pSDwf with only $\tilde{\beta}_1$. The site 0 is empty. f-fermions are represented by green spin, and d-fermion is represented by red spin. Black valence bonds are bonds with of f-fermions, while red valence bond has a d-fermion. Note that the position of d-fermion is shifted by $-\hat{y}$ by $\tilde{\beta}_1$ term effect (red dotted line). This figure shows another contribution to the overlap between pSDwf and spin basis $|1_\uparrow 3_\uparrow 2_\downarrow 4_\downarrow 0_{emp}\rangle$, with *spin of f-fermion on site 2 and spin of d-fermion on site 0 are anti-parallel..* It gives rise to state: $|\uparrow_{1f}\downarrow_{0f}\uparrow_{3f}\downarrow_{2f}\uparrow_{0d}\downarrow_{4f}\rangle = -|\uparrow_{1f}\uparrow_{3f}\downarrow_{2f}\downarrow_{4f}(\uparrow_{0d}\downarrow_{0f})\rangle$. Note that there is a contribution for $\langle 1_\uparrow 3_\uparrow 0_\downarrow 4_\downarrow 2_{emp}|\Phi^{SC}_{PSD}(\tilde{\beta}_0)\rangle$, with the same valence bond map, where $|1_\uparrow 3_\uparrow 0_\downarrow 4_\downarrow 2_{emp}\rangle$ is the result state after a hopping along $\hat{y}$ acting on original state $|1_\uparrow 3_\uparrow 2_\downarrow 4_\downarrow 0_{emp}\rangle$. That one would give a state $|\uparrow_{1f}\downarrow_{0f}\uparrow_{3f}\downarrow_{2f}\uparrow_{2d}\downarrow_{4f}\rangle = |\uparrow_{1f}\uparrow_{3f}\downarrow_{0f}\downarrow_{4f}(\uparrow_{2d}\downarrow_{2f})\rangle$. The minus sign in the shifted d-fermion overlap comes from fermi statistics.

4.3 How to measure the mixing β_k? –Physical Meaning of spinon excitation and dopon excitation

From Eq.(4.34,4.33), we know what at the mean-field level, β_k can be measured by spectral weight Z. After projection, it is natural to expect that Z is also closely related to β_k. But how to calculate Z after projection? Basically through Eq.(4.32,4.31), we need a good trial ground state and excited state. The ground state would be nothing but pSDwf. What is a good excited state? To be specific, let us study Z_-, then the question is how to obtain $|N-1\rangle$?

In pBCSwf, the good excited state (referred as quasi-particle state) is found to be:

$$|N-1\rangle_{qp}^{PBCS} = P_D c_p P_N |BCS\rangle, \tag{4.60}$$

where P_N project into fixed N_f number of electrons. The way we construct excited state here is simple: first find a excited state on the mean-field level, then do a projection. In pSDwf, which includes pBCSwf as a limit, we should have a similar formula. But now we have two possible ways to construct excitation states, since on mean-field level we have two types of fermions f and d, they correspond to two types of excitations. Now it is important to understand what each type of excitations looks like. It turns out that *the f-type excitation corresponds to the quasi-particle excitation, and d-type excitation corresponds to bare hole excitation.* Thus the quasi-particle state $|N-1\rangle$ for calculating Z_- is the f-type excitation.

The main result for this section is Eq.(4.70,4.71) for f-excitation and Eq.(4.76) for d-excitation. One can see that the f-excitation of pSDwf is just the quasi-particle excitation in pBCSwf together with hopping terms acting on it. And d-excitation is the bare hole on a pSDwf ground state. Let's see how those happen:

For f-excitation,

$$\begin{aligned} |N-1\rangle_f &= P_{SD} f_{-p}^\dagger P_N |\Phi_{SD}^{SC}\rangle \\ &= P_{SD} f_{-p}^\dagger \left(\sum_k b(k)(f_{k\uparrow}^\dagger + \tilde{\beta}_k d_{k\uparrow}^\dagger)(f_{-k\downarrow}^\dagger + \tilde{\beta}_k d_{-k\downarrow}^\dagger) \right)^{\frac{N+N_h}{2}} |0\rangle. \end{aligned} \tag{4.61}$$

Here $|N-1\rangle_f$ has $N_f - 1$ number of electrons, because before projection there are totally $N + N_h + 1$ fermions, and we know projection enforces one f-fermion per site,

so totally there are $N_h + 1$ d-fermions, i.e., holes. What does this wavefunction look like after projection?

To understand this we first try to understand the excitation of pBCSwf. What is the excited state in terms of spin basis? One way to see it is to identify:

$$|N-1\rangle_{qp}^{PBCS} = P_D c_{p\uparrow}\left(\sum_k a(k) c_{k\uparrow}^\dagger c_{-k\downarrow}^\dagger\right)^{N_f/2}|0\rangle \tag{4.62}$$

$$\propto P_D c_{-p\downarrow}^\dagger\left(\sum_k a(k) c_{k\uparrow}^\dagger c_{-k\downarrow}^\dagger\right)^{N_f/2-1}|0\rangle. \tag{4.63}$$

In this form the overlap with a spin basis $\{\mathbf{R}_{i\uparrow}, \mathbf{R}_{j\downarrow}\}$ is easy to see. Notice now the number of up spins is $N_f/2-1$, and the number of down spins is $N_f/2$, so there is one more site in $\{\mathbf{R}_{j\downarrow}\}$. The only fashion to construct a spin basis is: let $c_{-p\downarrow}^\dagger$ create an electron somewhere, then let $a(k)c_{k\uparrow}^\dagger c_{-k\downarrow}^\dagger$ create the valence bonds. After observation, the overlap is:

$$\begin{aligned}&\langle\{\mathbf{R}_{i\uparrow}, \mathbf{R}_{j\downarrow}\}|N-1\rangle_{qp}^{PBCS}\\ =&\begin{vmatrix} a(\mathbf{R}_{1\downarrow}-\mathbf{R}_{1\uparrow}) & a(\mathbf{R}_{1\downarrow}-\mathbf{R}_{2\uparrow}) & \cdots & a(\mathbf{R}_{1\downarrow}-\mathbf{R}_{\frac{N_f}{2}-1,\uparrow}) & e^{-ip\mathbf{R}_{1\downarrow}}\\ a(\mathbf{R}_{2\downarrow}-\mathbf{R}_{1\uparrow}) & a(\mathbf{R}_{2\downarrow}-\mathbf{R}_{2\uparrow}) & \cdots & a(\mathbf{R}_{2\downarrow}-\mathbf{R}_{\frac{N_f}{2}-1,\uparrow}) & e^{-ip\mathbf{R}_{2\downarrow}}\\ \vdots & \vdots & \ddots & \vdots & \\ a(\mathbf{R}_{\frac{N_f}{2}\downarrow}-\mathbf{R}_{1\uparrow}) & a(\mathbf{R}_{\frac{N_f}{2}\downarrow}-\mathbf{R}_{2\uparrow}) & \cdots & a(\mathbf{R}_{\frac{N_f}{2}\downarrow}-\mathbf{R}_{\frac{N_f}{2}-1\uparrow}) & e^{-ip\mathbf{R}_{\frac{N_f}{2}\downarrow}}\end{vmatrix}.\end{aligned} \tag{4.64}$$

But to compare with pSDwf formalism, we want to see the same result in a different way. Let us do a particle-hole transformation, just like what we did in Eq.(4.50).

$$\begin{aligned}&|N-1\rangle_{qp}^{PBCS}\\ =&P_D c_{p\uparrow}\left(\sum_k a(k) c_{k\uparrow}^\dagger c_{-k\downarrow}^\dagger\right)^{N_f/2}|0\rangle \propto P_D h_{-p\downarrow}^\dagger\left(\sum_k b(k) h_{k\uparrow}^\dagger h_{-k\downarrow}^\dagger\right)^{(N+N_h)/2}|0\rangle.\end{aligned} \tag{4.65}$$

The only way to construct a spin basis in hole representation $\{\tilde{\mathbf{R}}_{i\uparrow}, \tilde{\mathbf{R}}_{j\downarrow}\}_h$ is to let $h_{-p\downarrow}^\dagger$ construct a hole somewhere, and let $b(k)h_{k\uparrow}^\dagger h_{-k\downarrow}^\dagger$ construct the valence bonds to

fill the lattice. The overlap in hole representation is:

$$\langle\{\mathbf{R}_{i\uparrow},\mathbf{R}_{j\downarrow}\}|N-1\rangle_{qp}^{PBCS}=\langle\{\tilde{\mathbf{R}}_{i\uparrow},\tilde{\mathbf{R}}_{j\downarrow}\}_h|N-1\rangle_{qp}^{PBCS}$$

$$=\begin{vmatrix} b(\tilde{\mathbf{R}}_{1\downarrow}-\tilde{\mathbf{R}}_{1\uparrow}) & b(\tilde{\mathbf{R}}_{1\downarrow}-\tilde{\mathbf{R}}_{2\uparrow}) & \cdots & b(\tilde{\mathbf{R}}_{1\downarrow}-\tilde{\mathbf{R}}_{\frac{N+N_h}{2}\uparrow}) & e^{-ip\tilde{\mathbf{R}}_{1\downarrow}} \\ b(\tilde{\mathbf{R}}_{2\downarrow}-\tilde{\mathbf{R}}_{1\uparrow}) & b(\tilde{\mathbf{R}}_{2\downarrow}-\tilde{\mathbf{R}}_{2\uparrow}) & \cdots & b(\tilde{\mathbf{R}}_{2\downarrow}-\tilde{\mathbf{R}}_{\frac{N+N_h}{2}\uparrow}) & e^{-ip\tilde{\mathbf{R}}_{2\downarrow}} \\ \vdots & \vdots & \ddots & \vdots & \\ b(\tilde{\mathbf{R}}_{\frac{N+N_h}{2}+1\downarrow}-\tilde{\mathbf{R}}_{1\uparrow}) & b(\tilde{\mathbf{R}}_{\frac{N+N_h}{2}+1,\downarrow}-\tilde{\mathbf{R}}_{2\uparrow}) & \cdots & b(\tilde{\mathbf{R}}_{\frac{N+N_h}{2}+1,\downarrow}-\tilde{\mathbf{R}}_{\frac{N+N_h}{2}\uparrow}) & e^{-ip\tilde{\mathbf{R}}_{\frac{N+N_h}{2}+1,\downarrow}} \end{vmatrix}. \tag{4.66}$$

Now let us go back to pSDwf. What is an f-type excitation? The only way to construct a spin basis, $|\{\tilde{\mathbf{R}}_{i\uparrow},\tilde{\mathbf{R}}_{j\downarrow}\}_h\rangle$, is to let $f_{-p}^\dagger$ construct an f-fermion somewhere, then let $b(k)(f_{k\uparrow}^\dagger+\tilde{\beta}_k d_{k\uparrow}^\dagger)(f_{-k\downarrow}^\dagger+\tilde{\beta}_k d_{-k\downarrow}^\dagger)$ construct the valence bonds to fill the whole lattice. We first consider the case $\tilde{\beta}_k=\tilde{\beta}_0$. In this case, the constructing precess is in exactly the same fashion as in Eq.(4.66), except for one difference: there is a coefficient of $\sqrt{2}\tilde{\beta}_0$ for each hole. That is because for each hole there are two contributions, one from $|\uparrow_f\downarrow_d\rangle$, the other from $|\uparrow_d\downarrow_f\rangle$, each with coefficient of $\sqrt{1/2}\tilde{\beta}_0$; unless that the hole and the spinon created by $f_{-p}^\dagger$ are on the same site, in which case we have only one contribution. If we ignore the last effect (since it is an infinitesimal change to the wavefunction in the low doping limit, and it also comes as an artifact of our projective construction), we conclude that:

$$\langle\{\mathbf{R}_{i\uparrow},\mathbf{R}_{j\downarrow}\}|N-1,\tilde{\beta}_0\rangle_f=\langle\{\tilde{\mathbf{R}}_{i\uparrow},\tilde{\mathbf{R}}_{j\downarrow}\}_h|N-1,\tilde{\beta}_0\rangle_f=(\sqrt{2}\beta_0)^{N_h+1}.$$

$$\begin{vmatrix} b(\tilde{\mathbf{R}}_{1\downarrow}-\tilde{\mathbf{R}}_{1\uparrow}) & b(\tilde{\mathbf{R}}_{1\downarrow}-\tilde{\mathbf{R}}_{2\uparrow}) & \cdots & b(\tilde{\mathbf{R}}_{1\downarrow}-\tilde{\mathbf{R}}_{\frac{N+N_h}{2}\uparrow}) & e^{-ip\tilde{\mathbf{R}}_{1\downarrow}} \\ b(\tilde{\mathbf{R}}_{2\downarrow}-\tilde{\mathbf{R}}_{1\uparrow}) & b(\tilde{\mathbf{R}}_{2\downarrow}-\tilde{\mathbf{R}}_{2\uparrow}) & \cdots & b(\tilde{\mathbf{R}}_{2\downarrow}-\tilde{\mathbf{R}}_{\frac{N+N_h}{2}\uparrow}) & e^{-ip\tilde{\mathbf{R}}_{2\downarrow}} \\ \vdots & \vdots & \ddots & \vdots & \\ b(\tilde{\mathbf{R}}_{\frac{N+N_h}{2}+1\downarrow}-\tilde{\mathbf{R}}_{1\uparrow}) & b(\tilde{\mathbf{R}}_{\frac{N+N_h}{2}+1,\downarrow}-\tilde{\mathbf{R}}_{2\uparrow}) & \cdots & b(\tilde{\mathbf{R}}_{\frac{N+N_h}{2}+1,\downarrow}-\tilde{\mathbf{R}}_{\frac{N+N_h}{2}\uparrow}) & e^{-ip\tilde{\mathbf{R}}_{\frac{N+N_h}{2}+1,\downarrow}} \end{vmatrix} \tag{4.67}$$

$$=(\sqrt{2}\beta_0)^{N_h+1}\langle\{\mathbf{R}_{i\uparrow},\mathbf{R}_{j\downarrow}\}|N-1\rangle_{qp}^{PBCS}, \tag{4.68}$$

so

$$|N-1,\tilde{\beta}_0\rangle_f\propto|N-1\rangle_{qp}^{PBCS}. \tag{4.69}$$

The point is that f-type excitation describes the spin-charge separation picture of the excitation, because the hole and the unpaired spinon created by $f_{-p}^\dagger$ can be arbitrarily separated. And it turns out to be the low energy excitation of t-J model.

What if the mixing β_k has momentum dependence? Similar to our study for the ground state wavefunction leading to Eq.(4.55,4.56), one can convince oneself that, in the one hole case

$$\begin{aligned}|N-1,\tilde{\beta}_0,\tilde{\beta}_1,\tilde{\beta}_2,\tilde{\beta}_3\rangle_f \propto & |N-1\rangle_{qp}^{PBCS}+\left(\frac{-\tilde{\beta}_1}{2\tilde{\beta}_0}\right)P_D\sum_{i,\delta=\pm\hat{x},\pm\hat{y}}c_{i+\delta,\alpha}^{\dagger}c_{i,\alpha}|N-1\rangle_{qp}^{PBCS}\\ &+\left(\frac{-\tilde{\beta}_2}{2\tilde{\beta}_0}\right)P_D\sum_{i,\delta=\pm(\hat{x}+\hat{y}),\pm(\hat{x}-\hat{y})}c_{i+\delta,\alpha}^{\dagger}c_{i,\alpha}|N-1\rangle_{qp}^{PBCS}\\ &+\left(\frac{-\tilde{\beta}_3}{2\tilde{\beta}_0}\right)P_D\sum_{i,\delta=\pm2\hat{x},\pm2\hat{y}}c_{i+\delta,\alpha}^{\dagger}c_{i,\alpha}|N-1\rangle_{qp}^{PBCS}. \end{aligned} \tag{4.70}$$

And for multi-hole case, similar to Eq.(4.59)

$$|N-1,\tilde{\beta}_0,\tilde{\beta}_\delta\rangle_f \propto P_D \exp_{n_{hop}=0,1}\left(1+\sum_{i,\delta}\frac{-\tilde{\beta}_\delta}{2\tilde{\beta}_0}c_{i+\delta,\alpha}^{\dagger}c_{i,\alpha}\right)|N-1\rangle_{qp}^{PBCS}. \tag{4.71}$$

For d-excitation, story is different. It turns out d-excitation corresponds to bare hole excitation. What is a bare hole excitation $|N-1\rangle_{bh}$? For a pBCSwf,

$$|N-1\rangle_{bh}^{PBCS}=c_{p\uparrow}|\Phi_{PBCS}\rangle, \tag{4.72}$$

in terms of spin basis, it is easy to show that:

$$\begin{aligned}&\langle\{\mathbf{R}_{i\uparrow},\mathbf{R}_{j\downarrow},\mathbf{R}_{k0}\}|N-1\rangle_{bh}^{PBCS}=\langle\{\mathbf{R}_{i\uparrow},\mathbf{R}_{j\downarrow},\mathbf{R}_{k0}\}|c_{p\uparrow}|\Phi_{PBCS}\rangle\\ &\propto\sum_k e^{-ip\mathbf{R}_{k0}}\langle\{\{\mathbf{R}_{i\uparrow},\mathbf{R}_{k0}\},\mathbf{R}_{j\downarrow}\}|\Phi_{PBCS}\rangle\\ &=\sum_k e^{-ip\mathbf{R}_{k0}}\begin{vmatrix} a(\mathbf{R}_{1\downarrow}-\mathbf{R}_{1\uparrow}) & a(\mathbf{R}_{1\downarrow}-\mathbf{R}_{2\uparrow}) & \cdots & a(\mathbf{R}_{1\downarrow}-\mathbf{R}_{\frac{N_f}{2}-1\uparrow}) & a(\mathbf{R}_{1\downarrow}-\mathbf{R}_{k0})\\ a(\mathbf{R}_{2\downarrow}-\mathbf{R}_{1\uparrow}) & a(\mathbf{R}_{2\downarrow}-\mathbf{R}_{2\uparrow}) & \cdots & a(\mathbf{R}_{2\downarrow}-\mathbf{R}_{\frac{N_f}{2}-1\uparrow}) & a(\mathbf{R}_{2\downarrow}-\mathbf{R}_{k0})\\ \vdots & \vdots & \ddots & \vdots & \vdots\\ a(\mathbf{R}_{\frac{N_f}{2}\downarrow}-\mathbf{R}_{1\uparrow}) & a(\mathbf{R}_{\frac{N_f}{2}\downarrow}-\mathbf{R}_{2\uparrow}) & \cdots & a(\mathbf{R}_{\frac{N_f}{2}\downarrow}-\mathbf{R}_{\frac{N_f}{2}-1\uparrow}) & a(\mathbf{R}_{\frac{N_f}{2}\downarrow}-\mathbf{R}_{k0})\end{vmatrix}. \end{aligned} \tag{4.73}$$

What is a d-type excitation in terms of spin basis? We first consider the case

where $\tilde{\beta}_k = \tilde{\beta}_0$,

$$|N-1,\tilde{\beta}_0\rangle_d = P_{SD} d^\dagger_{-p\downarrow} P_N |\Phi^{SC}_{SD}\rangle$$
$$= P_{SD} d^\dagger_{-p\downarrow} \left(\sum_k b(k)(f^\dagger_{k\uparrow} + \tilde{\beta}_k d^\dagger_{k\uparrow})(f^\dagger_{-k\downarrow} + \tilde{\beta}_k d^\dagger_{-k\downarrow}) \right)^{\frac{N+N_h}{2}} |0\rangle. \quad (4.74)$$

One can see that the only way to construct a spin basis, $|\{\tilde{\mathbf{R}}_{i\uparrow}, \tilde{\mathbf{R}}_{j\downarrow}\}_h\rangle$, is to let $b(k)(f^\dagger_{k\uparrow} + \tilde{\beta}_k d^\dagger_{k\uparrow})(f^\dagger_{-k\downarrow} + \tilde{\beta}_k d^\dagger_{-k\downarrow})$ construct the valence bonds to fill the whole lattice, then find a site occupied by one $f_\uparrow$-fermion only, and let $d^\dagger_{-p\downarrow}$ construct a hole there. By observation, we conclude,

$$|N-1,\tilde{\beta}_0\rangle_d \propto |N-1\rangle^{PBCS}_{bh}. \quad (4.75)$$

If $\tilde{\beta}_k$ has k-dependence, one can also convince oneself that

$$|N-1,\tilde{\beta}_0,\tilde{\beta}_\delta\rangle_d \propto c_p |\Phi^{SC}_{PSD}(\tilde{\beta}_0,\tilde{\beta}_\delta)\rangle \equiv |N-1\rangle^{PSD}_{bh}, \quad (4.76)$$

i.e., d-type excitation corresponds to the bare hole in pSDwf.

To summarize, we have the following identification: f-type excitation corresponds to the low energy quasi-particle excitation, i.e., a state constructed by putting c_p operator inside the projection; d-type excitation corresponds to the bare hole excitation, i.e., a state constructed by putting c_p operator outside the projection.

4.4 Numerical Methods and Results

We use Variational Monte Carlo (VMC) method to calculate the ground state energy (of 2 holes), the excited state energy (of 1 hole) of pSDwf and pBCSwf and the spectral weight $Z_{-,k}$.

Our pBCSwf calculation is mostly traditional. Nevertheless the previous calculation of Z_-[80] is indirect and having uncontrolled error bars inside the fermi surface. We developed a straightforward technique to calculate Z_-. Let us recall the definition of Z_- Eq.(4.31). For pBCSwf, if we relabel $|N-1\rangle^{PBCS}_{bh}$ as $|bh\rangle$ and $|N-1\rangle^{PBCS}_{qp}$ as

$|qp\rangle$ to save notation:

$$\begin{aligned} Z_{-,k} &= \frac{|\langle qp|bh\rangle|^2}{\langle qp|qp\rangle\langle\Phi_{PBCS}|\Phi_{PBCS}\rangle} \\ &= \frac{|\langle qp|bh\rangle|^2}{\langle qp|qp\rangle\langle bh|bh\rangle}\frac{\langle bh|bh\rangle}{\langle\Phi_{PBCS}|\Phi_{PBCS}\rangle} \\ &= \frac{|\langle qp|bh\rangle|^2}{\langle qp|qp\rangle\langle bh|bh\rangle}n_k, \end{aligned} \tag{4.77}$$

where n_k is the occupation number of particles at momentum k. n_k can be calculated by VMC approach pretty straightforwardly[86]. In particular, one can easily show that at low doping limit, which is the case considered in this chapter, $n_k = \frac{1}{2}$ independent of k exactly. The only thing one needs to worry about is the overlap prefactor between $|qp\rangle$ and $|bh\rangle$. Instead of calculating the factor itself, one can split the calculation into two. If we denote a spin basis as $|s\rangle$,

$$\frac{\langle qp|bh\rangle}{\langle qp|qp\rangle} = \sum_s \frac{\langle qp|s\rangle\langle s|bh\rangle}{\langle qp|qp\rangle} = \sum_s \frac{\langle s|bh\rangle}{\langle s|qp\rangle}\frac{|\langle qp|s\rangle|^2}{\langle qp|qp\rangle} = \sum_s \frac{\langle s|bh\rangle}{\langle s|qp\rangle}\rho_{qp}(s), \tag{4.78}$$

$$\frac{\langle bh|qp\rangle}{\langle bh|bh\rangle} = \sum_s \frac{\langle bh|s\rangle\langle s|qp\rangle}{\langle bh|bh\rangle} = \sum_s \frac{\langle s|qp\rangle}{\langle s|bh\rangle}\frac{|\langle bh|s\rangle|^2}{\langle bh|bh\rangle} = \sum_s \frac{\langle s|qp\rangle}{\langle s|bh\rangle}\rho_{bh}(s). \tag{4.79}$$

Since both $\langle s|qp\rangle$ and $\langle s|bh\rangle$ are Slater determinant or sum of Slater determinants (see Eq.(4.64) and Eq.(4.73)), the above two quantities can be calculated by Metropolis program in a straightforward fashion. Then the product of the two gives the $Z_{-,k}$. This algorithm works for finite doping case, too.

For pSDwf, because we include k-dependent mixing, in each step of Metropolis random walk, we need to keep track of all the $(1+n_{shift})^{n_h}$ matrices, which limit the calculation for few holes.

4.4.1 Ground state at half filling and 2 holes

The calculation is done for t-t'-t''-J model on 10 by 10 lattice, where $t = 1$, $t' = -0.3$, $t'' = 0.2$ and $J = 0.3$. We choose periodic boundary condition in x-direction, and anti-periodic boundary condition in y-direction.

For variational parameters, we choose the lowest-energy ansatz in Eq.(4.7)[87] with parameters

$$\chi = 1, \qquad \Delta = 0.55, \qquad \mu = 0. \tag{4.80}$$

energy per bond	$\vec{S}_i \cdot \vec{S}_{i+1}$
-0.1710(1)	-0.3200(1)

Table 4.1: half-filling ground state on 10 by 10 lattice

wavefunction	$\frac{\Delta}{\chi}$	$\frac{\chi'}{\chi}$	$\frac{\chi''}{\chi}$	$\frac{\tilde{\beta}_1}{\tilde{\beta}_0}$	$\frac{\tilde{\beta}_2}{\tilde{\beta}_0}$	$\frac{\tilde{\beta}_3}{\tilde{\beta}_0}$	total energy per bond	$\langle \vec{S}_i \cdot \vec{S}_{i+1} \rangle$ per bond	T_1	T_2	T_3
pBCSwf	0.55	0	0	0	0	0	-0.1872(1)	-0.2977(2)	2.64(1)	0.52(1)	0.48(1)
pBCSwf (optimal)	0.55	-0.4	0.0	0	0	0	-0.1890(1)	-0.2947(2)	2.66(1)	0.06(1)	1.07(1)
pSDwf	0.55	-0.5	0.1	0	0	0	-0.1885(1)	-0.2872(2)	2.66(1)	-0.23(1)	1.52(1)
pSDwf (optimal)	0.55	0	0	-0.3	0.3	-0.1	-0.1918(1)	-0.2943(2)	2.86(1)	-0.46(1)	0.77(1)

Table 4.2: Two holes on 10 by 10 lattice. $t = 1$, $t' = -0.3$, $t'' = 0.2$ and $J = 0.3$. T_1, T_2 and T_3 stand for nearest neighbor hopping per hole $\frac{1}{N_h}\sum_{i,\delta=\pm\hat{x},\pm\hat{y}}\langle c_i^\dagger c_{i+\delta}\rangle$, next nearest neighbor hopping per hole $\frac{1}{N_h}\sum_{i,\delta=\pm(\hat{x}+\hat{y}),\pm(\hat{x}-\hat{y})}\langle c_i^\dagger c_{i+\delta}\rangle$ and third nearest neighbor hopping per hole $\frac{1}{N_h}\sum_{i,\delta=\pm 2\hat{x},\pm 2\hat{y}}\langle c_i^\dagger c_{i+\delta}\rangle$ respectively. We compare pBCSwf of d-wave ansatz, pBCSwf with longer range hoppings χ' and χ'', and pSDwf with non-local mixings. The best trial pSDwf has an energy 1.5% below that of the best trial pBCSwf with longer range hoppings. Comparing the first and the last line which have the same spin correlation, we find that the energy of a hole in pSDwf is $0.46t$ lower than that of a hole in pBCSwf. Note that pBCSwf with longer range hoppings destroys the d-wave spin background. As a result, the attempt to lower the hopping energy by tuning χ' and χ'' is not effective since it would increase the spin energy a lot.

The energy for half-filling ground state is listed in Table 4.1.

For two holes, we compare the energy of ground states of pBCSwf and pSDwf. For pSDwf, to lower the t hopping energy, since $t < 0$, by Eq.(4.59), the sign of $\tilde{\beta}_1$ should be negative. Similarly since $t' > 0, t'' < 0$, the parameters lowering t' and t'' hopping energy have signs $\tilde{\beta}_2 > 0$ and $\tilde{\beta}_3 < 0$. We did a variational search for the optimal values of $\tilde{\beta}_i$. The results are listed in Table 4.2, where we also compare it with pBCSwf with longer range hoppings (see Section 4.4.5).

We find that the energy of the best pSDwf is lower than the energy of the best pBCSwf. We note that the pSDwf and pBCSwf are identical at half filling. So the energy difference between the two states is purely a doping effect. Comparing the first and the last line in table 4.2 which have the same spin correlation, we see that the total energies of the two states differ by 0.0046×200 since the the 10 by 10 lattice has 200 links. This energy difference is due to the presence of two holes. So the energy of a hole in pSDwf is $0.46t$ lower than that of a hole in pBCSwf. This energy difference is big, indicating that the charge-spin correlation is much better described

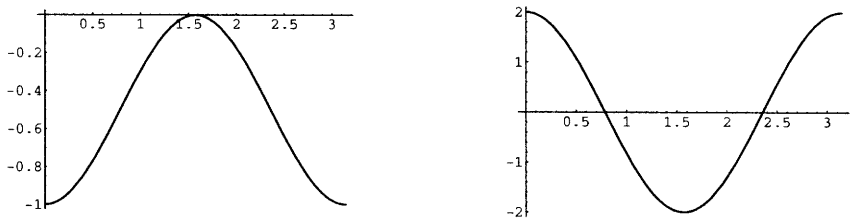

Figure 4-5: Shapes of functions $\cos k_x \cos k_y$ (left) and $\cos 2k_x + \cos 2k_y$ (right) along diagonal direction from $(\pi, 0)$ to $(0, \pi)$.

by pSDwf than pBCSwf.

4.4.2 Hole doped case, quasi-particle excitations and Z_-.

In this section we study the excitations of t-t'-t''-J model, which is one hole on 10x10 lattice. We also compare pSDwf with pBCSwf. We know from Eq.(4.71) that the pSDwf f-excitation state goes back to pBCSwf quasi-particle excitation state when all non-local mixings $\tilde{\beta}_\delta = 0$. Also from Eq.(4.71), one can see that to lower the t, t' and t'' hopping energy, we should also have $\tilde{\beta}_1 < 0$, $\tilde{\beta}_2 > 0$ and $\tilde{\beta}_3 < 0$. Actually in the low doping limit, one should expect the non-local mixing $\tilde{\beta}_\delta$ for quasi-particle excited states (f-excitation) to be same as the ground state. Here we adopt the values of $\tilde{\beta}_\delta$ from our study of 2-hole system ground state.

Our VMC calculation shows that the pSDwf or pBCSwf has finite Z_- deep inside the fermi surface even in the low doping limit $x \to 0$. This is physically wrong because deep inside fermi surface there is no well-defined quasi-particle, and the idea of calculating Z_- by a single particle excited state is also incorrect. Nevertheless, because the low energy excitation is more and more quasi-particle like as one approaches the fermi surface, we expect that the Z_- calculation remains valid close to fermi surface, roughly speaking, along the diagonal direction from $(\pi, 0)$ to $(0, \pi)$.

From Eq.(4.33), we know that at the mean-field level, the modulation of Z_- is controlled by β_k^2. It is important to study the shapes of β_k^2 for various cases. In Fig. 4-5 we plot the shapes of functions $\cos k_x \cos k_y$ and $\cos 2k_x + \cos 2k_y$ along the diagonal direction. If $\beta_k = \beta_0 + 2\beta_1(\cos k_x + \cos k_y)$, β_k^2 remains constant along the diagonal direction. If $\beta_k = \beta_0 + 4\beta_2 \cos k_x \cos k_y$, for small $\beta_2 > 0$, β_k^2 is reduced at the anti-nodal point. If $\beta_k = \beta_0 + 2\beta_3(\cos 2k_x + \cos 2k_y)$, for small $\beta_3 < 0$, β_k^2 is enhanced at the nodal point and suppressed at the anti-nodal point. Let us remember this trend: positive β_2 and negative β_3 drive the modulation of Z_- in the way consistent with dichotomy for hole doped samples.

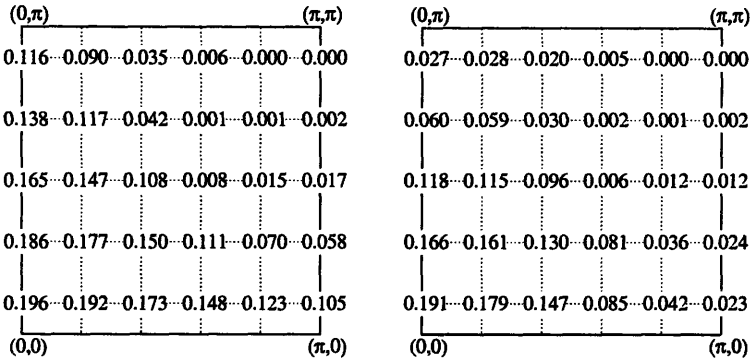

Figure 4-6: For one hole on 10 by 10 lattice, we plot $Z_{-,k}$ of pBCSwf (left, $\chi = 1$, $\Delta = 0.55$) and pSDwf (right, $\chi = 1$, $\Delta = 0.55$, $\frac{\tilde{\beta}_1}{\tilde{\beta}_0} = -0.3$, $\frac{\tilde{\beta}_2}{\tilde{\beta}_0} = 0.3$, $\frac{\tilde{\beta}_1}{\tilde{\beta}_0} = -0.1$). pBCSwf has almost constant Z_- along diagonal direction from $(\pi, 0)$ to $(0, \pi)$; while pSDwf has Z_- suppressed at anti-nodal point.

For small values of β_k we know that $\tilde{\beta}_k \approx \beta_k$. Eq.(4.33) suggests that along the diagonal direction

$$Z_{-,k} \propto (\tilde{\beta}_0 + 4\tilde{\beta}_2 \cos k_x \cos k_y + 2\tilde{\beta}_3(\cos 2k_x + \cos 2k_y))^2. \tag{4.81}$$

But as a mean-field result, one should expect that the above equation is only valid qualitatively. In fact to crudely fit the relation of the modulation of Z_- and $\tilde{\beta}$, we found it is better to have some order of unity extra factor in front of $\tilde{\beta}$ terms, and $\tilde{\beta}_1$ also contributes to the modulation of Z_- as a uniform shift.

$$Z_{-,k} \propto (\tilde{\beta}_0 + \frac{\tilde{\beta}_1}{2} + \tilde{\beta}_2 \cos k_x \cos k_y + \frac{\tilde{\beta}_3}{2}(\cos 2k_x + \cos 2k_y))^2. \tag{4.82}$$

For t-J model without t' and t'', there is no reason to develop a finite value of β_2 and β_3 since there is no longer range hoppings. As a result, one expects that Z_- remains almost constant along the diagonal direction.

For t-t'-t''-J model with $t > 0$, $t' < 0$, $t'' > 0$, we know that $\tilde{\beta}_2 > 0$ and $\tilde{\beta}_3 < 0$ have to be developed to favor longer range hoppings. So one expect Z_- should develop dichotomy shape along the diagonal direction.

In Fig.4-6 we compare the $Z_{-,k}$ of pBCSwf and pSDwf. One can see that pSDwf shows strong dichotomy.

In Fig.4-7 we compare the energy dispersion of one-hole quasi-particle excitations of pBCSwf and pSDwf. The energy of a doped hole in pSDwf is $0.38t$ lower than that of a hole in pBCSwf.

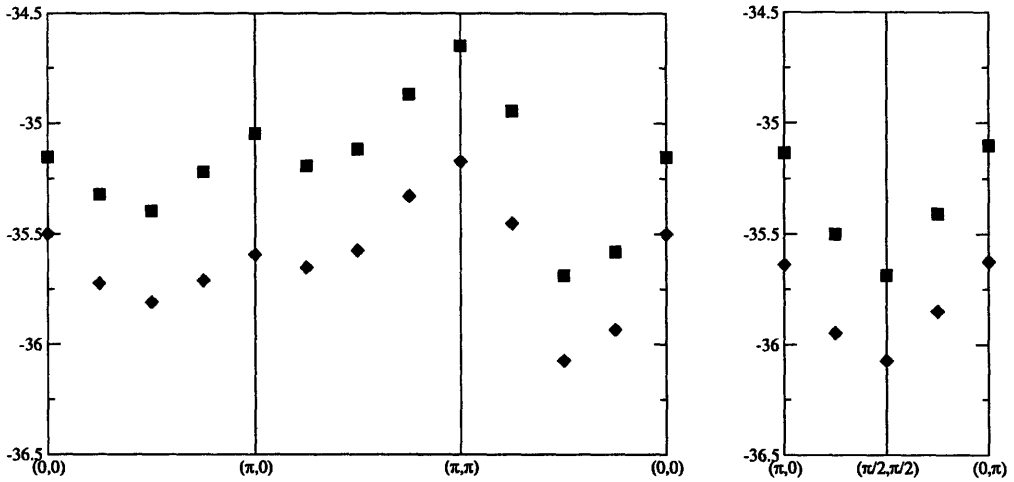

Figure 4-7: Quasi-particle spectrum for one hole on 10 by 10 lattice. $t = 1$, $t' = -0.3$, $t'' = 0.2$ and $J = 0.3$. The black square shows the spectrum of d-wave pBCSwf with $\chi = 1$ and $\Delta = 0.55$, and the red diamond shows the spectrum of pSDwf with $\chi = 1$, $\Delta = 0.55$, $\frac{\tilde{\beta}_1}{\tilde{\beta}_0} = -0.3$, $\frac{\tilde{\beta}_2}{\tilde{\beta}_0} = 0.3$ and $\frac{\tilde{\beta}_3}{\tilde{\beta}_0} = -0.1$. One can see the first hole doped to $(\pi/2, \pi/2)$. The energy of a doped hole in pSDwf is $0.38t$ lower than that of a hole in pBCSwf.

4.4.3 Electron doped case

In electron-doped case, one can do a particle-hole transformation, then multiply a (-1) for the odd lattice electron operators. By doing so, the original electron-doped t-J model with parameters t, t', t'', J transformed into hole-doped t-J model with parameters $t, -t', -t'', J$, together with a (π, π) shift in momentum space.

The approach outlined in Eq.(4.78) and Eq.(4.79) still applies here. But because of the particle-hole transformation, we are calculating Z_+ of the original electron-doped system. Because $t' > 0$ and $t'' < 0$, to favor longer range hoppings, we must have $\tilde{\beta}_2 < 0$ and $\tilde{\beta}_3 > 0$, which differ from hole-doped case by a sign flip. As a result, the Z_+ now will be suppressed at nodal point, but enhanced at the anti-nodal point. This is exactly what people observed in exact diagonalization[72].

We did a variational search for the optimal variational parameters for pBCSwf with longer range hoppings χ' and χ'', and pSDwf with non-local mixings. In Table 4.3 we compare the energy of pBCSwf and pSDwf with 2 electron doped on 10 by 10 lattice. In Fig.4-8 we plot the Z_+ map of pSDwf, one can see pSDwf has spectral weight of anti-dichotomy shape.

In Fig.4-9 we compare the energy dispersion of one-electron quasi-particle excitations of pBCSwf and pSDwf. The energy of a doped electron in pSDwf is $0.25t$ lower

wavefunction	$\frac{\Delta}{\chi}$	$\frac{\chi'}{\chi}$	$\frac{\chi''}{\chi}$	$\frac{\tilde{\beta}_1}{\tilde{\beta}_0}$	$\frac{\tilde{\beta}_2}{\tilde{\beta}_0}$	$\frac{\tilde{\beta}_3}{\tilde{\beta}_0}$	total energy per bond	$\langle \vec{S}_i \cdot \vec{S}_{i+1} \rangle$ per bond	T_1	T_2	T_3
pBCSwf	0.55	0	0	0	0	0	-0.1884(1)	-0.2977(2)	2.64(1)	0.52(1)	0.48(1)
pBCSwf (optimal)	0.55	0.2	0.0	0	0	0	-0.1888(1)	-0.2964(2)	2.61(1)	0.70(2)	0.20(2)
pSDwf (optimal)	0.55	0	0	-0.5	-0.3	0.3	-0.1910(1)	-0.2971(2)	2.57(1)	0.86(2)	-0.72(2)

Table 4.3: Two electrons on 10 by 10 lattice. $t = 1$, $t' = -0.3$, $t'' = 0.2$ and $J = 0.3$, and we mapped it into a hole-doped model with $t = 1$, $t' = 0.3$, $t'' = -0.2$ and $J = 0.3$ with a (π, π) shift in momentum space. T_1, T_2 and T_3 stand for nearest neighbor hopping per hole $\frac{1}{N_h}\sum_{i,\delta=\pm\hat{x},\pm\hat{y}}\langle c_i^\dagger c_{i+\delta}\rangle$, next nearest neighbor hopping per hole $\frac{1}{N_h}\sum_{i,\delta=\pm(\hat{x}+\hat{y}),\pm(\hat{x}-\hat{y})}\langle c_i^\dagger c_{i+\delta}\rangle$ and third nearest neighbor hopping per hole $\frac{1}{N_h}\sum_{i,\delta=\pm 2\hat{x},\pm 2\hat{y}}\langle c_i^\dagger c_{i+\delta}\rangle$ respectively. We compare pBCSwf of d-wave ansatz, pBCSwf with longer range hoppings χ' and χ'', and pSDwf with non-local mixings. The best trial pSDwf has energy lowered by 1.2% from the best trial pBCSwf with longer range hoppings. And comparing the first line and the last line which have the same spin correlations, we find that the energy of a doped electron in pSDwf is $0.26t$ lower than that of an electron in pBCSwf.

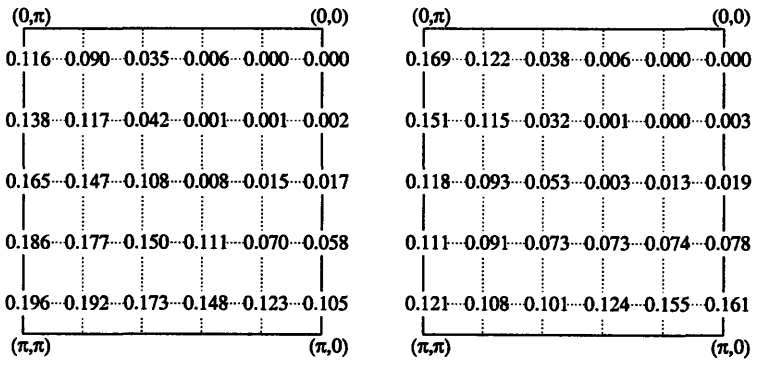

Figure 4-8: For one electron on 10 by 10 lattice, we plot $Z_{+,k}$ of pBCSwf(left, $\chi = 1$, $\Delta = 0.55$) and pSDwf(right, $\chi = 1$, $\Delta = 0.55$, $\frac{\tilde{\beta}_1}{\tilde{\beta}_0} = -0.5$, $\frac{\tilde{\beta}_2}{\tilde{\beta}_0} = -0.3$, $\frac{\tilde{\beta}_1}{\tilde{\beta}_0} = 0.3$). By particle-hole symmetry, the Z_+ of one electron pBCSwf is identical to the Z_- of one hole pBCSwf together with a (π, π) momentum shift. pBCSwf has almost constant Z_+ along the direction from $(\pi, 0)$ to $(0, \pi)$; while pSDwf has Z_+ suppressed at nodal point and enhanced at anti-nodal point.

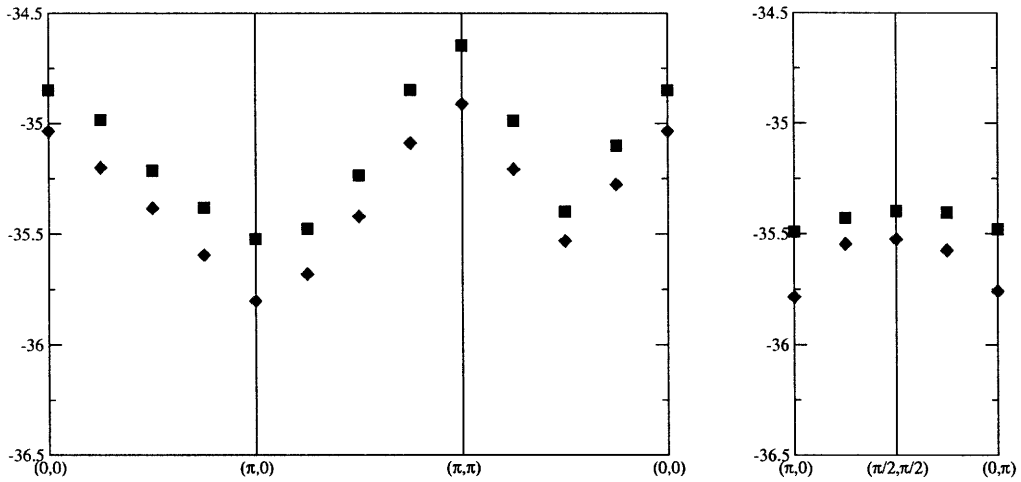

Figure 4-9: Quasi-particle spectrum for one electron on 10 by 10 lattice. $t = 1$, $t' = -0.3$, $t'' = 0.2$ and $J = 0.3$ (one can map it into a hole-doped model with $t = 1$, $t' = 0.3$, $t'' = -0.2$ and $J = 0.3$ with a (π, π) shift in momentum space.). The black square shows the spectrum of d-wave pBCSwf with $\chi = 1$ and $\Delta = 0.55$, and the red diamond shows the spectrum of pSDwf with $\chi = 1$, $\Delta = 0.55$, $\frac{\tilde{\beta}_1}{\tilde{\beta}_0} = -0.5$, $\frac{\tilde{\beta}_2}{\tilde{\beta}_0} = -0.3$ and $\frac{\tilde{\beta}_3}{\tilde{\beta}_0} = 0.3$. One can see the first electron doped to $(\pi, 0)$. The energy of a doped electron in pSDwf is $0.25t$ lower than that of an electron in pBCSwf.

than that of an electron in pBCSwf.

4.4.4 A prediction

In hole-doped and electron-doped case, $t > 0$ and t' and t'' have opposite signs, and as a result Z_- develops strong k dependence along diagonal direction. What if t' and t'' have the same sign? If both $t' > 0$ and $t'' > 0$, one expects that $\tilde{\beta}_2 < 0$ and $\tilde{\beta}_3 < 0$ to favor longer range hoppings. But they drive the modulation of Z_- in opposite ways. As a result, one expects that for certain ratio of values of $t' > 0$ and $t'' > 0$ of order 1, their effects cancel and Z_- remains constant along the diagonal direction, but with an enhanced value of Z_- than the case of pure t-J model. Similarly for certain ratio of values of $t' < 0$ and $t'' < 0$ of order 1, Z_- remains constant along the diagonal direction, but with a suppressed value of Z_- than the case of pure t-J model. These predictions can be checked by exact diagonalization.

4.4.5 pBCSwf with longer range hoppings

One can view pSDwf as an improved pBCSwf. We choose the d-wave pairing wavefunction $b(k)$ with only nearest hopping χ and pairing Δ parameters. Then β_2 and β_3

wavefunction	$\frac{\Delta}{\chi}$	$\frac{\chi'}{\chi}$	$\frac{\chi''}{\chi}$	$\frac{\tilde{\beta}_1}{\tilde{\beta}_0}$	$\frac{\tilde{\beta}_2}{\tilde{\beta}_0}$	$\frac{\tilde{\beta}_3}{\tilde{\beta}_0}$	total energy per bond	$\langle \vec{S}_i \cdot \vec{S}_{i+1} \rangle$ per bond	T_1	T_2	T_3
pBCSwf	0.55	0	0	0	0	0	-0.1793(1)	-0.3075(2)	2.65(2)	0.43(2)	0.65(2)
pBCSwf	0.55	-0.4	0.0	0	0	0	-0.1796(1)	-0.3043(2)	2.66(2)	0.02(2)	1.21(2)
pSDwf	0.55	0	0	-0.3	0.3	-0.1	-0.1815(1)	-0.3058(2)	2.86(2)	-0.49(2)	0.87(2)

Table 4.4: Two holes on 14 by 14 lattice. $t = 1$, $t' = -0.3$, $t'' = 0.2$ and $J = 0.3$. T_1, T_2 and T_3 stand for nearest neighbor hopping, next nearest neighbor hopping and third nearest neighbor hopping respectively. Although the spin energy of pBCSwf with finite longer range hoppings $\chi' = -0.4$ is slightly lower than that of pSDwf on 10 by 10 lattice, it is much higher on 14 by 14 lattice.

encode some second-neighbor and third-neighbor correlations. The price to pay is to include more than one Slater determinants in spin basis. One may naturally ask, suppose we insist working on pBCSwf, if one puts in longer range hopping parameters like χ' and χ'' in the pairing wavefunction $b(k)$, one also encodes some second-neighbor and third-neighbor correlations, which may lower the second-neighbor and third-neighbor hopping energies. But in this way one can still work with a single Slater determinant. If our pSDwf with no-local mixing is physically similar to pBCSwf with longer range hoppings, why should one bother to work with many Slater determinants?

We want to emphasize that our pSDwf is physically different from pBCSwf even after we include longer range hoppings χ' and χ''. We note that, in the infinite-lattice limit with a few holes, the pBCSwf cannot have longer range hoppings (*i.e.* $\chi' = \chi'' = 0$). Otherwise we are considering some other spin wavefunction instead of d-wave wavefunction, which will increase the spin energy by a finite amount per site. Therefore χ' and χ'' have to vanish in low doping limit. In contrast, for our pSDwf, the the spin energy is not affected by finite β_i in the zero doping limit. Thus in the low doping limit, the spin energy is perturbed only slightly by a finite β_2 and β_3. On the other hand a finite β_2 and β_3 make the hopping energy much larger than that of pBCSwf. So in the infinite-lattice limit with a few holes, β_i will be finite and the energy of one hole will be lowered by a finite amount by turning on a finite β_i.

Physically this means that β_2 and β_3 characterize the charge correlations, while χ' and χ'' characterize the spin correlations. The above claim is supported by 2-hole system on larger lattice, i.e., by lower the doping. In Table 4.4 we list the energies of pBCSwf with longer range hopping and pSDwf on 14 by 14 lattice. Comparing with Table 4.2 one can see the spin energy for pSDwf is lowered further than that for pBCSwf.

Another way to see that these two wavefunctions are different is by calculating Z_-. Numerical results show that pSDwf has dichotomy whereas pBCSwf does not.

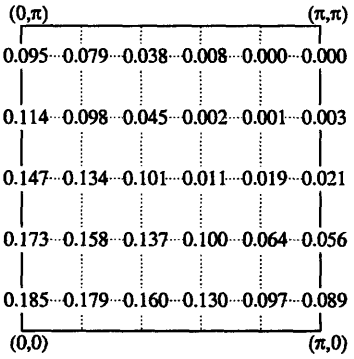

Figure 4-10: For one hole on 10 by 10 lattice, we plot $Z_{-,k}$ of pBCSwf with longer range hopping $\chi' = -0.4$ ($\chi = 1$, $\Delta = 0.55$).

Actually on the mean-field level, a negative χ' and/or positive χ'' even make the Z_- larger on the anti-nodal point than on the nodal point. After projection, we observe that Z_- still remains almost constant along the diagonal direction for pBCSwf with longer range hoppings. In Fig.4-10 we plot the Z_- map of pBCSwf with longer range hopping $\chi' = -0.4$.

4.5 Conclusion

In this chapter we studied a new type of variational wavefunction, pSDwf. It can be viewed as an improved pBCSwf, and the improvement is that pSDwf correctly characterizes the charge dynamics and the correlation between the doped holes/electrons and the nearby spins. This physics was missed by the previous pBCSwf. As a result, pSDwf correctly reproduces the dichotomy of hole-doped and electron-doped Mott insulator.

In pSDwf, we introduced two types of fermions, spinon f and dopon d. Spinons f carry spin but no charge. They form a d-wave paired state that describes the spin liquid background. Dopons d carry both spin and charge and correspond to a bare doped hole. The mixing between spinons and dopons described by β_0, β_1, β_2 and β_3 leads to a d-wave superconducting state. The charge dynamics (such as electron spectral function) is determined by those mixings. β_0 is the on-site mixing (or local mixing), and β_1, β_2 and β_3 are non-local mixings corresponding to mixing with first, second and third neighbors respectively. If pSDwf has only local mixing, it is identical to pBCSwf. With non-local mixings, pSDwf corresponds to pBCSwf with hopping terms acting on it. Therefore the wavefunction develops finite non-local mixings to lower the hopping energies. In particular, for the hole-doped case, to lower t' and t''

energies, the mixing is described by $\beta_2 > 0$ and $\beta_3 < 0$.

The pSDwf can also be obtained by projecting the spinon-dopon mean-field wavefunction into the physical subspace. Therefore, one expects that some properties of pSDwf can be understood from the mean-field theory. In the mean-field theory, it is clear that the modulation of $Z_{-,k}$ in k space is controlled by the non-local mixings. Our numerical calculation of $Z_{-,k}$ shows that the above mean-field result is valid even for the projected wave function. We find that $\beta_2 > 0$ and $\beta_3 < 0$ give exactly the dichotomy of $Z_{-,k}$ observed in the hole doped samples. Because $\beta_2 > 0$ and $\beta_3 < 0$ are driven by t' and t'', the dichotomy is also driven by t' and t''. Thus to lower the hopping energy, the spectral weight is suppressed in some region in k-space. This result conflicts a naive guess: to lower the hopping energy, the excitation should be more quasi-particle like. We also predict that the dichotomy will go away if t' and t'' have the same sign and similar magnitude. In summary, we found a mean-field theory and the associated trial wavefunction capturing the dichotomy physics.

Traditionally, in projected wavefunction variational approach, for example pBCSwf, people use wavefunctions which in real space correspond to a single Slater determinant. The reason to do so is simply to make the computation easier. Our study shows what kinds of important physics that may be missed by doing so. In real space, the pSDwf is sum of $(1 + n_{shift})^{n_{hole}}$ number of Slater determinants, because each hole can either do not hop, or hop into one of n_{shift} sites. So our calculation is limited to few-hole cases. However, the idea of introducing many Slater determinant is quite general. For example, one can study another improved pBCSwf, which allows each hole to hop once but forbids two holes hopping together, therefore the number of Slater determinant is $(1 + n_{shift})n_{hole}$ and many-hole cases are computationally achievable. This new improved pBCSwf is the first order approximation of pSDwf and remains to be studied. For a long time there is a puzzle that doped Mott-insulator (*ie* the spin disordered metallic state) seems to be energetically favorable only at high doping $x > 0.3$. For $x < 0.3$ the doped spin density wave state have a lower energy. Our pSDwf may push this limit down to low doping which agrees with experiments better. This is because that including many Slater determinants can lower the energy per hole by a significant amount (about $0.4t$).

As we have stressed, pSDwf provides a better description of spin-charge correlation, or more precisely, the spin configuration near a doped hole. This allows us to reproduce the dichotomy in quasiparticle spectral weights observed in experiments. The next question is whether the better understanding of the spin-charge correlation can lead to new experimental predictions. In the following, we will describe one such

prediction in quasi-particle current distribution.

We know that a finite supercurrent $\boldsymbol{J}_s$ shifts the superconducting quasiparticle dispersion $E_{\boldsymbol{k}}$. To the linear order in $\boldsymbol{J}_s$, we have

$$E_{\boldsymbol{k}}(\boldsymbol{A}) = E_{\boldsymbol{k}}(0) + c^{-1}\boldsymbol{j}_{\boldsymbol{k}} \cdot \boldsymbol{A},$$

where c is the speed of light and we have introduced the vector potential $\boldsymbol{A}$ to represent the supercurrent: $\boldsymbol{J}_s = \frac{n_s e^2}{mc}\boldsymbol{A}$. $\boldsymbol{j}_{\boldsymbol{k}}$ is a very important function that characterizes how excited quasiparticles affect superfluid density ρ_S. We call $\boldsymbol{j}_{\boldsymbol{k}}$ quasiparticle current. According to the BCS theory

$$\boldsymbol{j}_{\boldsymbol{k}} = e\frac{\partial \epsilon_{\boldsymbol{k}}}{\partial \boldsymbol{k}} = e\boldsymbol{v}_{\text{normal}}, \tag{4.83}$$

where $\epsilon_{\boldsymbol{k}}$ is the normal state dispersion which is roughly given by $\epsilon_{\boldsymbol{k}} = -2t[\cos(k_x) + \cos(k_y)]$.

The previous study[79] of quasi-particle current for pBCSwf shows that the quasi-particle current is roughly given by the BCS result (4.83) scaled down by a factor α. Such a quasi-particle current has a smooth distribution in k-space. Here we would like to stress that since the charge dynamics is not capture well by the pBCSwf, the above result from pBCSwf may not be reliable. We expect that the quasi-particle current of pSDwf should has a strong k-dependence, *ie* a large quasi-particle current near the nodal point where Z_k is large and small quasi-particle current near the anti-nodal point where Z_k is small. Such a quasi-particle current distribution may explain the temperature dependence of superfluid density [82].

Indeed, the mean-field spinon-dopon approach does give rise to a very different quasi-particle current distribution which roughly follows Z_k. For more detailed study in this direction and possible experimental tests, see Ref. [88].

Chapter 5

Summary of results and outlook

Let me summarize the understandings that we discussed in this thesis for exotic phases and phase transitions in Table 5.1. Note to make the table logically complete, I also include the gapped exotic phases, which are not discussed in this thesis. There are also fascinating new physics associated with gapped exotic phases[89, 90].

Basically we are in the process of building a new paradigm to replace the traditional Landau's theory of phases and phase transitions. Here we made some attempts to find the mathematical language to characterize the new phases and describe the new type of phase transitions. However one should note that currently the understanding of exotic phases and transitions are more like case by case, and different attempts come with different formalism. It will be very interesting and important to unify them in a same framework. For example, find a systematic way to write down the wavefunction and low energy effective theory for these new states of matters.

The current mathematical language of low energy excitations is mainly field theory. Exotic phases simply mean exotic stable fixed points in the RG sense. How much do we know about stable exotic fixed points in field theory? The answer is very limited. Basically all the known stable exotic fixed points involve gauge fields. We showed that the low energy excitations of an exotic phase usually involves gauge fields, but that could be a result of our limitation of language. Therefore exploring new languages, for example string theory, may bring us completely new understandings.

We proposed that by starting with a pure spin model, the low energy effective theory can be QED or QCD. That means the QED and QCD in our real life, in principle, can be the low energy theory of some spin model. Spin model may be the microsopic theory of the high energy physics. There are recent works on realizing gravitational interaction from a spin model[91, 92, 93]. Just like string theory, spin model may deserve equal attention as a potential way to unify gravity with other

	Conventional phase	Exotic phase
Examples	spin ordered phase fermi liquid, CDW...	quantum hall liquid spin liquid
Characterization	order parameter symmetry breaking Symmetry group	Quantum order No symmetry breaking PSG
Excitations	gapped gapless with free fermion or free boson no fractionalization	gapped with GS degeneracy gapless but strongly interacting in IR fractionalization
Phase transition	fluctuating order parameter Landau-Ginzburg-Wilson	usually involves gauge theory

Table 5.1: Summary of conventional and exotic phases and phase transitions.

fundamental interactions.

We used projected wavefunction technique to study the doped and undoped spin liquids. It is a very efficient way to construct spin disordered state, and it can provide very good energetics, but there are a lot of issues remain unsolved. First of all whether a projected wavefunction can be a ground state of any short-ranged hamiltonian is unclear. In one-dimension we know a projected fermi-sea is the ground state of Heisenberg model with a power law interaction[94, 95], and there are no results like that available for higher dimensions. By studying projected wavefucntion, hopefully we can answer the questions of the long range physics of the spin liquid ground state. However the relation between projected wavefunction and the low energy effective theory need to be further studied before any conclusive claim about long range physics is made. For example for the U(1)-Dirac state discussed in chapter 3, one key issue is whether the long range properties of the projected wavefunction is correctly described by the low energy effective theory of QED3. We can measure the correlation functions like spin-spin correlation or bond-bond correlations in the projected wavefunction, but are they the same as those given by QED3? A lattice-QED calculation is really necessary to answer this question, because by doing so we can compare the results from the two approaches.

Projected wavefunction is just one numerical attempt of writing down a variational state. There are other attempts such as the tensor product states[96, 97]. Is it

possible to unify the different approaches and give a systematic way to write down disordered ground state wavefunction? Instead of variational approaches, are there quasi-exact numerical techniques to address the ground state issues? We know that quantum monte-carlo seems to have unavoidable difficulties on frustrated spin models or general fermionic models, which is called sign-problem. Are there ways to bypass the sign-problem? All those questions are challenges in the numerical studies.

The above future directions are more or less "principle" motivated. There are also experiment motivated issues. Currently there are a few candidate materials which may have spin liquid ground states. But we still need smoking-gun experiments to identify them. Designing such a smoking-gun experiment is extremely important for the whole field of exotic studies. As usually happens in experiments, the material will not be described by a pure Heisenberg model. There will be non-magnetic or magnetic impurities, DM-interactions, phonon interactions(lattice distortion), etc. In order to make a comparison with experiments, including these extra interactions may be required. Spin-liquids coupled to impurities, phonons, and spin liquids in a system with DM-interaction, are open and important issues. Studying these issues can help us to identify spin liquid phase.

Suppose an exotic phase is identified, due to our understanding of the exotic phase transitions, all the transition from that phase to neighboring phases necessarily contain new physics. The first issue is what those neighboring phases are. For example, what will happen if we apply magnetic field on the kagome material? Studying those phase transitions would be very interesting and may provide extra ways to design experiments to identify exotic phases.

Appendix A

Detailed calculation of anomalous dimension γ

The scaling dimension of staggered spin-spin correlation function $\langle(-)^{\boldsymbol{x}}\mathbf{S}(\boldsymbol{x})(S)(\mathbf{0})\rangle$ is calculated by the large-N_f expansion of quantum field theory. In our formalism, one can show that the staggered spin-spin correlation function is just the fermion mass operator $\langle\bar{\psi}\psi(\boldsymbol{x})\bar{\psi}\psi(\mathbf{0})\rangle$ correlation function in the effective theory Eq.(2.119). By power counting, the scaling behavior should be $\langle\bar{\psi}\psi(\boldsymbol{x})\bar{\psi}\psi(\mathbf{0})\rangle = \frac{1}{x^4}$, but quantum fluctuations change it into $\langle\bar{\psi}\psi(\boldsymbol{x})\bar{\psi}\psi(\mathbf{0})\rangle = \frac{1}{x^{4+2\gamma_{\bar{\psi}\psi}}}$, where $\gamma_{\bar{\psi}\psi}$ is called the anomalous dimension of fermion mass operator. It turns out that the easiest way of calculating $\gamma_{\bar{\psi}\psi}$ is not to calculate $\langle\bar{\psi}\psi(\boldsymbol{x})\bar{\psi}\psi(\mathbf{0})\rangle$ directly, but to calculate the correlation function of fermion field ψ: $\langle\psi(\boldsymbol{x})\bar{\psi}(\mathbf{0})\rangle$, and the three-point correlation function $\langle\bar{\psi}\psi(\boldsymbol{x})\bar{\psi}(\boldsymbol{y})\psi(\mathbf{0})\rangle$.

Let us firstly calculate the staggered spin-spin correlation function in $SU(2)$-linear phase, where the low energy effective theory is Eq.(2.40). We need to understand the gauge interaction. In the large-N_f limit, the gauge field is strongly screened by fermions, and under renormalization group the coupling g will flow to an IR stable conformal invariant fixed point $g_*^2 \sim \frac{\Lambda}{N_f}$. Here Λ is the UV cut-off of our theory. To

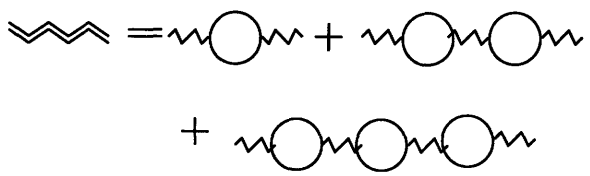

Figure A-1: The dressed gauge propagator in the leading order of large N_f limit, which is nothing but the one-loop correction in polarization.

Figure A-2: Gauge dressed fermion propagator at first order of $\frac{1}{N_f}$

the leading order of $\frac{1}{N_f}$, the dressed gauge propagator is as Fig.A-1. Let us work within Euclidean space and Landau gauge, where the bare gauge propagator is:

$$G^{ab}_{\mu\nu}(x,y) = \left\langle A^a_\mu(x) A^b_\nu(y) \right\rangle \tag{A.1}$$
$$= \int \frac{dk^3}{(2\pi)^3} e^{ik\cdot(x-y)} \frac{g^2\delta^{ab}}{k^2}(\delta_{\mu\nu} - \frac{k_\mu k_\nu}{k^2})$$

The bare fermion propagator is:

$$\left\langle \psi_i(x)\bar{\psi}_j(y) \right\rangle = \int \frac{dp^3}{(2\pi)^3} e^{ip\cdot(x-y)} \frac{-i\not{p}\delta_{ij}}{p^2} \tag{A.2}$$

where i, j label the gauge components. The dressed gauge propagator can be calculated as:

$$G^{ab}_{\mu\nu,dressed}(k) = \frac{g^2\delta^{ab}}{k^2(1+\Pi)}\left(\delta_{\mu\nu} - \frac{k_\mu k_\nu}{k^2}\right) \tag{A.3}$$

where if we do Pauli-Villar regularization,

$$(k^2\delta_{\mu\nu} - k_\mu k_\nu)\Pi = N_f g^2 T_F \int \frac{dq^3}{(2\pi)^3} \frac{\mathrm{Tr}\left[\gamma_\mu \not{q} \gamma_\nu (\not{q} - \not{k})\right]}{q^2(q-k)^2}$$
$$=(k^2\delta_{\mu\nu} - k_\mu k_\nu) N_f g^2 T_F (\frac{1}{8k} - \frac{1}{6\pi\Lambda}) \tag{A.4}$$

in which

$$\mathrm{Tr}[\tau^a\tau^b] = T_F\delta^{ab} \qquad \Rightarrow \qquad T_F = \frac{1}{2} \tag{A.5}$$

At the fixed point, where $g^2_* = \frac{6\pi\Lambda}{N_f T_F}$, the dressed gauge propagator is:

$$G^{ab}_{\mu\nu,dressed}(k) = \frac{8\delta^{ab}}{N_f T_F k}\left(\delta_{\mu\nu} - \frac{k_\mu k_\nu}{k^2}\right) \tag{A.6}$$

we now study the fermion correlation function with first order correction in $\frac{1}{N_f}$

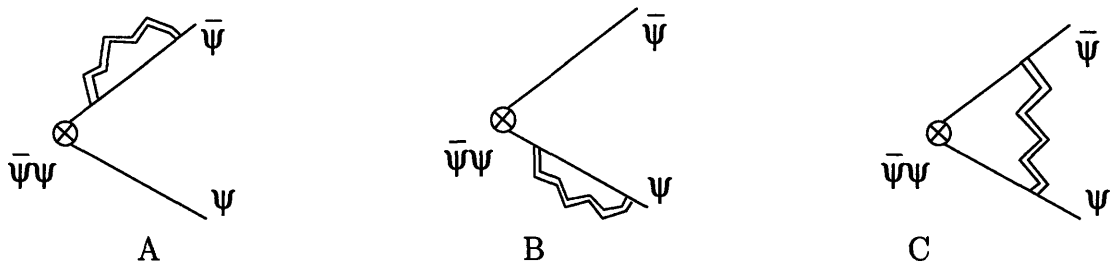

Figure A-3: Gauge dressed three point correlation function at order of $\frac{1}{N_f}$

expansion, as shown in Fig.A-2. The dressed fermion propagator is:

$$S_{ij}(k) = \frac{-i\not{k}\delta_{ij}}{k^2}(1+\Sigma) \tag{A.7}$$

where

$$\begin{aligned} \not{p}\Sigma &= i\int \frac{dq^3}{(2\pi)^3}\frac{\gamma_\mu(-i)(\not{k}+\not{q})\gamma_\nu}{(k+q)^2}\frac{C_F 8}{N_f T_F q}\left(\delta_{\mu\nu}-\frac{q_\mu q_\nu}{q^2}\right) \\ &= -\not{p}\frac{8C_F}{3\pi^2 N_f T_F}log(\frac{k}{\Lambda}) \end{aligned} \tag{A.8}$$

and

$$\tau^a\tau^a = C_F\mathbf{I} \qquad \Rightarrow \qquad C_F = \frac{3}{4} \tag{A.9}$$

Thus we know that the anomalous dimension of ψ is:

$$\gamma_\psi = -\frac{1}{2}\frac{8C_F}{3\pi^2 N_f T_F} \tag{A.10}$$

Then we look at the dressed three-point correlation function $\langle\bar{\psi}\psi(\boldsymbol{x})\bar{\psi}(\boldsymbol{y})\psi(\mathbf{0})\rangle$ at the order of $\frac{1}{N_f}$, as shown in Fig.A-3. Suppose we fix the momentum of $\bar{\psi}\psi$ to be $2k$, while $\bar{\psi}$ and ψ each carry momentum k, then the tree level three point correlation function will be $G_3(2k,k,k) = \frac{-i\not{k}}{k^2}\frac{-i(-\not{k})}{k^2} = \frac{1}{k^2}$. From the contributions of diagrams in Fig.A-3, we will have the dressed three point correlation function:

$$G_3(2k,k,k) = \frac{1}{k^2}\left(1+(A+B+C)log(\frac{k}{\Lambda})\right) \tag{A.11}$$

where A, B, C are the contributions from each corresponding diagram. Actually we know that $A+B+C = \gamma_{\bar{\psi}\psi} + 2\gamma_\psi$. So by calculating $A+B+C$, we will know the

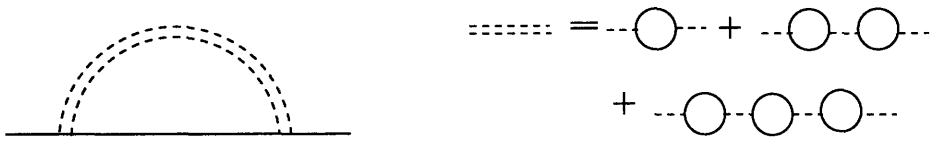

Figure A-4: The contribution of σ-boson to fermion propagator at order of $\frac{1}{N_f}$, where the double dashed line is the dressed σ-boson propagator at leading order.

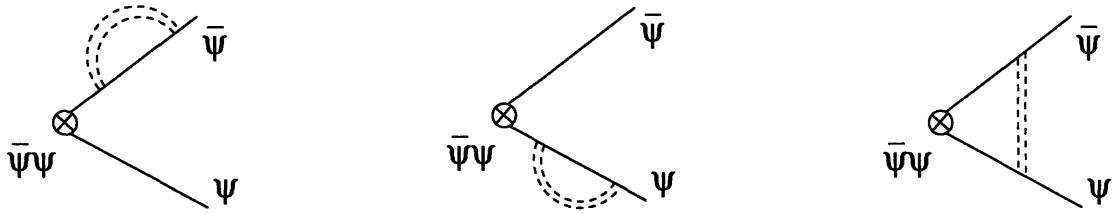

Figure A-5: Contributions of σ-boson to three point correlation function at order of $\frac{1}{N_f}$

anomalous dimension of fermion mass operator $\gamma_{\bar{\psi}\psi}$.

It is easy to see that A, B are just from the dressed fermion propagator, which has been calculated above: $A = B = 2\gamma_\psi$. New calculation needs to be done for vertex correction in C.

$$\begin{aligned} & Clog(\frac{k}{\Lambda}) \\ =&\frac{8C_F}{N_f T_F}\int \frac{dq^3}{(2\pi)^3}\frac{\gamma_\mu(\not{q}+\not{k})(\not{q}-\not{k})\gamma_\nu}{(q+k)^2(q-k)^2 q}\left(\delta_{\mu\nu}-\frac{k_\mu k_\nu}{k^2}\right) \\ =&-\frac{8C_F}{\pi^2 N_f T_F} log(\frac{k}{\Lambda}) \end{aligned} \tag{A.12}$$

Now we can compute $\gamma_{\bar{\psi}\psi}$:

$$\begin{aligned} \gamma_{\bar{\psi}\psi} =& A + B + C - 2\gamma_\psi = C + 2\gamma_\psi \\ =&-\frac{32C_F}{3\pi^2 N_f T_F} = -\frac{16}{\pi^2 N_f} \end{aligned} \tag{A.13}$$

We can also calculate the spin-spin correlation function at the critical point in a similar fashion. The only difference is that the σ boson becomes massless at critical point and contributes to the anomalous dimension of correlation functions. The contribution of σ boson to fermion propagator and three-point correlation function

are shown in Fig.A-4 and Fig.A-5. After similar calculation, we find that at the critical point,

$$\gamma_{\bar{\psi}\psi} = -\frac{16}{\pi^2 N_f} + \frac{4}{3\pi^2 N_f} \tag{A.14}$$

where the second term comes from the contribution of massless σ-boson. The change of scaling behavior during this phase transition is shown in Fig.2-12.

Appendix B

A simple algorithm to do local projection

Suppose the wavefunction before projection is the ground state of some fermionic quadratic Hamiltonian. One can always diagonalize the Hamiltonian so that all two-point correlation functions of fermion operators can be calculated exactly. For our SDwf, that means quantities like $\langle f_i^\dagger f_j\rangle$, $\langle d_i^\dagger f_j\rangle$,$\langle d_i^\dagger d_j\rangle$... can be calculated.

Projection is supposed to remove the unphysical states. For a site i, the following operator removes the unphysical states.

$$P_i = n_{f,i}(n_{f,i}-2)(\frac{1}{2}n_{d,i}^2 - \frac{1}{2}n_{d,i}+1)\cdot(1-\frac{1}{2}n_{d,i}(\vec{S}_{f,i}+\vec{S}_{d,i})^2). \tag{B.1}$$

It obviously ensures that $n_{f,i}=1$, $n_{d,i}\neq 2$ and f and d fermions form local singlet. To calculate energy, we do local projection on the relevant sites. For example, to calculate the J term energy, one actually calculates

$$\langle \vec{S}_i\cdot\vec{S}_j\rangle_{prj} = \frac{\langle P_iP_j(\vec{S}_{f,i}+\vec{S}_{d,i})\cdot(\vec{S}_{f,j}+\vec{S}_{d,j})P_iP_j\rangle}{\langle P_iP_j\rangle}. \tag{B.2}$$

The denominator accounts for the wavefunction normalization due to projection. One can write operators $P_i\vec{S}_i\cdot\vec{S}_jP_j$ and $P_i\vec{S}_i\cdot\vec{S}_jP_j$ in terms of fermion operators. By Wick's theorem, the expectation values of these operators reduce to a sum of products of fermion two-point correlation functions, which are known. Similarly for t term energy, one calculates for example,

$$\langle c_{i\uparrow}^\dagger c_{j\uparrow}\rangle_{prj} = \frac{\langle P_iP_jf_{i\uparrow}^\dagger h_j^\dagger h_i f_{j\uparrow}P_iP_j\rangle}{\langle P_iP_j\rangle}, \tag{B.3}$$

where $h_i^\dagger = \frac{1}{\sqrt{2}}(f_{i\uparrow}^\dagger d_{i\downarrow}^\dagger - f_{i\downarrow}^\dagger d_{i\uparrow}^\dagger)$ is the operator that creates a hole at site i.

One may ask whether we can do local projections on more and more sites, then the result will be closer and closer to the one of full projection. Unfortunately this cannot be done, because the number of terms in the summation when we expand $P_{i1}P_{i2}\ldots P_{in}$ increases exponentially fast as we increase n. Therefore we are limited to few sites. The above method can only be viewed as some renormalized mean-field approach.

Bibliography

[1] L. D. Landau, Sov. Phys. JETP **3**, 920 (1956).

[2] L. D. Landau, Phys. Z. Sowjetunion **11**, 26 (1937).

[3] L. D. Landau and E. M. Lifschitz, *Statistical Physics - Course of Theoretical Physics Vol 5* (Pergamon, London, 1958).

[4] X.-G. Wen, Int. J. Mod. Phys. B **4**, 239 (1990).

[5] X.-G. Wen, Advances in Physics **44**, 405 (1995).

[6] P. W. Anderson, Science **235**, 1196 (1987).

[7] G. Baskaran, Z. Zou, and P. Anderson, Solid State Commun. **63**, 973 (1987).

[8] N. F. Mott, Proc. Phys. Soc. A **62**, 416 (1949).

[9] S. A. Trugman, Phys. Rev. B **41**, 892 (1990).

[10] B. I. Shraiman and E. D. Siggia, Phys. Rev. Lett. **61**, 467 (1988).

[11] C. L. Kane, P. A. Lee, and N. Read, Phys. Rev. B **39**, 6880 (1989).

[12] T. Senthil, A. Vishwanath, L. Balents, S. Sachdev, and M. P. A. Fisher, Science **303**, 1490 (2004).

[13] Y. Ran and X.-G. Wen, cond-mat/0609620 (2006).

[14] Y. Ran, M. Hermele, P. A. Lee, and X.-G. Wen, Phys. Rev. Lett. **98**, 117205 (2007).

[15] Y. Ran and X.-G. Wen, cond-mat/0611034 (2006).

[16] G. Baskaran, Z. Zou, and P. W. Anderson, Solid State Comm. **63**, 973 (1987).

[17] G. Baskaran and P. W. Anderson, Phys. Rev. B **37**, 580 (1988).

[18] I. Affleck, Z. Zou, T. Hsu, and P. W. Anderson, Phys. Rev. B **38**, 745 (1988).

[19] E. Dagotto, E. Fradkin, and A. Moreo, Phys. Rev. B **38**, 2926 (1988).

[20] X.-G. Wen and P. A. Lee, Phys. Rev. Lett. **76**, 503 (1996).

[21] P. A. Lee, N. Nagaosa, T.-K. Ng, and X.-G. Wen, Phys. Rev. B **57**, 6003 (1998).

[22] D. H. Kim and P. A. Lee, Annals of Physics **272**, 130 (1999).

[23] W. Rantner and X.-G. Wen, Phys. Rev. B **66**, 144501 (2002).

[24] P. A. Lee and X.-G. Wen, Phys. Rev. Lett. **78**, 4111 (1997).

[25] X.-G. Wen and P. A. Lee, Phys. Rev. Lett. **80**, 2193 (1998).

[26] J. B. Marston and I. Affleck, Phys. Rev. B **39**, 11538 (1989).

[27] X.-G. Wen, Phys. Rev. B **65**, 165113 (2002).

[28] V. Kalmeyer and R. B. Laughlin, Phys. Rev. Lett. **59**, 2095 (1987).

[29] X.-G. Wen, F. Wilczek, and A. Zee, Phys. Rev. B **39**, 11413 (1989).

[30] N. Read and S. Sachdev, Phys. Rev. Lett. **66**, 1773 (1991).

[31] X.-G. Wen, Phys. Rev. B **44**, 2664 (1991).

[32] C. Mudry and E. Fradkin, Phys. Rev. B **49**, 5200 (1994).

[33] T. Senthil and M. P. A. Fisher, Phys. Rev. B **62**, 7850 (2000).

[34] X.-G. Wen and Y.-S. Wu, Phys. Rev. Lett. **70**, 1501 (1993).

[35] W. Chen, M. P. A. Fisher, and Y.-S. Wu, Phys. Rev. B **48**, 13749 (1993).

[36] T. Senthil, J. B. Marston, and M. P. A. Fisher, Phys. Rev. B **60**, 4245 (1999).

[37] N. Read and D. Green, Phys. Rev. B **61**, 10267 (2000).

[38] X.-G. Wen, Phys. Rev. Lett. **84**, 3950 (2000).

[39] X.-G. Wen, *Quantum Field Theory of Many-Body Systems – From the Origin of Sound to an Origin of Light and Electrons* (Oxford Univ. Press, Oxford, 2004).

[40] C. Dasgupta and B. I. Halperin, Phys. Rev. Lett. **47**, 1556 (1981).

[41] I. Affleck and J. B. Marston, Phys. Rev. B **37**, 3774 (1988).

[42] A. Tanaka and X. Hu, Phys. Rev. Lett. **95**, 036402 (2005).

[43] M. Hermele, T. Senthil, and M. P. A. Fisher, Phys. Rev. B **72**, 104404 (2005).

[44] T. Appelquist, A. Ratnaweera, J. Terning, and L. C. R. Wijewardhana, Phys. Rev. D **58**, 105017 (1998).

[45] T. Appelquist and D. Nash, Physical Review Letters **64**, 721 (1990/02/12).

[46] T. Appelquist, J. Terning, and L. Wijewardhana, Physical Review Letters **75**, 2081 (11 Sept. 1995).

[47] M. Moshe and J. Zinn-Justin, Physics Reports **385**, 69 (2003/10/).

[48] J. Gracey, Physics Letters B **317**, 415 (1993).

[49] M. Ciuchini, S. Derkachov, J. Gracey, and A. Manashov, Physics Letters B **458**, 117 (1999).

[50] F. Wegner, J. Math. Phys. **12**, 2259 (1971).

[51] J. S. Helton *et al.*, cond-mat/0610539.

[52] O. Ofer *et al.*, cond-mat/0610540.

[53] P. Mendels *et al.*, cond-mat/0610565.

[54] M. B. Hastings, Phys. Rev. B **63**, 014413 (2000).

[55] X.-G. Wen, Phys. Rev. B **65**, 165113 (2002).

[56] M. Hermele, T. Senthil, M. P. A. Fisher, P. A. Lee, N. Nagaosa, and X.-G. Wen, Phys. Rev. B **70**, 214437 (2004).

[57] G. Kotliar and J. Liu, Phys. Rev.B **38**, 5142 (1988).

[58] J. Marston and C. Zeng, J. Appl. Phys. **69**, 5962 (1991).

[59] C. Waldtmann *et al.*, Eur. Phys. Jour. B **2**, 501 (1998).

[60] C. Gros, Annals of Physics **189**, 53 (1989).

[61] P. Lee, N. Nagaosa, and X.-G. Wen, Rev. Mod. Phys. **78**, 17 (2006).

[62] D. J. J. Farnell, R. F. Bishop, and K. A. Gernoth, Phys. Rev. B **63**, 220402 (2001).

[63] L. Arrachea, L. Capriotti, and S. Sorella, Phys. Rev. B **69**, 224414 (2004).

[64] D. H. Kim, P. A. Lee, and X.-G. Wen, Phys. Rev. Lett. **79**, 2109 (1997).

[65] A. Damascelli, Z. Hussain, and Z.-X. Shen, Rev. Mod. Phys. **75**, 473 (2003).

[66] Z.-X. Shen and J. Schrieffer, Phys. Rev. Lett. **78**, 1771 (1997).

[67] X. Zhou *et al.*, Phys. Rev. Lett. **92**, 187001 (2004).

[68] S. Pan, J. O'Neal, R. Badzey, C. Chamon, H. Ding, J. Engelbrecht, Z. Wang, H. Eisaki, S. Uichada, A. Gupta, K.-W. Ng, E. Hudson, K. Lang, and J. Davis, Nature **413**, 282 (2001).

[69] C. Howald, P. Fournier, and A. Kapitulnik, Phys. Rev. B **64**, 100504 (2001).

[70] K. McElroy, D.-H. Lee, J. E. Hoffman, K. M. Lang, J. Lee, E. W. Hudson, H. Eisaki, S. Uchida, and J. C. Davis, Phys. Rev. Lett. **94**, 197005 (2005).

[71] P. W. Leung and R. J. Gooding, Phys. Rev. B **52**, R15711 (1995).

[72] P. W. Leung, B. O. Wells, and R. J. Gooding, Phys. Rev. B **56**, 6320 (1997).

[73] H. Fong, P. Bourges, Y. Sidis, L. Regnault, A. Ivanov, G. Gu, N. Koshizuka, and B. Keimer, Nature **398**, 588 (1999).

[74] J. Tranquada, B. Sternlieb, J. Axe, Y. Nakamura, and S. Uchida, Nature **375**, 561 (1995).

[75] G. Aeppli, T. Mason, S. Hayden, H. Mook, and J. Kulda, Science **278**, 1432 (1997).

[76] K. Yamada, C. H. Lee, K. Kurahashi, J. Wada, S. Wakimoto, S. Ueki, H. Kimura, Y. Endoh, S. Hosoya, G. Shirane, R. J. Birgeneau, M. Greven, M. A. Kastner, and Y. J. Kim, Phys. Rev. B **57**, 6165 (1998).

[77] F. Zhang and T. Rice, Phys. Rev. B **37**, 3759 (1988).

[78] C. Gros, Phys. Rev. B) **38**, 931 (1988).

[79] C. Nave, D. Ivanov, and P. Lee, Phys. Rev. B **73**, 104502 (2006).

[80] S. Bieri and D. Ivanov, condmat/0608047 (2006).

[81] T. C. Ribeiro and X.-G. Wen, Phys. Rev. Lett. **95**, 1 (2005).

[82] R. Liang, D. A. Bonn, W. N. Hardy, and D. Broun, Phys. Rev. Lett. **94**, 117001 (2005).

[83] P. Lee and N. Nagaosa, Physical Review B **46**, 5621 (1992).

[84] T. C. Ribeiro and X.-G. Wen, Phys. Rev. B **74**, 155113 (2006).

[85] T. C. Ribeiro and X.-G. Wen, Phys. Rev. Lett. **97**, 057003 (2006).

[86] A. Paramekanti, M. Randeria, and N. Trivedi, Phys. Rev. Lett. **87**, 217002 (2001).

[87] D. A. Ivanov and P. A. Lee, Phys. Rev. B **68**, 132501 (2003).

[88] T. C. Ribeiro, X.-G. Wen, and A. Vishwanath, (to be published).

[89] X.-G. Wen, Phys. Rev. D **68**, 065003 (2003).

[90] M. Levin and X.-G. Wen, Phys. Rev. B **67**, 245316 (2003).

[91] Z.-C. Gu and X.-G. Wen, gr-qc/0606100 (2006).

[92] S.-S. Lee, gr-qc/0609107 (2006).

[93] C. Xu, Phys. Rev. B **74**, 224433 (2006).

[94] F. D. M. Haldane, Phys. Rev. Lett. **60**, 635 (1988).

[95] B. S. Shastry, Phys. Rev. Lett. **60**, 639 (1988).

[96] M. M. Wolf, G. Ortiz, F. Verstraete, and J. I. Cirac, Phys. Rev. Lett. **97**, 110403 (2006).

[97] F. Verstraete and J. I. Cirac, Phys. Rev. B **73**, 094423 (2006).